



Rensselaer

The MANE Student Research and Design Journal

Featuring:

Inventor's Studio Innovations
(Partially funded by VentureWell)

Published by:

Department of Mechanical, Aerospace & Nuclear Engineering
Rensselaer Polytechnic Institute
110 8th Street Troy, NY

**Department of Mechanical, Aerospace, & Nuclear Engineering
Rensselaer Polytechnic Institute**

Editorial Staff

Brian Waite
Nicholas Thompson
Alex Angilella
Dannah Laguitan
Amanda Youmans
Daniel Spatcher
Eva Mungai

Editor-in-Chief

Adam Wertz

Advisory Committee

Dr. Asish Ghosh
Dr. Suvranu De



The MANE Student Research and Design Journal is published annually by the Department of Mechanical, Aerospace, & Nuclear Engineering (MANE) Department at Rensselaer Polytechnic Institute (RPI) located at 110 8th St. Troy, NY 12180. Responsibility for the contents rests upon the authors and not upon the MANE Department at RPI. Abstracting is permitted with credit to the source. All rights reserved. Copyright © 2016 by the Department of Mechanical, Aerospace, & Nuclear Engineering at Rensselaer Polytechnic Institute.

Research Content

| | |
|--|----|
| Letter from the Editor | 1 |
| Cascaded PID Controller Design for a Modular Quadrotor Vehicle | 2 |
| Attitude Estimation with Inertia/Magnetic Sensors | 7 |
| Effects of Synthetic Jets on Performance Enhancement of an Airfoil Model with a Control Surface | 12 |
| Finite Element Implementation of a Dynamic Residual-Based LES Model | 16 |
| Measurement of the $^{59}\text{Co}(n,\gamma)$ Cross Section Using a Lead Slowing-Down Spectrometer | 19 |
| Directional Neutron Detection with Solid-State Neutron Detectors | 23 |
| Sensitivity Calibration of a Real-Time Neutron Detection System Using Solid-State Silicon Carbide Detectors and Silver Foil Activation | 27 |

Design Content: Inventor's Studio at Rensselaer

| | |
|---|----|
| Piezoelectric Nanowire Wind-Harvester | 31 |
| A Deferred Action Battery for Home Backup Power | 36 |
| Utilizing Regulations and Standards as Design Criteria in Innovative Design | 41 |
| Low-Cost Skeletal Tracking System for a Wearable Consumer Product | 45 |
| Personal Face Warming Device | 47 |
| Application of Bell Housing for LED Cooling and Light Deflection | 49 |
| Spoiler Alert Wasteless Refrigerator | 52 |
| Pressure Washing in the 21 st Century | 55 |
| LifeSource: Daily Vital Sign Monitoring System | 58 |
| SolarSystem: A New Solar Powered Battery System | 61 |
| Reload: An Automatic Ordering System | 63 |
| Inter-Connecting Clamp (ICC) | 65 |
| Limb Ease: A New Concept for Transfemoral Prosthetic Sockets | 68 |
| Autonomous UAS Target Identification | 75 |

June 2016

Dear RPI Community,

I am pleased to introduce the first annual issue of RPI's MANE Student Research and Design Journal. The Journal showcases some of the impactful research and innovative design work performed by undergraduate and co-terminal students within cutting-edge laboratories across The MANE Department at RPI.

The task of initiating a student-run research journal was taken by The MANE Department's Student Advisory Council under the direction of the Department Head—Dr. Suvranu De—and Professor of Inventor's Studio—Dr. Asish Ghosh. Otherwise, the Journal is completely student-run; it's composed entirely of students' contributions to research and innovative solutions to design problems developed by students. The editorial staff is composed of graduate students in the MANE Department, who have experience publishing research in peer-reviewed technical journals. Thanks to Brian Waite, Nicolas Thompson, Alex Angelini, Dannah Laguitan, Amanda Youmans, Dan Spatcher, and Eva Mungai for serving on the editorial staff.

I hope you enjoy this issue of the MANE Student Research and Design Journal, as it is the product of hard work and commitment on from many talented students. We are very proud of the students who contribute to research at RPI. Hopefully this is the first of many issues which will help student researchers to become prolific authors of impactful research publications.

Sincerely,



Adam Wertz

Editor-in-Chief

Nuclear Engineering Ph.D. Candidate at RPI

CASCADED PID CONTROLLER DESIGN FOR A MODULAR QUADROTOR VEHICLE

Gregory S. Grebe, Botao Hu, Sandipan Mishra
Intelligent Systems Automation and Control Lab
Rensselaer Polytechnic Institute

In this experiment, a two level, cascaded PID controller was created to fly a rigidly connected group of flying modules arranged as a quadcopter. The PID controller was tuned using standard methods until it was able to achieve stable hovering about a given point. The system is capable of hovering at a given point with less than 100mm of oscillation or drift.

I. INTRODUCTION

The Distributed Flight Array [1] is a modular Vertical Take-Off and Landing (VTOL) vehicle first proposed by researchers at ETH Zurich. The concept is to create many modular flying units that, once docked together in a feasible configuration, are capable of stable hovering flight. The ETH Zurich implementation uses a model based control strategy. In this experiment, we attempt to replicate their results and achieve stable hovering flight using a PID controller and four modules. Section II will briefly introduce the system. Section III will introduce the dynamics model and section IV will introduce the PID controller design. Section V will detail the experimental results.

II. SYSTEM DESCRIPTION

The quadrotor system is composed of four identical hexagonal modules, each containing a motor and propeller, an Electronic Speed Controller, and a battery (Figure 1). A single central Arduino Mini microcontroller sends the appropriate Pulse Width Modulated (PWM) signal to each of the four speed controllers. These speed controllers are hard-wired to the motors, each of which has a three-blade fixed-pitch propeller attached. The red propellers (numbered 1 and 2) rotate clockwise, while the black propellers (numbered 3 and 4) rotate counterclockwise. An equal number of counter-rotating propellers are required to cancel out the rotor's reaction torques during flight. An off-board 3D Motion-Capture Camera system is the only sensor used in the system. The sensor uses IR reflecting markers attached to the vehicle in order to

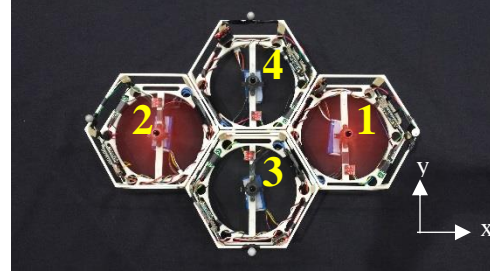


Figure 1: Quadrotor System.

localize it in space with less than 1mm of error. In the future, this system will be replaced with sensors placed locally on the modules to expand the vehicles range.

III. DYNAMICS MODEL

The system is modeled as a rigid body that is capable of producing four independently controlled positive thrust vectors, located at the center of each propeller, and directed upwards perpendicular to the plane of the vehicle. The body frame is fixed at the vehicle's center of mass, which is assumed the geometric center of the vehicle. The axes in *Figure 1* show the alignment of the body frame (denoted B) with respect to the vehicle.

The 3D Motion-Capture system provides the location and orientation of the vehicle-fixed body frame with respect to the global inertial frame (denoted as I). The location is given as a (x, y, z) coordinate in the I frame. For simplicity, the origin of the inertial frame is assumed coincident with the origin of the body frame while the vehicle is at rest before takeoff. The orientation of the body frame is described by the ZYX-Euler angles, which are used to represent the roll α , pitch β and yaw γ acting around the x, y and z axes respectively. The orientation of the body frame with respect to the inertial frame can therefore be expressed as a single rotation matrix:

$${}^I R_{xyz} = R_x(\alpha)R_y(\beta)R_z(\gamma). \quad (1)$$

The system is actuated by altering the speed of the rotors, which is proportional to the upward thrust vector, as well as the reaction torque produced. The speed controller allows us to control the rotor's angular velocity $\boldsymbol{\omega}_i$. The thrust produced is quadratically proportional to the angular velocity, so we therefore assume that the thrust is also proportional to the PWM commands ($\mathbf{u}_1, \mathbf{u}_2, \mathbf{u}_3, \mathbf{u}_4$). The steady-state thrust generated by rotor i is given by

$$f_i = k_f u_i. \quad (2)$$

Similarly, the reaction torque τ_i acting on the body of the vehicle that is generated by rotor i is given by

$$\tau_i = k_\tau u_i. \quad (3)$$

The coefficients k_f and k_τ are both constants, and are a function of several rotor parameters as well as air density. These parameters are usually determined using static thrust tests. The torque τ_i can be approximated as a linear function of thrust by

$$\tau_i = c_i f_i, \quad (4)$$

where c_i is a constant with the same magnitude for all i , and its sign depends on the handedness of the propeller.

As a rigid body, standard rigid body dynamics apply here. The entire system is assumed to have mass m , and moment of inertia J that is subjected to the forces $\mathbf{f} = [0, 0, \sum_i^4 f_i]$, and torques $\boldsymbol{\tau} = [0, 0, \sum_i^4 \tau_i]$ produced by the rotors. The equations of motion are given by

$$\dot{\mathbf{p}} = \mathbf{v} \quad (5)$$

$$m\dot{\mathbf{v}} = {}^I_B \mathbf{R}_{xyz} \mathbf{f} \quad (6)$$

$${}^I_B \dot{\mathbf{R}}_{xyz} = {}^I_B \mathbf{R}_{xyz} \boldsymbol{\omega}^\times \quad (7)$$

$$J\dot{\boldsymbol{\omega}} = -\boldsymbol{\omega} \times J\boldsymbol{\omega} + \boldsymbol{\tau}. \quad (8)$$

The vectors $\mathbf{p} = [x, y, z]$ and $\mathbf{v} = [\dot{x}, \dot{y}, \dot{z}]$, represent the position and velocity respectively of the body in the inertial frame. The vector $\boldsymbol{\omega} = [p, q, r]$ denotes the angular velocities in the body frame. The superscript \times denotes the skew symmetric matrix of that vector.

The equations of motion in their full form are nonlinear. They can however be linearized about the hover point, which is considered an equilibrium point for the vehicle. The simplified linearized equations of motion are expressed as follows

$$\ddot{x} = \beta g \quad (9)$$

$$\ddot{y} = -\alpha g \quad (10)$$

$$\mathbf{M} [\ddot{z} \quad \ddot{\alpha} \quad \ddot{\beta} \quad \ddot{\gamma}]^T = \mathbf{P} k_f \mathbf{u}, \quad (11)$$

where \mathbf{M} is a matrix and \mathbf{u} is the system input defined as

$$\mathbf{M} = \text{diag}(m, I_x, I_y, I_z) \quad (12)$$

$$\mathbf{u} = [u_1, u_2, u_3, u_4]^T \quad (13)$$

and the matrix \mathbf{P} is a 4×4 matrix that encodes the location and handedness of each of the rotors

$$\mathbf{P} = \begin{bmatrix} 1 & y_1 & -x_1 & c_1 \\ 1 & y_2 & -x_2 & c_2 \\ 1 & y_3 & -x_3 & c_3 \\ 1 & y_4 & -x_4 & c_4 \end{bmatrix}. \quad (14)$$

IV. CASCADED PID CONTROLLER DESIGN

To control a quadrotor, many researchers have proposed different controllers, including linear controllers such as the PID controller [2], the Iterative Learning Controller [3] and nonlinear controllers such as the adaptive controller [4] and the back stepping controller [5]. A comprehensive review can be found in [6].

In this paper, a cascaded PID controller is designed. Given the dynamics in the previous section, the purpose of the PID controller is to derive the control input \mathbf{u} to stabilize the quadrotor at a given position (x_d, y_d, z_d) . While simplistic, and useful only for a standard configuration of four modules, the PID controller designed is useful for benchmarking future controller designs. It also provides a working flying testbed to experiment with vehicle and controller design.

From (11), the quadrotor position (x, y) is not directly controllable, but the three angular accelerations are directly controllable. The idea is to first get the desired angles $(\alpha_d, \beta_d, \gamma_d)$ from

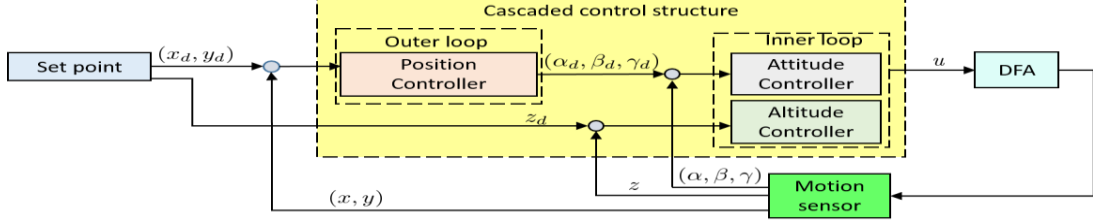


Figure 2. Proposed Cascaded Controller Architecture.

(x_d, y_d) and then design a controller that stabilizes the quadrotor angle (α, β, γ) to $(\alpha_d, \beta_d, \gamma_d)$. The overall controller is designed in a cascaded architecture (Figure 2). It consists of an inner loop and an outer loop. The outer level seeks to control the global (x, y) position and output the desired angles $(\alpha_d, \beta_d, \gamma_d)$, while the inner level determines the required values for the control output \mathbf{u} to track $(\alpha_d, \beta_d, \gamma_d, z_d)$ and achieve that position. The inner control loop is run at 100Hz while the outer control loop is run at half of that value, 50Hz. In this paper, to simplify the problem, we set γ_d to always be zero.

IV.A. The outer loop controller design

The outer controller takes desired position (x_d, y_d) and current position (x, y) as input, and outputs (α_d, β_d) .

$$\ddot{x}_d = k_{px}(x_d - x) + k_{ix} \int (x_d - x)dt + k_{dx}(\dot{x}_d - \dot{x}) \quad (15)$$

$$\ddot{y}_d = k_{py}(y_d - y) + k_{iy} \int (y_d - y)dt + k_{dy}(\dot{y}_d - \dot{y}) \quad (16)$$

$$\alpha_d = -\frac{\dot{y}_d}{g} \quad (17)$$

$$\beta_d = \frac{\dot{x}_d}{g}. \quad (18)$$

(α_d, β_d) are bounded to within ± 0.2 radians to ensure that the quadcopter does not roll or pitch too extremely. These values, as well as the desired height z_d are then passed to the inner controller.

IV.A. The inner loop controller design

The inner controller is again a PID controller. It maps (α_d, β_d, z_d) to $\mathbf{u} = (f_1, f_2, f_3, f_4)$ as follows:

$$\ddot{\alpha}_r = k_{p\alpha}(\alpha_d - \alpha) + k_{i\alpha} \int (\alpha_d - \alpha)dt + k_{d\alpha}(\dot{\alpha}_d - \dot{\alpha}) \quad (19)$$

$$\ddot{\beta}_r = k_{p\beta}(\beta_d - \beta) + k_{i\beta} \int (\beta_d - \beta)dt + k_{d\beta}(\dot{\beta}_d - \dot{\beta}) \quad (20)$$

$$\ddot{z}_r = k_{pz}(z_d - z) + k_{iz} \int (z_d - z)dt + k_{dz}(\dot{z}_d - \dot{z}) \quad (21)$$

$$\ddot{\gamma}_r = k_{p\gamma}(-\gamma) + k_{i\gamma} \int (-\gamma)dt + k_{d\gamma}(-\dot{\gamma}) \quad (22)$$

$$\mathbf{u} = \frac{1}{k_f} \mathbf{P}^{-T} \mathbf{M} [\ddot{z}_r \quad \ddot{\alpha}_r \quad \ddot{\beta}_r \quad \ddot{\gamma}_r]^T \quad (23)$$

This effort is then distributed amongst the various rotors by multiplying the output vector by the following distribution matrix:

$$\mathbf{P}^{-T} = \begin{bmatrix} 0.25 & 0 & 0.5 & -0.25 \\ 0.25 & 0 & -0.5 & -0.25 \\ 0.25 & 0.5 & 0 & 0.25 \\ 0.25 & -0.5 & 0 & 0.25 \end{bmatrix} \quad (24)$$

IV.C. Tuning

The system was first tuned systematically by attempting to isolate the various parameters and tune them individually. The system was hung on wires to isolate a single parameter, and all gains except for the parameter of interest were set to zero. The four directly controllable parameters were tuned first. Once the individual parameters had all been tuned, a series of hover tests, in which the system was released while already hovering, were conducted to further tune these parameters to achieve a stable hovering configuration. Once suitable controller gains were found for these parameters the x and y position controller gains were tuned until the system was capable of hovering at a given location with less than 100mm of drift or oscillation. The final PID gains are listed in Table 1.

Table 1: PID Gains.

| Parameter | Kp | Ki | Kd |
|-----------|--------|-------|---------|
| α | 150 | 40 | 30 |
| β | 80 | 30 | 30 |
| γ | 500 | 120 | 60 |
| z | 0.2 | 0.2 | 0.1 |
| x | 0.001 | 0.001 | 0.00008 |
| y | 0.0015 | 0.001 | 0.00002 |

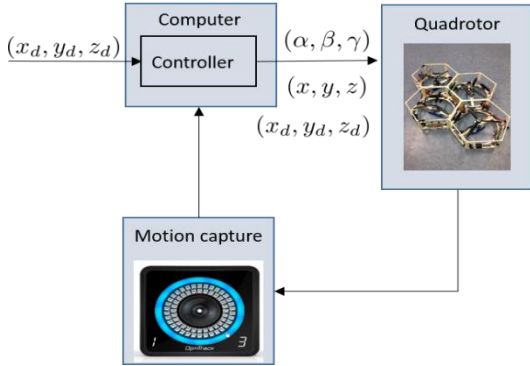


Figure 4: Experimental setup.

V. EXPERIMENTAL VALIDATION

In order to validate the effectiveness of the cascaded PID Controller, an experiment is performed. Four IR markers are fixed to the quadrotor and these markers are captured by the motion capture system. The system sends accurate position and Euler angle measurement to the computer at 100 Hz. The computer then sends the measurement wirelessly to the quadrotor through an XBee serial connection. All of the controller computation is carried out with an Arduino controller onboard the quadrotor.

With the given PID controller, the system is found to be capable of stable hovering. It is also able to takeoff from the ground and settle to hovering at a given location within a reasonable response time. While running the experiment, the controller was set to hold a constant position and yaw angle, 250mm directly above its starting ground position. *Figure 3* shows the position of the system throughout the flight with data obtained from the motion capture sensor. The system takes off and quickly climbs to the appropriate height. There is some initial overshoot in the z control, however it eventually settles to the correct level. While the settling time

and steady state error of the response could be improved, it was not deemed significant to the overall experiment and further tuning was not done. Once hovering, the x and y position show some slight oscillations about the set point, however these oscillations are never more than 100mm in amplitude, and are barely perceptible to the human

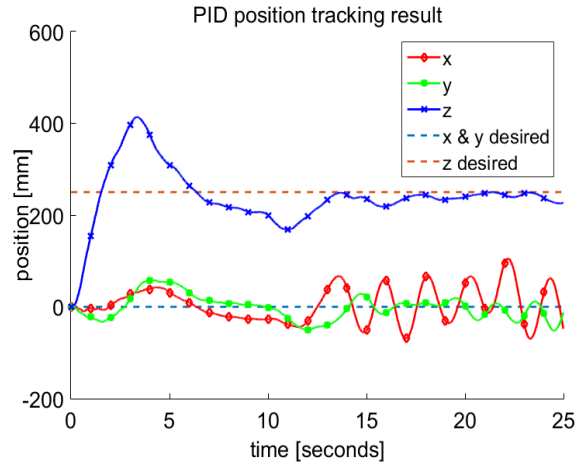


Figure 3. Position of System in Flight.

eye. Our system is not required to have pinpoint accuracy and response, so the controller was deemed an appropriate and acceptable benchmark for future experiments.

VI. CONCLUSIONS

Through this experiment it was shown that it is possible to create a simple PID controller for a nontraditional, module based quadrotor. This experiment examined the most basic test case, in which the modules were arranged much like any quadcopter would be. However, it has provided a very useful benchmark for creating new controllers that make use of additional modules or more advanced control strategies. Overall, the experiment showed that the PID controller is effective for the system to hover at a given point with little fluctuation in position.

ACKNOWLEDGMENTS

The authors would like to acknowledge Dr. Jacopo Tani (PhD) and the entire RPI Distributed Flight Array team that participated in this experiment.

REFERENCES

- [1] R. Oung and R. D'Andrea, "The Distributed Flight Array: Design, Implementation, and Analysis of a Modular Vertical Take-Off and Landing Vehicle," *The International Journal of Robotics Research*, 2013.
- [2] N. D. M. Q. L. a. V. K. Michael, "The GRASP multiple micro-UAV testbed," *Robotics & Automation Magazine*, vol. 17, no. 3, pp. 56-65, 2010.
- [3] O. a. R. D. Purwin, "Performing and extending aggressive maneuvers using iterative learning control," *Robotics and Autonomous Systems*, vol. 59, no. 1, pp. 1-11, 2011.
- [4] Z. T. M. A. E. L. Dydek, "Adaptive control of quadrotor UAVs: A design trade study with flight evaluations." Control Systems Technology," *Control Systems Technology, IEEE Transactions on* , vol. 21, no. 4, pp. 1400-1406, 2013.
- [5] A. B. T. Madani, "Backstepping Control for a Quadrotor Helicopter," in *Intelligent Robots and Systems, 2006 IEEE/RSJ International Conference on*, Beijing, 2006.
- [6] F. Kendoul, "Survey of advances in guidance, navigation, and control of unmanned rotorcraft systems," *Journal of Field Robotics*, vol. 29, no. 2, pp. 315-378, 2012.

Attitude Estimation with Inertia/ Magnetic Sensors

Yaser A. Khalil, Botao Hu, and Sandipan Mishra
Rensselaer Polytechnic Institute
Department of Mechanical, Aerospace, and Nuclear Engineering
khaliy@rpi.edu

In this paper, an estimation algorithm is designed for determining the orientation of a rigid body based on the measurements from an integrated inertial measurement sensor: a gyroscope sensor, an accelerometer and a magnetometer. An Extended Kalman Filter is used to estimate the attitude. Experimental comparison with a high accuracy motion caption system demonstrates the effectiveness of the attitude estimation method.

I. INTRODUCTION

With the proliferation of sensing capability embedded in smart devices, an accurate estimation of the attitude of a rigid body is becoming increasingly important. Attitude estimation a rigid is the estimation of the orientation or angular position of a rigid body. It can enable an intuitive interaction with such devices. This interaction, for example, can be seen when a smart phone rotates the screen after detecting changes in orientation. Attitude estimation can usually be achieved with low cost inertia measurement sensors such as a gyroscope sensor, an accelerometer sensor, and a magnetic sensor. However, these sensors usually have a biased output and they are affected by measurement noise. This paper provides an efficient estimator which accurately estimates the attitude based on the measurements of these sensors.

In state-of-the-art inertia measurement sensor packages, the gyroscopic sensor measures angular velocity and can therefore be used to obtain attitude by integration. However, the slow time varying bias in the measurement leads to unbounded drift after integration. The accelerometer can obtain drift free inclination estimates while the magnetometer can obtain drift-free heading estimates [1]. These estimates, however, are sensitive to high frequency noise in the measurement. In summary, a single sensor is incapable of obtaining accurate attitude estimation, but by fusing the measurements from these three sensors, it is possible to obtain high accuracy estimates.

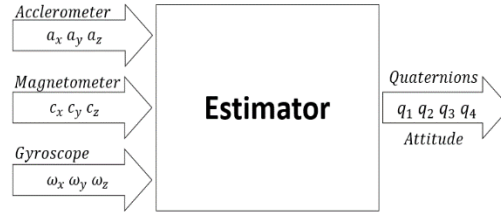


Figure 1: The proposed attitude estimator.

Sensor fusion for attitude estimation has been explored by many researchers. Some of the widely used methods are: the complementary filter [2], the Extended Kalman Filter (EKF) [1][3][4], the Unscented Kalman Filter (UKF) [5], and the Particle Filter (PF) [6]. A comprehensive survey for attitude estimation can be found in [4]. In this paper, a six-axis motion sensor that integrates a gyroscope ,an accelerometer (MPU-6050, InvenSense Inc), and a tri-axis magnetometer (HMC5883L, Honeywell Inc) are used for attitude estimation. As shown in Fig. 1, the estimator takes in measurements from the accelerometer, magnetometer and the gyroscope and outputs unit quaternions, which is a representation for rotation [7]. The estimator designed in this paper is based on the Extended Kalman Filter and it is similar to the estimator presented in [1]. The main difference is that in this study, the biases of the magnetometer and accelerometer are calibrated before sensor fusion instead of using the biases as states of the system. This helps reduce the number of state variables and decrease computational requirement.

The paper is organized as follows. Section II introduces the process and measurement model of the estimator. Section III then introduces the implementation of the Extended Kalman Filter. Finally, Section IV shows the experimental result while section V concludes the paper.

II. MODEL DESCRIPTION

In this paper, the attitude is represented by a unit quaternion vector. Compared to commonly used

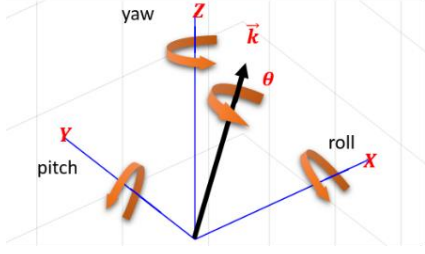


Figure 2: Euler angles and the axis angle representation.

Euler angles, the unit quaternion representation does not have singularities and is used by [1,3,4] as the representation for rotation. This section will introduce the unit quaternion representation, followed by the sensor reading model. The process model and measurement model will be described last.

The attitude estimator is built based on the following assumptions:

1. The accelerometer is only affected by the gravitational acceleration. The magnetic field around the magnetometer is time invariant.
2. The bias of the gyroscope measurement is slowly time varying or time invariant.
3. The systematic error of the accelerometer and magnetometer are carefully calibrated.

II.A. The unit quaternion representation

A rotation can be described as a result of sequential rotations. The Euler angles include the roll angle, pitch angle, and yaw angle. They are defined as the rotations about x , y , and z -axis respectively.

A rotation can also be described as a result of a single rotation of angle θ about a unit axis $\vec{k} = [k_1, k_2, k_3]$. This is called the axis angle representation. Fig. 2 shows the definition of Euler angles and the axis angle representation. The unit quaternion is then defined based on the axis angle representation. The unit quaternion vector \vec{q} has four elements q_1, q_2, q_3 , and q_4 which are defined as

$$q_1 = k_1 \sin\left(\frac{\theta}{2}\right) \quad (1)$$

$$q_2 = k_2 \sin\left(\frac{\theta}{2}\right) \quad (2)$$

$$q_3 = k_3 \sin\left(\frac{\theta}{2}\right) \quad (3)$$

$$q_4 = \cos\left(\frac{\theta}{2}\right) \quad (4)$$

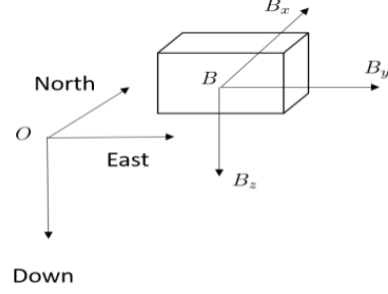


Figure 3: Coordinate axis definition.

The elements in the unit quaternion vector satisfy the constraints

$$q_1^2 + q_2^2 + q_3^2 + q_4^2 = 1 \quad (5)$$

II.B. Sensor reading model

For this experiment, the inertia frame is denoted as O frame and the direction is defined as North-East-Down (NED). The body-fixed frame is denoted as B frame with three right-handed orthonormal bases as shown in Fig 3. The gyroscope measures the angular velocities around the body axes, denoted as $\omega = [\omega_1, \omega_2, \omega_3]$. The gravitational acceleration is denoted as g . The accelerometer and the magnetometer measure the gravitational vector, and the magnetic field in the body frame respectively. By denoting the measurements in the inertia frame as $a_O = [0, 0, g]^T$ and $c_{O\boxtimes}$ the measurements in B frame can be represented as:

$$a_B = R_{BO} a_O \quad (6)$$

$$c_B = R_{BO} c_O, \quad (7)$$

R_{BO} is the representation of the rotation of the O frame with respect to the B frame. It can be presented by the unit quaternion vector [7].

$$R = \begin{bmatrix} r_{11} & r_{12} & r_{13} \\ r_{21} & r_{22} & r_{23} \\ r_{31} & r_{32} & r_{33} \end{bmatrix} \quad (8)$$

$$r_{11} = 2q_1^2 + 2q_4^2 - 1 \quad (9)$$

$$r_{12} = 2(q_1q_2 - q_3q_4) \quad (10)$$

$$r_{13} = 2(q_1q_3 + q_2q_4) \quad (11)$$

$$r_{21} = 2(q_1q_2 + q_3q_4) \quad (12)$$

$$r_{22} = 2q_2^2 + 2q_4^2 - 1 \quad (13)$$

$$r_{23} = 2(q_2q_3 - q_1q_4) \quad (14)$$

$$r_{31} = 2(q_1q_3 - q_2q_4) \quad (15)$$

$$r_{32} = 2(q_2q_3 + q_1q_4) \quad (16)$$

$$r_{33} = 2q_3^2 + 2q_4^2 - 1 \quad (17)$$

The measurements from all three sensors are ideal except the bias error in the gyroscope measurement. However, in reality, the measurements are usually affected by systematic errors and non-systematic errors. The systematic errors include the scalar error and the bias error. The calibration method for the systematic errors of the accelerometer and gyroscope can be found at [8]. In this paper, it is assumed that the systematic errors are calibrated.

II.C. Process model

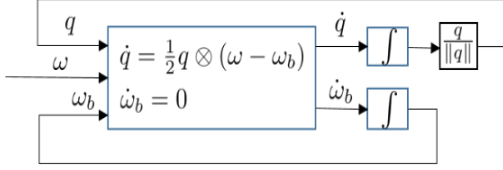


Figure 4: The process model.

For the chosen model, the elements of the unit quaternions and biases of the gyroscope sensor are used as the states of the estimator. Denote the state vector as $x = [x_1, x_2, x_3, x_4, x_5, x_6, x_7]$, where $q = [x_1, x_2, x_3, x_4]$ is the unit quaternion vector and $\omega_b = [x_5, x_6, x_7]$ is the bias vector consists of biases in the measurement of the gyroscope. The equations that govern the evolution of the unit quaternion vector and the bias vector are defined as

$$\dot{q} = \frac{1}{2} q \otimes (\omega - \omega_d) \quad (18)$$

$$\dot{\omega}_d = 0. \quad (19)$$

II.D. System measurement model

The outputs of the system are the accelerometer and the magnetometer readings in the body frame.

$$\begin{aligned} z &= \begin{bmatrix} a_B \\ c_B \end{bmatrix} = h(x, a_o, c_o) \\ &= \begin{bmatrix} R_{BO} & 0 \\ 0 & R_{BO} \end{bmatrix} \begin{bmatrix} a_O \\ c_O \end{bmatrix} \end{aligned} \quad (20)$$

The rotation matrix R_{BO} is a function of the quaternions as shown in (8). Notice that the measurements are nonlinear functions of the states.

III. IMPLEMENTATION OF THE EKF

This part is a brief introduction to the implementation of the Extended Kalman Filter. Detailed implementations can be found in [1,3,4]. The implementation of the EKF includes

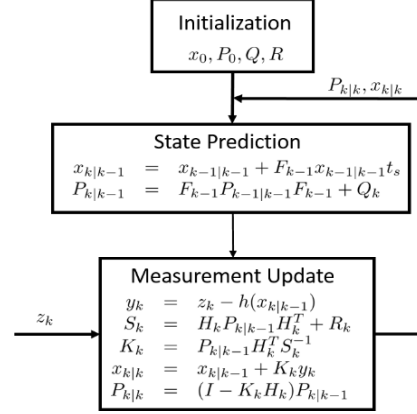


Figure 5: Implementation of the EKF.

initialization, state prediction, and measurement update as shown in Fig. 5.

III.A. Initialization

The first step for the EKF is initialization. Define the initial body frame B to be coincident with the inertia frame O , so the initial state is defined as

$$x_o = [0 \ 0 \ 0 \ 1 \ 0 \ 0 \ 0]. \quad (21)$$

The initial value for the covariance matrix P_o is defined as the identity matrix. The covariance matrix Q that describes the process model and covariance matrix R that describes the measurement error can be initialized as diagonal matrices.

III.B. State prediction

The second step is state prediction. It is governed by the equations in Fig. 5. The $x_{k-1|k-1}$ is the previous state estimate, and $x_{k|k-1}$ is the predicted state. The prediction is based on the first order linearization of the process model (18) and (19). t_s is the sampling time, F is the linearized state evolution dynamics, and Q_k is the process noise covariance matrix.

III.C. Measurement update

The third step is the measurement update. This step uses the measurement z_k with predicted states $x_{k|k-1}$ and covariance matrix $P_{k|k-1}$ to update the estimated states $x_{k|k}$ and the covariance matrix $P_{k|k}$. This step is summarized in the Fig.5, where R_k is the measurement noise covariance matrix. After the update, a new iteration can be started with the

updated state estimate and the updated covariance matrix.

IV. EXPERIMENTAL VALIDATION

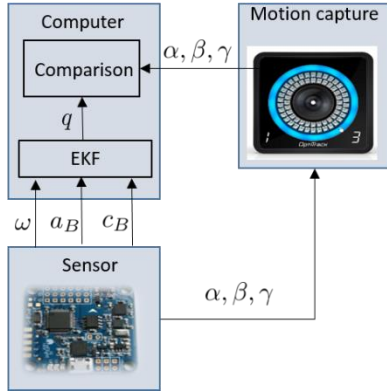


Figure 6: Experimental setup.

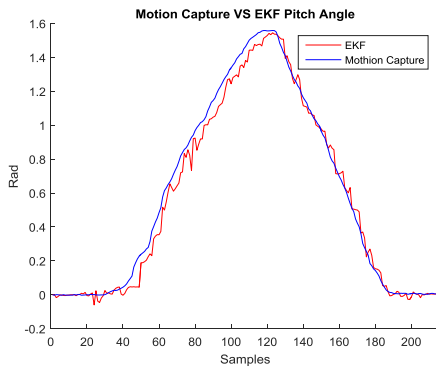


Figure 7: Pitch angle comparison.

To verify the effectiveness of the attitude estimator, an experiment comparison is implemented. The experimental setup is shown in Figure 6. The sensor is fixed to a rigid platform where markers are attached. The markers are captured by several motion capture cameras. These motion capture cameras are able to provide accurate Euler angle measurements α, β, γ to the computer at 100 Hz. The sensor measurements ω, a_B, c_B are also obtained at 100 Hz. The EKF is performed in Matlab and the estimation results q are transformed into Euler angles for comparison with the ground truth values from the motion capture system.

Simple rotations about the x, y, and z axes are performed. The roll, pitch, and yaw angles from the EKF are compared with the ground truth from the motion capture camera. The comparison results are shown in Fig. 7, 8 and 9. From all figures, it is clear that this attitude estimation scheme works well.

V. CONCLUSION

This paper presents an estimator based on the Extended Kalman Filter to estimate the attitude with

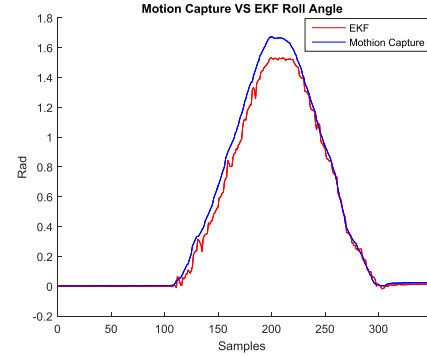


Figure 8: Roll angle comparison.

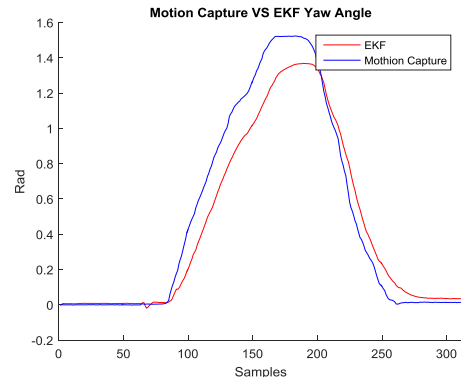


Figure 9: Yaw angle comparison.

an accelerometer, a gyroscope, and a magnetometer sensor. The experimental result shows that the attitude estimation works well. In this test, the motion of the movement is slow, and future work could focus on implementing the estimator onto a quadrotor during flight to test the performance.

ACKNOWLEDGEMENT

This project is part of the Distributed Flight Array project. The author would like to thank Prof. Mishra, Dr. Tani Jacopo and Ph.D. student Botao Hu for their help in this paper.

REFERENCES

- [1] Sabatini, Angelo Maria. "Kalman-filter-based orientation determination using inertial/magnetic

- sensors: Observability analysis and performance evaluation." *Sensors*, 11.10 (2011): 9182-9206.
- [2] Gallagher, Anthony, Yoky Matsuoka, and Wei-Tech Ang. "An efficient real-time human posture tracking algorithm using low-cost inertial and magnetic sensors." *Intelligent Robots and Systems, 2004.(IROS 2004). Proceedings. 2004 IEEE/RSJ International Conference on*. Vol. 3. IEEE, 2004.
- [3] Yun, Xiaoping, and Eric R. Bachmann. "Design, implementation, and experimental results of a quaternion-based Kalman filter for human body motion tracking." *Robotics, IEEE Transactions on*, Vol. 22.6 (2006): 1216-1227.
- [4] Sabatini, Angelo Maria. "Estimating three-dimensional orientation of human body parts by inertial/magnetic sensing." *Sensors*, Vol.11.2 (2011): 1489-1525.
- [5] Cheon, Yee-Jin, and Jong-Hwan Kim. "Unscented filtering in a unit quaternion space for spacecraft attitude estimation." *Industrial Electronics, 2007. ISIE 2007. IEEE International Symposium on*. IEEE, 2007.
- [6] Cheng, Yang, and John L. Crassidis. "Particle filtering for attitude estimation using a minimal local-error representation." *Journal of guidance, control, and dynamics*, Vol. 33.4 (2010): 1305-1310.
- [7] Trawny, Nikolas, and Stergios I. Roumeliotis. "Indirect Kalman filter for 3D attitude estimation." *University of Minnesota, Dept. of Comp. Sci. & Eng., Tech. Rep, 2* (2005): 2005.
- [8] Tedaldi, David, Alberto Pretto, and Emanuele Menegatti. "A robust and easy to implement method for IMU calibration without external equipments." *Robotics and Automation (ICRA), 2014 IEEE International Conference on*. IEEE, 2014.

Effects of Synthetic Jets on Performance Enhancement of an Airfoil Model with a Control Surface

Annika Lindstrom, Jason Roman, Marianne Monastero, and Dr. Michael Amitay
Department of Mechanical, Aerospace, and Nuclear Engineering
Rensselaer Polytechnic Institute

For a typical passenger aircraft the vertical tail is larger than required for standard flight. It is sized to provide the yaw needed to compensate for a worst case scenario of asymmetric engine failure in a heavy crosswind during takeoff. With active flow control, this yaw produced by the tail may be increased enough so that the entire vertical tail could be downsized, thus decreasing weight, drag, and fuel costs.

Previous research on scaled models has shown that the side force increased when synthetic jets were active, but the spacing between the jets was an area where further research was needed [1]. To study the effects of jet spacing, a model was designed that could be tested at various sideslip, sweep, and control surface deflection angles and with several different jet configurations.

This paper discusses the application of synthetic jet technology, the previous results obtained, the particle image velocimetry (PIV) and pressure tests performed, and the direction the research is heading.

I. INTRODUCTION

The active flow control used in this study is based on synthetic jet actuators, which are devices that add momentum to the flow using vortices that are generated near the surface with no additional mass. These jets, shown in Figure 1, are created from alternating suction and blowing from the time-periodic deformations of piezoelectric discs [1].

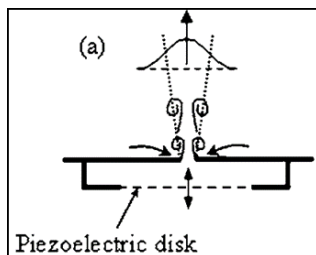


Figure 1: Diagram of Synthetic Jet [2].

Synthetic jets have a wide range of applications in the aerospace industry and beyond. They have been shown to be beneficial in controlling separation on wind turbines unmanned aerial vehicles and in inlet ducts [3,4]. By controlling the flow separation, it is possible to reduce drag on an airfoil, which ultimately reduce the fuel costs of an aircraft and increase its performance.

Previous work done by Rathay et al. found that by using synthetic jet actuators on vertical tail models, a non-dimensional side force could be increased by as much as 34% [1]. It was also found that the spacing between synthetic jets on a vertical tail model was an important parameter affecting the side force coefficient. On a smaller, 1/19th scale model, it was found that increased spacing resulted in lower side force enhancement. On a larger model, 1/9th scale model, the spacing had unexpected effects that partially agreed with the smaller model at certain side slip angles, while at others it had a reversed effect.

The focus of this study is to look more closely into jet spacing on a vertical tail model. A model based on a vertical tail geometry with multiple configurations can vary the separation severity and the spanwise flow component to study the spacing effect in these conditions. The separation severity can be changed by changing the angle of attack or the rudder deflection, whereas the spanwise flow component can be varied by changing the sweep of the model.

II. EXPERIMENTAL SETUP

In order to test the effectiveness of the synthetic jets, a new wind tunnel model was designed and fabricated. It was made using computer-aided design software and then 3D printed and fabricated out of a combination of Stereolithography plastic (SLA) and aluminum. The model, shown in Figure 2, was tested in Rensselaer Polytechnic Institute's Subsonic Wind Tunnel, with a blockage of 17.2%. The

approximate location of the jets is shown also. There is no sweep and no taper in this configuration. The model was designed to enable measurements of surface pressure around the airfoil using pressure ports that are organized in chordwise rows in seven locations along the span, with 30 pressure ports each. There are extra pressure ports on the jets themselves.

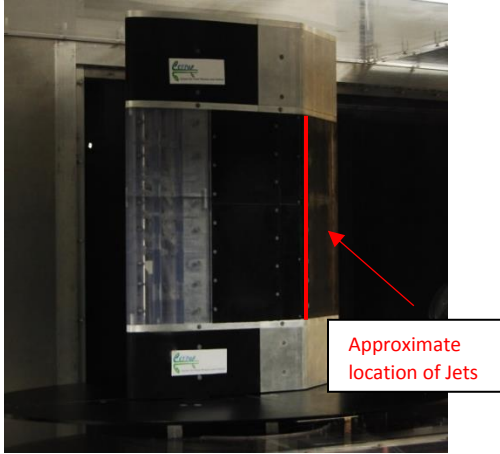


Figure 2: Model in RPI Subsonic Wind Tunnel [5].

The model had a modified NACA 0012 airfoil cross-section, a chord of 0.538 m, and a rudder chord of 33% of the total chord. Tests were run at a chord Reynolds number, $Re_c = 720,000$, with a sideslip angle of 0 and 5 degrees. The synthetic jets were placed upstream of the rudder hinge line just before the separation point where the effect of the jets would be greatest. Baseline data were acquired without the jets being actuated and then the effect of the jets was tested in different configurations, varying the spacing of the actuated jets. Particle image velocimetry (PIV) was obtained for the baseline case and pressure data was taken for each configuration.

III. RESULTS

PIV was performed on the baseline unactuated model and provided detailed information about the behavior of the flow over the suction side of the model, showing the point of separation. The results are shown in Figure 3, which depicts a portion of the rudder on the model with a side sweep angle of 5 degrees, denoted by β . Free-stream velocity, denoted by

U_∞ , is from left to right. The arrows in the figure show the velocity vectors at that point in the flow, and the scale on the right shows the streamwise velocity of the flow at that point, the warmer colors showing higher velocity positive direction flow and dark blue indicating negative flow, representing separated flow. The large area of dark blue indicates the large separation that occurs over the rudder. These results show the severity of the separation over the control surface and solidified the need for actuation because of the loss of momentum caused by this separation.

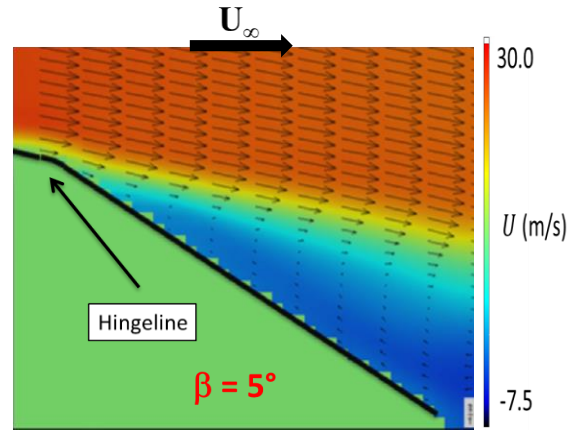


Figure 3: PIV Results on the Model [5].

The pressure data for the center spanwise row are shown in Figure 4 for both the baseline (unactuated) case, represented with black dots, and the actuated case, represented with the red triangles. Coefficient of pressure (C_p) is shown on the flipped vertical axis in the figure, and the normalized location along the chord is shown on the horizontal axis, each point corresponds to a pressure reading that was acquired through pressure ports along the model. As shown by the figure, actuating the jets yields an increase in the magnitude of C_p at certain chordwise locations, which corresponds to an increase in the integrated side force. An increase in side force due to synthetic jet actuation was shown to be as much as 17% under certain conditions, demonstrating the effectiveness of the jets.

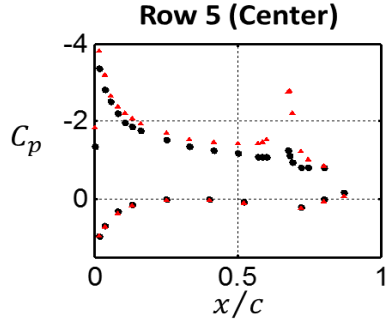


Figure 4: Pressure Data Results [5].

Once the positive effects of the jets were established, the spacing between jets was investigated more closely. Several configurations were tested, with every jet, every other, every third, every fourth, and only the center jet being actuated. Figure 5 presents the pressure distributions at the center pressure row for each of these spacings, showing the coefficient of pressure vs. normalized chordwise location. As seen in the graph, the case with all jets active has the highest suction peak, and the lowest is the baseline case with no jets active. This trend continues as an increased suction or magnitude of C_p is correlated with the decrease in spacing. These results were similar to those seen in Rathay et al. [1].

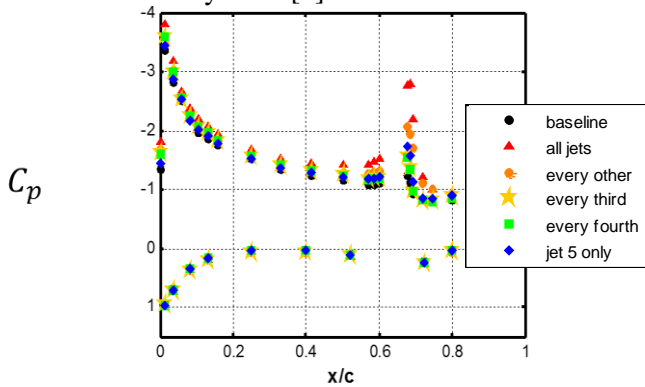


Figure 5: Pressure data with various jet configurations [5].

To look at the effects of the jets on the side force, the pressure coefficient distributions were integrated to obtain the side force coefficient. This integration was performed for each spacing case and is shown in Figure 6, which is the average side force coefficient from all of the six pressure port rows versus the number of active jets. As the number of active jets increases (as the spacing decreases), the average side force

coefficient increases. This is what would be expected to be seen since more momentum is being added to the flow. With all the jets active, an increase of side force of up to 17% was seen.

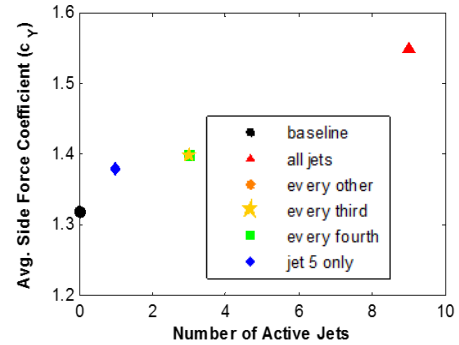


Figure 6: The variation of the side force coefficient with number of active jets [5].

IV. FUTURE WORK

The future work for this project is composed of two parts: model designing and fabrication and wind tunnel experiments.

Currently, most of the designing is focused on the control surface, with numerous configurations to be tested. The rudder will be deflected at two different angles, 20° and 30° , and the rudder length will be varied for different percentages of the chord. One current model is being designed for a control surface at 20% of the chord. It focuses on changing the control surface assembly and incorporating a support for the synthetic jets that allows them to move along the chord. Allowing for motion of the synthetic jets along the chord assists with finding the best streamwise location for the synthetic jets to be placed, which is another focus of the overall project. The control surface length will be varied in order to allow for the testing of the synthetic jets in different flows. An important aspect of the design is incorporating more SLA parts into the model to decrease the overall weight and make the project more cost efficient.

Future wind tunnel tests will be incorporating pressure measurements, stereo particle image velocimetry (SPIV), surface oil flow visualization, and tuft flow visualization to aid in understanding the effects of jet spacing on the aerodynamic performance of the model. Tests will be conducted on a model with a sweep angle of 20° , which will change the spanwise

flow over the rudder, with a control surface deflection of 20° and then the same sweep angle with a 30° control surface deflection to compare the results in separated flows with different severity levels.

V. CONCLUSIONS

Experiments were conducted to help study the effects that altering the spacing of synthetic jet actuators and the sideslip angle had on a simplified model. First, the jets were shown to be effective using pressure taps along the model, which showed an increase of up to 17% with all the jets active in side force when jets were turned on. Next, the spacing was investigated and was found to have similar results as previous studies, in that the number of active jets positively correlated with the side force enhancement.

For future study, the designs currently being worked on, namely the model with a 20° control surface deflection and a 20% chord, will eventually be used to understand the effects that varying the parameters of the control surface with respect to the chord, will have on the side force. More tests will be conducted at various sweep angles with different rudder configurations to continue to develop an understanding of the relationship between the spacing of the synthetic jets and the side force enhancement.

ACKNOWLEDGMENTS

The authors would like to thank Boeing's project manager Mr. Michael Beyar for his assistance, and The Boeing Company for their continued funding of the project.

REFERENCES

- [1] N. W. Rathay, M. J. Boucher, M. Amitay and E. Whalen, "Performance Enhancement of a Vertical Tail Using Synthetic Jet Actuators," *AIAA Journal*, vol. 52, no. 4, 2014.
- [2] M. Amitay and F. Cannelle, "Evolution of finite span synthetic jets," *Physics of*

Fluids, vol. 18, 2006.

- [3] K. Taylor and M. Amitay, "Dynamic stall process on a finite span model and its control via synthetic jet actuators," *Physics of Fluids*, vol. 27, 2015.
- [4] M. Monastero, M. Amitay and N. Rathay, "Effect of Actuator Spacing on Performance Enhancement of a Vertical Tail Model," in *1000 Island Fluids Mechanics Meeting*, 2014.
- [5] M. Monastero, A. Lindstrom M. Bayer, M. Amitay, "Parametric Study of Synthetic-Jet-Based Flow Control on a Vertical Tail Model," in *American Physical Society-Division of Fluid Dynamics*, Boston, 2015.

FINITE ELEMENT IMPLEMENTATION OF A DYNAMIC RESIDUAL-BASED LES MODEL

Nicholas Madonna, Assad Oberai
 Scientific Computation Research Center (SCOREC)
 Rensselaer Polytechnic Institute
 madonn@rpi.edu

A new dynamic model for k , the filtered fine-scale kinetic energy, is introduced in the context of the Residual-Based Variational Multiscale method (RBVMS) for Large Eddy Simulation (LES). The strong form of the equation for k is transformed into its stabilized finite element form. With this result, strides are taken toward implementing this model into PHASTA, an open source code for solving compressible and incompressible flows. Three test cases are conducted to verify the proper implementation of various components of the model. The results of these tests provide evidence to suggest that the current implementation of this new model into PHASTA is correct thus far.

I. INTRODUCTION

Turbulence is currently one of the biggest challenges in fluid mechanics. This is due to the fluctuations in pressure, velocity, and temperature associated with turbulent flow along with many other characteristics^[1]. One method for turbulence modeling is Large Eddy Simulation (LES)^[2]. In 2007, Bazilevs et al. applied the Residual-Based Variational Multi-Scale method (RBVMS) to LES^[3]. In 2016, Oberai and Hughes proposed an adaptation to the RBVMS method for LES^[4]. This proposed adaptation is the basis for this research.

II. THEORY

In the RBVMS method for LES, the flow field is divided into a coarse- and fine-scale ($\mathbf{u} = \bar{\mathbf{u}} + \mathbf{u}'$). The coarse-scale is solved for numerically, and the fine scale is approximated mathematically and inserted back into the equations for the coarse-scales. In the model by Oberai and Hughes the fine-scale flow field is approximated as

$$\mathbf{u}' = -\sqrt{2k} \frac{\mathcal{R}^m(\bar{\mathbf{U}})}{|\mathcal{R}^m(\bar{\mathbf{U}})|},$$

where k is the filtered fine-scale kinetic energy and $\mathcal{R}^m(\bar{\mathbf{U}})$ is the momentum residual of the coarse-

scales. The scalar equation for turbulent kinetic energy, k , is shown below.

$$k_{,t} + \bar{\mathbf{u}} \cdot \nabla k - C_1 |\nabla^s \bar{\mathbf{u}}|_F k - \nabla \cdot \left(\frac{\nu_T}{\sigma_k} \nabla k \right) + C_2 \frac{k^{\frac{3}{2}}}{\Delta} = |\mathcal{R}^m(\bar{\mathbf{U}})|_2. \quad (1)$$

Equation (1) is the strong form of the equation for k and it will be manipulated into a form that can be implemented into PHASTA. A number of test cases will be conducted to test its implementation.

III. EQUATION MANIPULATION

The equation must be transformed from the strong form to the weak form and discretized using the Galerkin method before being implemented in PHASTA. The finite element form of the equation for k^h (to be implemented into PHASTA) is,

$$\sum_{e=1}^{n_{el}} \left\{ \int_{\Omega^e} \left[N_a N_b \dot{k}_b + N_a [\bar{\mathbf{u}} \cdot (\nabla N_b k_B)] - C_1 N_a |\nabla^s \bar{\mathbf{u}}|_F N_b k_b + C_2 N_a \frac{(N_b k_b)^{\frac{3}{2}}}{\Delta} - N_a \sqrt{2 N_b k_b} |\mathcal{R}^m(\bar{\mathbf{U}})|_2 + \nabla N_a \cdot \left(\frac{\nu_T}{\sigma_k} \nabla N_b k_b \right) + (\bar{\mathbf{u}} \cdot \nabla N_a) \tau R(k^h) \right] d\Omega^e \right\} - \int_{\Gamma_h} N_a \left(\frac{\nu_T}{\sigma_k} \nabla N_b k_b \right) \cdot \bar{\mathbf{n}} d\Gamma_h = 0 \quad (2)$$

IV. RESULTS

After the finite element form is implemented into PHASTA, three test cases are conducted to verify that the implementation was done correctly. The idea behind these tests was to implement parts of the equation for k separately to simplify the problem. The results of these tests are shown below.

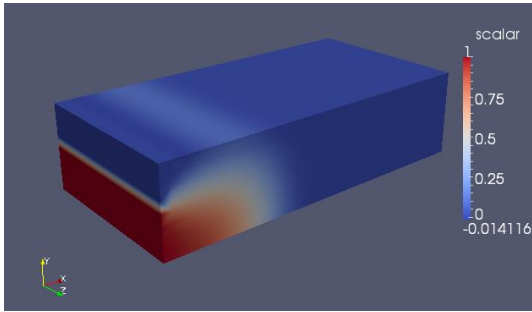


Figure 1: Results from Time Derivative, Advection, Diffusion Case after 10 Time Steps.

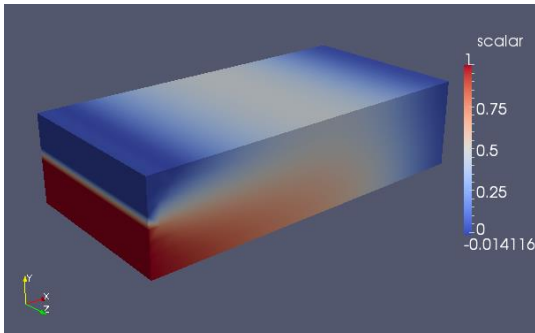


Figure 2: Results from Time Derivative, Advection, Diffusion Case after 30 Time Steps.

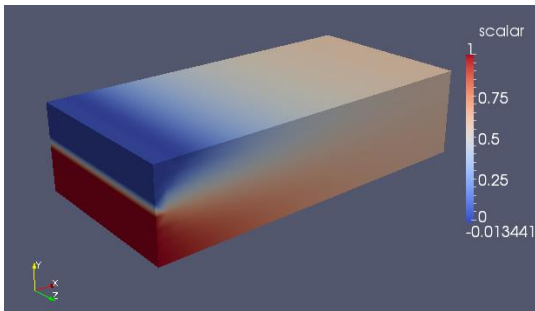


Figure 3: Results from Time Derivative, Advection, Diffusion Case after 90 Time Steps.

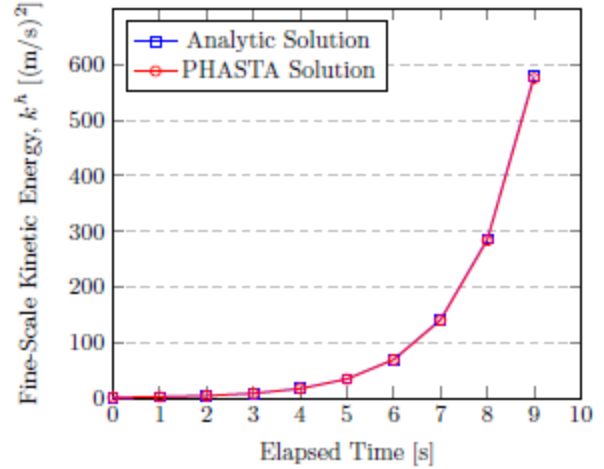


Figure 4: Plot of k^h from Analytic and PHASTA Solutions for Time, Production Case.

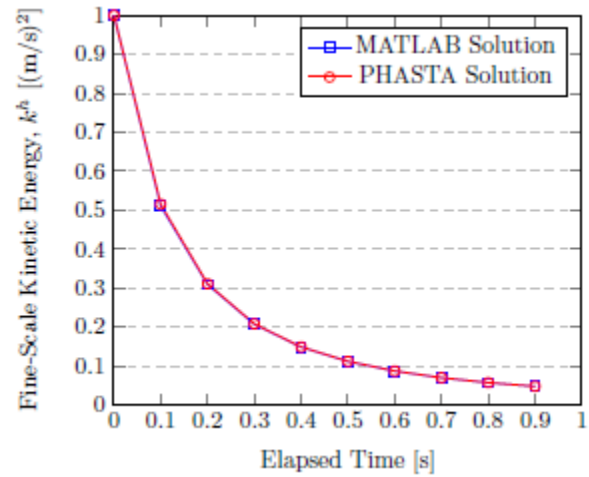


Figure 5: Plot of k^h from MATLAB and PHASTA Solutions for Time, Destruction Case.

Figures 1 through 3 are from the first test, Figure 4 from the second, and Figure 5 from the third. Figures 1 through 5 provide evidence to suggest that the finite element form of the equation for k^h has been implemented correctly. Figures 1 through 3 show results that align well with expectations. Figures 4 and 5 clearly show the agreement between the expected solution and the PHASTA solution.

V. CONCLUSIONS

A new dynamic turbulence model has been introduced for use with the RBVMS method for LES. This new model was manipulated into an appropriate form and implemented into PHASTA. Three tests were conducted to verify correct

implementation and the results of these tests do just that.

The next step for this new model is feeding it back into the coarse-scale equations so its effects can influence the flow field. With this in place, a turbulent flow simulation will be performed to shed light on the ability of this new model to accurately model turbulence.

ACKNOWLEDGMENTS

I would like to acknowledge my thesis committee, Professors Oberai, Sahni, and Shephard, for their support throughout this process and also my parents for making all of this possible.

REFERENCES

- [1] F. M. WHITE, *Viscous Fluid Flow*, New York: McGraw-Hill, 2006.
- [2] C. H. MOENG and P. P. SULLIVAN, "Large-Eddy Simulation," *Encyclopedia of Atmospheric Sciences*, vol. 4, no. 2, pp. 232-240, 2015.
- [3] Y. BAZILEVS, V. CALO, J. COTTRELL, T. HUGHES, A. REALI and G. SCOVAZZI, "Variational multiscale residual-based turbulence modeling for large eddy simulation of incompressible flows," *Computer Methods in Applied Mechanics and Engineering*, pp. 173-201, December 2007.
- [4] A. A. OBERAI and T. HUGHES, "A palette of fine-scale eddy viscosity and residual-based models for variational multiscale formulations of turbulence," *Computational Mechanics*, vol. 57, pp. 629-635, 2016.

MEASUREMENTS OF THE ^{59}Co (n, γ) CROSS SECTION USING A LEAD SLOWING-DOWN SPECTROMETER

J. Thai, N. Thompson, and Y. Danon
RPI Gaertner Linear Accelerator Center,
Rensselaer Polytechnic Institute
thaij@rpi.edu

Evaluating the neutron capture cross sections of materials commonly used in nuclear engineering is essential for design and operation of nuclear technologies. It is important to understand how a material may interact with radiation before implementing it into a system. Cobalt is a sample of particular interest because of the large differences in cross sections (an 89.61% difference) between JEFF and the other libraries at around 10 keV. A measurement of the neutron capture cross sections for cobalt would yield more accurate nuclear data. Measurements for cobalt, as well as other samples, were made using a Lead Slowing-Down Spectrometer at the Rensselaer Polytechnic Institute's Gaertner Linear Accelerator Center. YAP:Ce scintillators were used to record the capture rate of neutrons as a function of time, which could then be converted to a function of incident neutron energy. The spectra for the cobalt measurements agreed with the current evaluations, with the exception of a small range from 400 eV to 1 keV.

I. INTRODUCTION

It is necessary to experimentally validate the neutron capture cross sections (the probability of neutron capture) of commonly used materials in nuclear engineering. For example, a reactor consists of fuel, fission products, coolants, and various structural materials, whose properties must all be analyzed before operation. One project at the RPI Gaertner Linear Accelerator Center (LINAC) involves using a Lead Slowing-Down Spectrometer (LSDS) to measure neutron capture cross sections. The pulse height spectra for various samples were compared to outputs from Monte Carlo N-Particle (MCNP) simulations that modeled the experimental setup. The purpose of comparing the measurements to the MCNP calculations is to validate nuclear data libraries; for this work, we focused on ENDF/B-VII.1, JEFF-3.2, and JENDL-4.0.

II. PHYSICS OF THE LEAD-SLOWING-DOWN SPECTROMETER

When the LINAC accelerates electrons to the target in the LSDS, the high energy electrons interact with the target and part of their energy is converted into electromagnetic radiation known as Bremsstrahlung radiation¹. High energy x-rays that are emitted from this process interact with the target, supplying enough excitation energy to target nuclei to emit photoneutrons. These neutrons scatter in the lead and lose energy over time. By placing a sample and a set of scintillators in the LSDS, neutrons are captured by the sample and some of the resulting gamma ray emissions are detected. Detector signals are recorded as a function of time and it can be converted into a function of incident neutron energy. Equation 1 shows the relationship between time and the incident neutron energy used for this conversion,

$$E(\text{eV}) = \frac{165000}{(t + 0.3)^2} \quad (1)$$

where the time, t , is in microseconds. The capture rate of the neutrons by the sample as a function of neutron energy can be used to determine the neutron capture cross section of the material.

All of the samples measured are frequently used in nuclear applications. Some samples such as tantalum were selected because databases generally agreed on the cross sections of that material, and it could be used to verify the accuracy of the measurements at the LINAC.

Other samples of particular interest were selected due to differences in cross section peaks between the different databases. Consider the evaluations in Figure 1 for the neutron capture cross sections of cobalt from 5 keV to 10 keV. At 9.7 keV, there is a significant

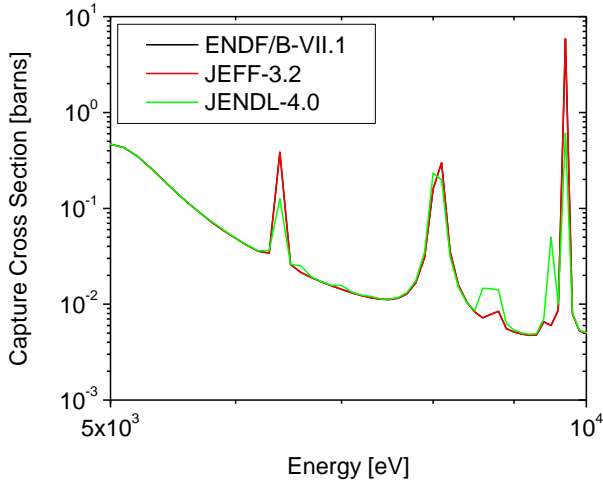


Figure 1: ENDF/B-VII.1, JEFF-3.2, and JENDL-4.0 evaluations of (n,γ) cross sections for cobalt-59 (^{59}Co) from 5 keV to 10 keV. Note, ENDF/B-VII.1 and JEFF-3.2 are identical in this region.

difference of approximately 5.25 barns (an 89.61% difference) between the JENDL-4.0 evaluation and the ENDF/B-VII.1 evaluation. Measurements for ^{59}Co using the LSDS can be used to better determine the correct cross section at 9.7 keV.

III. EXPERIMENTAL SETUP

The LSDS was configured with two different measurement ports; a sample and a detector were placed in each port. The detectors used during these measurements were Yttrium Aluminum Perovskite scintillators doped with Cerium (YAP:Ce). These detectors are high density inorganic scintillators with properties that yield a fast decay time and high light output². This makes these scintillators useful for high count rates and experiments that require precise timing. The samples placed in the LSDS were very small, with the largest sample being a 15.875 mm x 15.875 mm square that was 2 mm thick. The cobalt sample was cut into a 5/8" x 5/8" square sample that was 0.6 mm thick. An MCNP model of the LSDS is shown in Figure 2, and a detailed view of the sample and detector is shown in Figure 3.

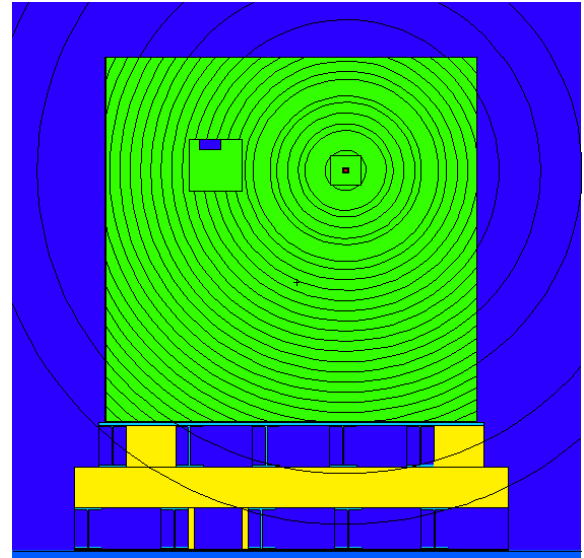


Figure 2: A diagram of the experimental setup of the LSDS.

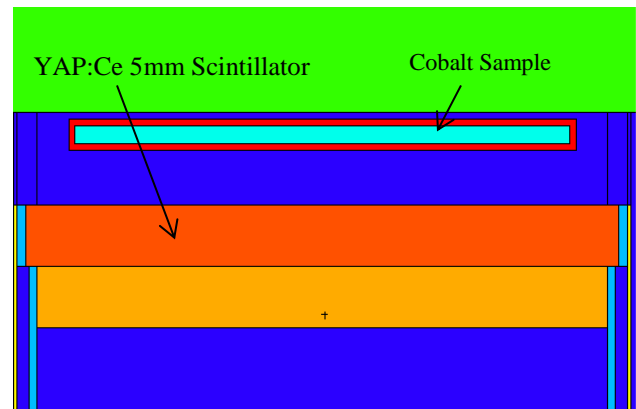


Figure 3: A detailed view of the MCNP modeled cobalt sample and detector.

In addition to the sample measurements, three background measurements were taken for each detector in their respective locations in the LSDS. For some of the samples, a ^{235}U flux monitor were placed in one port in the LSDS while a sample for neutron capture cross section measurements was placed in the other port. The data gathered from the ^{235}U flux monitor during these sets of measurements could be used to compare the different neutron fluxes of each measurement.

IV. RESULTS

IV.A. Background and Decay Correction

Three sets of measurements with no samples in the LSDS were made for the background counts, and this data was averaged to determine the background count rate of the system. The output of the detection system consisted of raw counts as a function of time, which could then be converted into a count rate as a function of incident neutron energy using Eq. 1. Figure 4 shows the background counts as a function

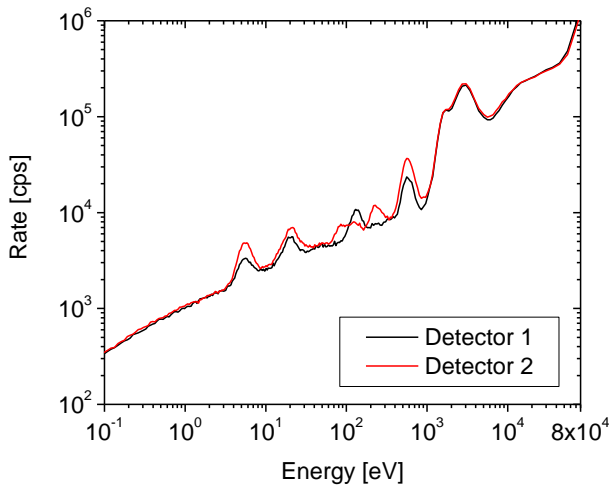


Figure 4: The background counts of detector 1 and detector 2.

of incident neutron energy for detectors 1 and 2. All of the raw sample data must be subtracted by a multiple of the background counts. The background counts may be multiplied by a scaling factor to correct for changes in neutron production from changing LINAC beam conditions. This scaling factor is computed by analyzing the data recorded by the ^{235}U flux monitor.

The detection system began recording data 2.46 μs before the measurements began. This data collected before the LINAC pulse was used to correct for radioactive decay in the sample count rate. The difference of the sums of the sample count rate and the background count rate before the LINAC pulse equals a constant that can be used for decay correction. The sample count rate must be subtracted by this count rate to correct for radioactive decay.

IV.B. Data

After the data from the cobalt measurements was decay corrected and the background was subtracted, the experimental spectrum of count rate as a function of energy was plotted against three different MCNP calculations. Each MCNP simulation contained the neutron capture cross sections of ENDF, JEFF, or JENDL, and an F4 card with an FM card was used to tally the number of particle-track lengths per unit volume in the cobalt sample³, multiplied by the capture cross section of that material. The relative errors of the tallies are presented in the MCNP output files as well, and this data was used to generate error bars for their corresponding curves.

Figure 5 shows the plot of the experimental data plotted with the simulated responses. With the exception of the counts from 400eV to 1 keV and at lower energies, the data from the LSDS agrees with the current evaluations. The most probable cause of disagreements in this region is that there may still be background effects that were not taken into consideration. Work must be done to properly propagate error for the experimental data. This requires a better understanding of the neutron flux that is being measured to determine which aspects of the LSDS and data acquisition system have uncertainties.

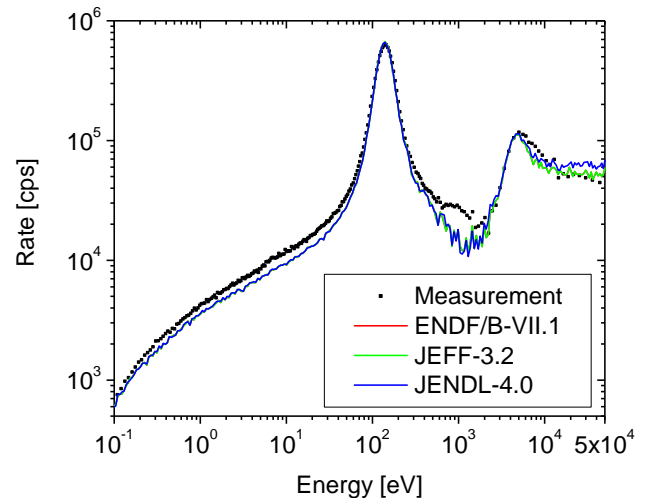


Figure 5: Experimental and simulated count rates as a function of incident neutron energy.

V. CONCLUSIONS

Measurements of the neutron capture cross sections of various samples have been made using the LSDS. The capture rate of neutrons in cobalt could be measured accurately with the LSDS, with the exception of a small range from 400eV to 1 keV. However, more work could be done to develop a pulse height weighting factor to minimize the error between the experimental data and the MCNP calculations, and improve detector response of the YAP:Ce scintillators. Additional research can be done to minimize the background effects in the system, which is a large cause of disagreement at low energies under 0.1 eV. With further data analysis, this measurement can assist in evaluating the cross sections of cobalt, which is widely used as a structural material in nuclear applications.

ACKNOWLEDGEMENTS

The authors would like to acknowledge the hard work and expertise of the LINAC technical staff. Without their knowledge in their respective fields, the research presented in this paper would not be possible.

REFERENCES

- [1] G. F. KNOLL, *Radiation Detection and Measurement*, 4th Ed., John Wiley & Sons, Inc., Hoboken, New Jersey (2010).
- [2] YAP:Ce, A Fast Inorganic Scintillation Material, 1997 Newbury (OH): Bicon.
- [3] T. Goorley, et al., "Initial MCNP6 Release Overview", *Nuclear Technology*, 180, pp 298-315 (Dec 2012).

Directional Neutron Detection with Solid State Neutron Detectors

B. Torres, A. Weltz, Y. Danon

Rensselaer Polytechnic Institute, 110 8th St., Troy, NY 12180, USA
blaketorres09@gmail.com

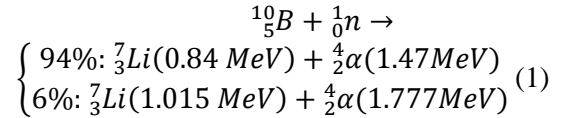
Directional neutron detectors are useful instruments for nuclear security and nuclear safeguards. These detection systems can be used to locate hidden special nuclear material (i.e. fissile uranium and plutonium) at national points of interest where materials are scanned for neutron radioactivity, such as border crossings, airports, shipyards, etc. While previous directional detection arrays have been designed with scintillating fiber neutron detectors, ³He proportional counters, and planar solid-state neutron detectors (SSNDs), this research outlines the design, construction, and testing of a modular directional neutron detector which uses high-efficiency and gamma-insensitive microstructured SSNDs developed at RPI [1, 2]. These microstructured solid-state neutron detectors were implemented into a cylindrical geometry of high density polyethylene (HDPE) as two rings of detectors with an angular spacing of 22.5 degrees in order to construct the modular directional neutron detector [3, 4].

I. INTRODUCTION & THEORY

Neutron detection is crucial in the fields of nuclear security and counterterrorism. The detection of neutron radiation is an indication of the presence of SNM, which is defined as plutonium or uranium enriched in isotopes ²³³U and ²³⁵U and is the fissile material used in nuclear weapons [5]. Once the presence of SNM has been identified, it is important to locate the source. Hand-held survey monitors can be used to search for the source, but an automated system which locates an unidentified neutron source can expedite the process. Microstructured SSNDs have been developed by multiple groups [3, 4, 5]. These solid state detectors are a promising replacement to expensive and bulky gas-filled neutron proportional counters (e.g. ³He and BF₃). These devices consist of a semiconductor substrate, i.e. silicon, which is etched in a repeated microstructure. The microscopic holes are filled with a neutron converting material, e.g. ¹⁰B, which readily absorbs thermal neutrons and produces energetic, charged particles.

The microstructured solid-state neutron detectors developed at Rensselaer Polytechnic

Institute utilize an etched honeycomb microstructure that is filled with 96% ¹⁰B. The thermal neutron absorption reaction of ¹⁰B can be seen in the equation below.



Neutron detection occurs when a neutron is incident on the boron-filled microstructure and is absorbed by ¹⁰B. The resulting charged particles can escape the neutron-converting region, reaching the semiconductor region with a fraction of their original energy. This results in the production of electron-hole pairs, which can cross the depletion region and produce a signal that can be amplified and registered as a neutron event. A picture demonstrating the hexagonal pattern of the aforementioned solid-state detectors developed at RPI can be seen in Figure 1; the diameter of the hexagonal holes is on the order of a few micrometers. These honeycomb detectors have demonstrated an intrinsic thermal neutron efficiency of ~28% with a gamma sensitivity below 10⁻⁶ corresponding to a 10 mR/hr ¹³⁷Cs source (E_γ=661.7 keV) [4]. Additionally, these devices show promise as an inexpensive neutron detector with low gamma sensitivity, zero bias requirement, and a flat and compact geometry.



Figure 1: The design of the hexagonal lattice used in RPI's solid state detectors [6].

II. MCNP SIMULATIONS

The first step in creating a directional detection system with the aforementioned SSNDs was designing the moderator geometry for the array. A cylindrical geometry was chosen due to its symmetry, and HDPE was chosen as the moderator due to its large hydrogen content and machinability. Additionally, the cylindrical construction allows for a modular design; additional detector rings can be stacked in order to improve the system sensitivity and angular resolution.

Monte Carlo n-Particle transport code (MCNP6.1) was used to find the appropriate height and radius of the cylinder, along with the optimal depth of the detection array. First, the optimal detector depth was determined. One of the microstructured detectors was simulated within the cylindrical moderator ($r=25$ cm), and the response of the detector (to an external ^{252}Cf neutron source) was simulated for incremental distances from the cylindrical surface. The external ^{252}Cf source was simulated five centimeters away from the edge of the cylinder, and ^{10}B absorption was tallied at various depths with intervals of 0.5 centimeters. The depth-dependent interaction rate was plotted (see Figure 2), and the optimal depth was found to be 3.5 cm. Next, the appropriate radius was determined by varying the radius of the cylindrical array, while keeping a constant detector depth and distance from the source. The results for this did not have a clear maximum, however it was found that a 15 cm radius provided enough moderation, achieving a detector response

>95% of that associated with an infinitely-wide cylinder. Finally, the desired height was determined by varying the height of the cylinder while keeping the other parameters constant. The cylindrical height which results in a detector response >99% of that associated with an exceedingly tall cylinder (100 cm) is 27.5 centimeters (or 5 slabs of HDPE). Thus, the optimal geometry for the detector array was determined [7].

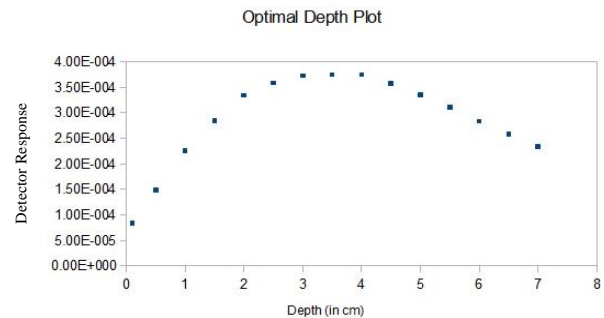


Figure 2: Detector response vs. depth of the detectors in the HDPE cylinder with a peak between 3 and 4cm.

While the part was milled, MCNP simulations were run in order to determine the relationship between the position of the ^{252}Cf source and the detection system. In the simulations, the source was kept at a constant 5 cm from the surface of the cylinder, while the angular position was changed by 5 degree intervals. One simulation with the source positioned at 22.5 degrees was performed in order to simulate the midpoint between two detectors. After these simulations were performed, the data was tabulated, and the counts in each simulation were normalized to the highest detector response. The difference between the 0° and 45° detectors in each simulation was then found and plotted with respect to the source angle (see Figure 3). As one can see from the graph, the relationship between these points is roughly linear. Knowing the relationship between the count difference and the change in angle proved to be crucial in writing a directional detection program.

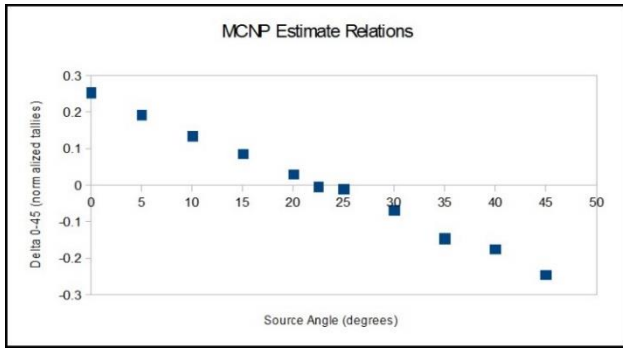


Figure 3: Difference in the largest normalized counts with respect to source angle.

III. EXPERIMENTAL PROCEDURE

The next step in creating a fully functional directional neutron detection system was to write a computer code that would output the direction of the source from detector counting data. Since this was a proof of concept, the program was written to determine the source position with a resolution of 22.5 degrees. The inputs consisted of the normalized counts for all eight detectors in the form of strings, which were then converted into integers. For the sake of simplicity, the detector variables were defined as compass positions (north, northwest, west, etc.). A series of sixteen boolean statements were then set up to define the position of the source with respect to the array. It was decided from MCNP results that if the difference in the two highest normalized counts was greater than 0.1, the source was somewhere between detectors and would be defined as such. An example of the boolean code for the source being closest to the north detector can be seen in Appendix A, along with the code for the source between the north and northeast detector.

The program would then identify the correct boolean through a series of if-then statements direction of the source in the user interface.

Experiments were performed with one of the aforementioned 4-cm² SSNDs developed at RPI. With the source set up approximately 1.15 meters from the edge of the array, the detector was inserted into one of the detector slots, and counts were measured over a period of five minutes. After the measurement was finished, the detector was re-positioned to the next angular location until all eight measurements had been taken. The entire array was then turned 22.5 degrees and this procedure was repeated.

IV. RESULTS

At the end of running this experiment, the normalized counts from detector positions at intervals of 22.5 degrees were tabulated and plotted with estimated values obtained from MCNP (see Figure 4).

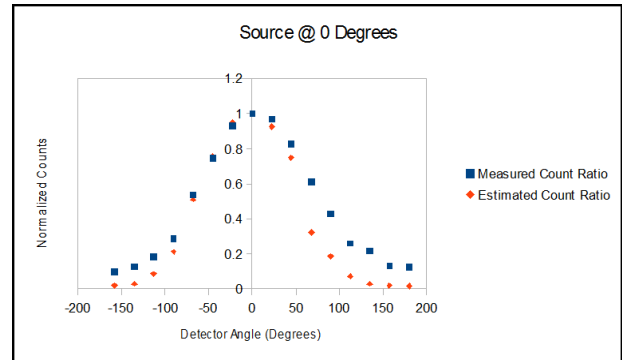


Figure 4: Normalized counts as measured and as initially calculated by MCNP.

As one can see from this graph, the MCNP simulations follow the shape of the normalized count rates measured during the experiments. However, there seems to have been some disagreement in the counts on one side of the array. This may be due to the fact that reflection of neutrons from the walls and floor were not accounted for in the MCNP code. As such, the MCNP simulations were run again with the walls and floor inputted as concrete with varying hydrogen content. Despite modifying the MCNP code for hydrogen content of 3% and 6% in the concrete, this was still not in agreement (see Figure 5). That said, the measured counts from the experiment still showed a clear peak in the counts with the front detector. As such, this can still be used for basic directional detection and is a successful proof of concept.

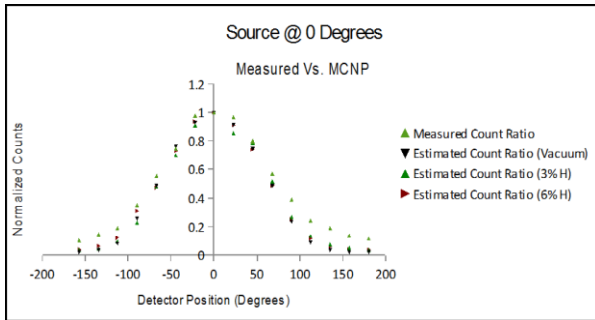


Figure 5: Normalized counts as measured and as calculated with MCNP with various hydrogen reflectors.

V. CONCLUSION

It has been shown that one can successfully use the microstructured SSNDs developed at RPI to develop a directional neutron detection array with reasonable angular resolution. This portable system can be employed in order to determine the direction of a hidden neutron source. Because of the efficiency, inexpensive and compact nature of microstructured SSNDs, this instrument can improve upon current methods of neutron directionality measurements.

REFERENCES

- [1] G.A. Wurden et al. (1995) "Scintillating-fiber 14 MeV neutron detector on TFTR during DT operation," *Review of Scientific Instruments*, Vol. 66, Issue 1.
- [2] United States Nuclear Regulatory Commission. (2015, February). Special Nuclear Material. *NRC*. Retrieved from <http://www.nrc.gov/materials/sp-nucmaterials.html>.
- [3] McGregor, D. et al. (2006) "Perforated Semiconductor Neutron Detector Modules," SMART Laboratory, Kansas State University.
- [4] Danon, Y.; Bhat I.; & Lu, J. (2013) "Development of a Self-Biased High Efficiency Solid-State Neutron Detector for MPACT Applications," *NEUP Project No. 10-852*.
- [5] Nikolic, R., Cheung C., Reinhardt, C., & Wang, T. (2006) "Future of Semiconductor Based Thermal Neutron Detectors (UCRL-PROC-219274)," Lawrence Livermore National Lab, CA, USA.
- [6] Danon, Y., Bhat I., Dingley, J., Lu, J., &

- LiCausi, N. (2008) "A Novel Solid-State Self Powered Neutron Detector," *SPIE Vol. 7079*.
- [7] Wetz, A. et al. (2015) "Development of a Modular Directional and Spectral Neutron Detection System Using Solid-State Detectors," *Nuclear Instrumentation and Methods in Physics Research, Section A*, 792, pp. 28-37.

APPENDIX A: Boolean code used for determination of the neutron source location

```
N = intN > intNE And intNE
> intE And intE > intSE
And intSE > intS And intN
> intNW And intNW > intW
And intW > intSW And intSW
> intS And (intN - intNE)
> 0.1 And (intN - intNW) >
0.1,
```

```
NxNE = intN > intNW And
intNW > intW And intW >
intSW And intNE > intE And
intE > intSE And intSE >
intS And -0.1 <= (intN -
intNE) And (intN - intNE)
<= 0.1.
```

SENSITIVITY CALIBRATION OF A REAL-TIME NEUTRON DETECTION SYSTEM USING A SILICON CARBIDE SOLID-STATE DETECTOR AND SILVER FOIL ACTIVATION

M. Wyatt, A. Weltz, R. Dahal, I. Bhat, and Y. Danon
Department of Mechanical, Aerospace, and Nuclear Engineering
Rensselaer Polytechnic Institute
wyattm@rpi.edu

The detection of pulsed neutron sources is of interest in order to characterize the neutron spectrum produced during criticality experiments and for safety applications that require characterization of accidental criticality excursions. Currently, pulsed neutron spectroscopy can be performed using a two-step process involving the activation of a foil and subsequent gamma spectroscopy and photopeak analysis. This multi-step method is time consuming and does not produce real-time data. A new method of pulsed neutron detection is introduced using a hybrid device composed of a silicon carbide (SiC) charged particle detector and a silver (Ag) activation foil. SiC detectors are solid-state, compact and robust, surviving large radiation fields and allowing for the Ag foil to be directly mounted on the device. The short half-life of the silver and subsequent energetic beta emission allow for real-time pulsed neutron detection.

I. MOTIVATION

The measurement of high-intensity neutron pulses has important applications in fields such as radiation protection, accelerator systems, and criticality excursion measurements. Traditional neutron detectors—e.g. proportional counters, solid-state devices, scintillating detectors, etc.—become saturated in a high-intensity field, losing information due to significant detector dead-time [1]. Therefore, passive neutron detectors, i.e. neutron activation foil systems, which can measure the intensity of neutron pulses, are used for such applications. Accelerator facilities use the aforementioned foil activation methods in order to track radiation doses [2]. Similarly, activation foils are used to measure pulsed sources associated with criticality excursions in order to determine their consequences [3].

However, the aforementioned passive neutron detection systems require long measurement times and do not provide any real-time data. The development of a real-time pulsed neutron detector would provide significant advantages for the aforementioned applications.

II. NEUTRON DETECTION WITH ACTIVATION FOILS

Neutron detection using activation foils is a process which begins by exposing a foil to a neutron source. As neutrons are absorbed by the foil, activation occurs. After this activation, the radioactivity of the foil can be measured using gamma spectroscopy. This activity—along with the flux-averaged cross-section of the foil and the efficiency of the gamma spectrometer—can be used to determine the intensity of the neutron field at the position of the foil. This two-step process introduces a delay between the irradiation of the foil and the subsequent gamma spectroscopy. Since no information is gathered until after the gamma spectroscopy is performed, there are no immediate, real-time data available.

Typical foils used for pulsed neutron detection include gold (Au) and dysprosium (Dy). These elements each have an isotope with a large thermal neutron absorption cross-section (^{198}Au and ^{165}Dy), which drives the sensitivity of the measurement. However, these isotopes associated with the Au and Dy foils have long half-lives (2.70 days and 2.33 hours, respectively). While an appreciable half-life is necessary due to the delay between the foil irradiation and gamma spectroscopy, a long half-life reduces the sensitivity and increases the time required to perform the measurement. This method of pulsed neutron detection is not limited to gold and dysprosium but has been demonstrated with many different activation foils [4].

III. DEVELOPMENT OF A REAL-TIME PULSED NEUTRON DETECTION SYSTEM

In order to improve upon the methods presented above, a real-time pulsed neutron detection system has been developed. This system uses a silver activation foil which is mounted directly on a SiC solid-state detector.

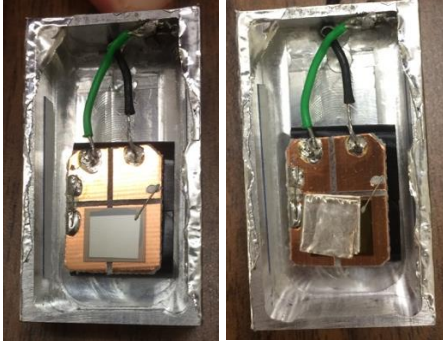
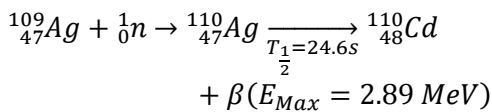


Figure 1: The SiC solid state detector with and without the silver foil mounted directly on it. Both the SiC and the Ag foil are approximately 1cm².

The development of this system is enabled by the compact nature of SiC detectors. This, along with its radiation hardness, allows for the detector and foil to be packaged together during the irradiation, eliminating the previous two-step process associated with traditional neutron activation foil methods [4]. In turn, this expands the breadth of available activation foils by allowing the use of foils with short half-lives. In particular, silver was used as the activation foil for this hybrid neutron detection system. ¹⁰⁹Ag, which accounts for 48.2% of natural Ag, has an appreciable thermal neutron absorption cross-section (87 barns at 0.0253 eV). The activation of ¹⁰⁹Ag leads to ¹¹⁰Ag, which decays via beta emission with a half-life of 24.6s. The emitted beta from ¹¹⁰Ag has a maximum energy of 2.89 MeV ($E_{Avg}=1.17$ MeV).



The use of short-lived Ag activation foils significantly improves the sensitivity and/or the measurement time associated with the

aforementioned methods because a target sensitivity can be achieved appreciably faster than with the Au and Dy foils. That is, to achieve the same sensitivity of the Au and Dy foils, it would take significantly less time. Conversely, if given the same time as the aforementioned foils, the Ag foil would reach a higher sensitivity. The shorter measurements associated with this Ag-SiC hybrid detection system—along with the ability to collect real-time data—opens the door to improved methods of pulsed neutron detection.

IV. SENSITIVITY CALIBRATION

The Ag-SiC hybrid detection system was created by mounting a silver foil directly on a 1-cm² SiC detector, and the foil and detector were mounted on the end of a rod for subsequent neutron exposure. In order to determine the sensitivity of this particular system, the device was exposed to a known neutron field. A californium (²⁵²Cf) spontaneous fission neutron source, which was housed in a block of high density polyethylene (HDPE), was used for this calibration. An exposure port provided access to the moderated neutron field. A schematic of the moderated neutron source can be seen in Figure 2.

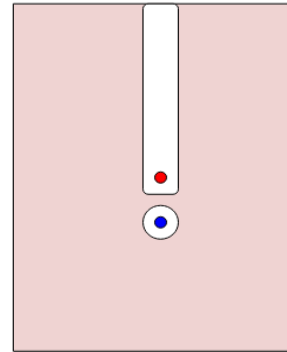


Figure 2: Front view schematic of the experimental setup. The ²⁵²Cf source (red) is housed in a block of HDPE and the detector system (blue) is inserted in the access port.

The Ag-SiC detection system was inserted to a depth of 10.75” below the HDPE surface. Previously, thermal neutron flux ($E < 0.5$ eV) at this position was determined to be 1226 ± 50 [n/cm²-s] using a gold foil analysis. The detector was operated in reverse bias with a

voltage of -7V, which improves the signal-to-noise ratio (SNR) compared to a zero bias state. A background measurement was performed in order to determine the intrinsic noise level of the device. Subsequently, the foil was irradiated in the configuration shown in Figure 2 for 100 seconds (about four half-lives) in order to approach saturation activity corresponding to the neutron flux at the aforementioned 10.75" location. Immediately after the 100 second irradiation, the source was removed and data collection was initiated. Data was collected for 100 seconds after saturation, in which time beta emission was detected by the SiC solid-state detector. Betas from ^{110}Ag escape the silver foil and impinge upon the SiC detector, depositing their residual energy to produce a distinguishable pulse in the detector. The results of this experiment can be seen in Figure 3. Some of the counts in the red background measurement are due to residual activity in the silver from previous irradiations.

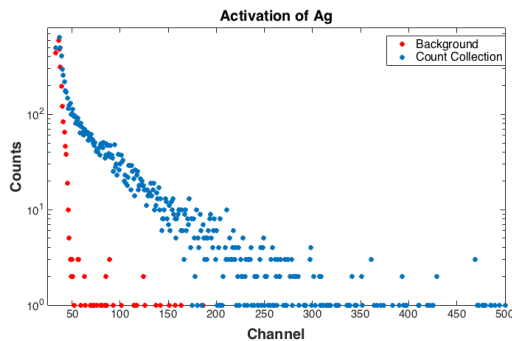


Figure 3: Background and neutron-exposed data used to demonstrate the sensitivity of the SiC-Ag detection system to thermal neutrons.

The measurement taken with the SiC-Ag pulsed neutron detector at the aforementioned 10.75" position with a previously-calibrated thermal neutron flux ($1226 \pm 50 \text{ n/cm}^2\text{-s}$) allows for the sensitivity of the detection system to be determined. Setting a lower limit of detection (LLD) above the background noise yields a count total of 3577 ± 60 neutrons, or a count rate of 35.8 ± 0.6 neutrons/second. Therefore, the sensitivity of the real-time pulsed neutron dosimeter is approximately 0.029 counts per incident thermal neutron for a constant 100 second irradiation. The sensitivity of the system can be improved by increasing the SiC detection

area and/or sandwiching detectors around a single foil.

V. CONCLUSIONS AND FUTURE WORK

A SiC-Ag hybrid pulsed neutron detector was constructed, tested, and a sensitivity measurement was performed using a moderated ^{252}Cf neutron source. Measurements demonstrate the system's ability to measure and quantify the intensity of an incident neutron pulse in real-time. Using the Ag-SiC hybrid system for detection in pulsed neutron environments will be important in moving towards applications in high intensity fields because it exceeds the limitations of the current devices. Future work will involve testing and determining the sensitivity of the Ag-SiC hybrid detector in the harsh environment associated with accelerator systems. Additionally, a pulsed neutron spectrometer will be developed using multiple Ag-SiC hybrid detectors embedded in a moderator in order to gather information about the energy spectrum of an incident pulse of neutrons.

REFERENCES

- [1] G. F. Knoll, *Radiation Detection and Measurement*, New York: John Wiley & Sons, 1999.
- [2] D. Thomas, A. Bardell and E. Macaulay, "Characterisation of a gold foil-based Bonner sphere set and measurements of neutron spectra at a medical accelerator," *Nuclear Instruments and Methods in Physics Research*, vol. 476, no. 1-2, pp. 31-35, January 2002.
- [3] T. Miller, M. Dunn, J. Wagner and K. McMahan, "2010 Criticality Accident Alarm System Benchmark Experiments At The Cea Valduc Silene Facility".
- [4] L. Serene, H. Friedlander, N. Herbert and S. Turkel, "Thermal Neutron Activation Cross Sections," *Physical Review*, vol. 72, no. 10, pp. 888-901, Nov 1947.
- [5] R. Firestone, *Table of the Isotopes Eighth Edition Volume I*, LLNL, 1996.



Rensselaer

The following section represents student design projects developed within Inventor's Studio Innovations partially funded by VentureWell.

Piezoelectric Nanowire Wind-Harvester

Orrin Amsden

Department of Mechanical, Aerospace, and Nuclear Engineering
Rensselaer Polytechnic Institute
amsdeo@rpi.edu

An alternative to current renewable energy sources is needed. Focusing on an urban environment, a device based on Zinc Oxide nanowires is designed that would allow for wind energy to be transformed into electrical energy via the piezoelectric effect. Simulations were run in order to calculate the maximum deflection of the nanowire, and it was found that the deflection grows as a power function of the aspect ratio.

I. INTRODUCTION

Global warming has been changing the climate of the entire world at an unprecedented and increasing rate for over half of the last century. Many countries are seeing record breaking temperatures that have been higher than any since the data has been recorded [1]. The rising temperature will have massive effects on many different aspects. Rising sea levels and increasing storm activity provide added challenges to the large portions of the human population that live in coastal areas. Droughts will be more intense and dry spells longer, which will destabilize many of the climates which are very important to our agriculture. Not only humans will be affected; many animals' native habitats will be damaged or changed in a potentially harmful way [2].

The cause of the increase in global warming is thought to be due to the increase in emissions called greenhouse gasses. One of the most prevalent, comprising of 76% of global greenhouse emissions in 2010, is Carbon Dioxide (CO_2). Whether the source is coal, oil, natural gas, or some other fuel, 25% of those emitted greenhouse gasses came from energy production [3].

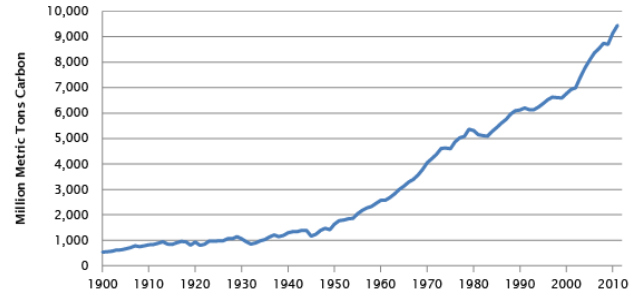


Figure 1: Global Carbon Emissions from Fossil-fuels 1900-2011 [3].

I.A. Current Solutions

Policies to curb emissions have been put into place and many countries are actively working together to help slow the rate of global warming [4]. There is an intense focus on replacing past sources of energy with new clean and renewable types. Already this trend can be seen by the increase in such technologies as wind, solar, and hydroelectric power, with around 13.4% of electricity in the United States generated via renewable sources [5].

Currently available renewable technologies are not without their drawbacks. For example, hydroelectric dams and wind turbines take up a very large volume and can be hard to integrate into urban areas. When they are in a more rural environment, they can be loud, effect the view, and still disrupt natural habitats [6]. Solar panels—while quiet and smaller in volume— can only be positioned on the tops of buildings and only work for a portion of the day, if they are located in a region of the earth that has adequate sunlight. In addition, they can be quite costly to manufacture and often use rare materials and dangerous and environmentally harmful chemicals during their fabrication [7].

I.B. Proposed Solution

Looking for a way to fill the gap of current renewable energy sources requires an innovation that is quiet, low volume, a low initial investment cost, and is relatively harmless to the environment. Given

that it will be small, so that it can fit in urban areas, technologies like geothermal and hydroelectric are most likely not as viable.

Moving away from the rotating blades of today's windmills, a solution that will not introduce any noise and have far less opportunity for failure due to moving parts, can be realized by nanoscale fabrication. Utilizing the single crystal form of the cheap and safe piezoelectric material Zinc Oxide (ZnO), which is safe enough to be a common ingredient in sunscreen, the wind can be captured and converted into electrical energy [8].

These can be fabricated quite simply, compared to many other micro- and nano- technologies, like those used in solar panels. Through a ZnO seeding step and a wet chemical growth, nanowires can be grown on a Gallium Nitride (GaN) wafer [9-10]. The product will be composed of an array of ZnO nanowires that will deform in the wind, creating an electric potential on the surface of the nanowires.

This structure can be repeated over to create panels as large as necessary. These panels can then be used anywhere that has a decent amount of wind blowing to generate energy. This has numerous applications in such places as on skyscrapers and other urban buildings, ships under constant wind on the ocean, or even as a supplement on the towers of current wind turbines to create even more electricity.

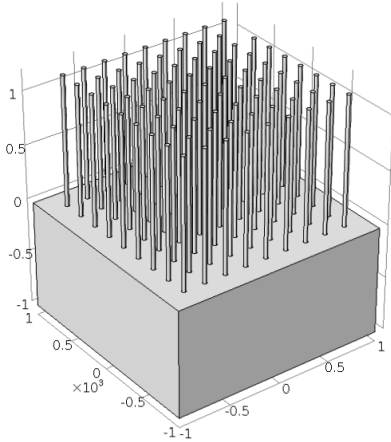


Figure 2: A CAD model of the ZnO nanowire array. The scale is in micrometers [μm].

II. PRODUCT DESCRIPTION

This product's main purpose will be to fill a niche market of electricity generation where currently there is no available method. The amount of tall buildings in cities bring about a large amount

of unused area as well as an increase in wind effects due to their height. Either stand alone or in conjunction with other modern technologies, it could help bring clean renewable energy to the world.

II.B. Mathematical Model

One of the largest and most iconic cities in the United States in New York City. With its numerous large structures it is a prime candidate for this technology. The measured values of an average of 12.2 mph (5.45 m/s) and a record of 40.7 mph (18.2 m/s) were used during the design process of this product [11].

These wind speeds are used as the two test points for the simulations of the nanowires. As can be seen in Eq. (1) and Eq. (2), which balance the mass and momentum of the wind, the flow, based on the density ρ , velocity u , the characteristic length l , dynamic viscosity μ , and temperature T , can be used to determine the force applied to the structure by the wind.

$$\rho(u \cdot \nabla)u = \nabla \cdot [-\rho l + \mu((\nabla u + (\nabla u)^T) + F) \quad (1)$$

$$\rho \nabla \cdot u = 0 \quad (2)$$

This force causes a stress and displacement on the nanowire. That in turn, based on Eqs. (3) - (8) calculates the stresses and displacement fields present in the material. This is what determines—based on the characteristics of the material—how far the nanowire has deflected.

$$-\nabla \cdot \sigma = Fv \quad (3)$$

$$\sigma = J^{-1}FSF^T \quad (4)$$

$$F = (l + -\nabla u) \quad (5)$$

$$J = \det(F) \quad (6)$$

$$s - s_0 = C: (\varepsilon - \varepsilon_0 - \varepsilon_{inel}) \quad (7)$$

$$\varepsilon = \frac{1}{2} [(\nabla u)^T + \nabla u + (\nabla u)^T \nabla u] \quad (8)$$

The stress and displacement are then turned into an electric potential via the piezoelectric effect. This charge, initially generated by the force of the wind acting on the nanowires, is then to be harvested and stored for later use.

$$-\nabla \cdot \sigma = Fv \quad (9)$$

$$\nabla \cdot D = \rho_v \quad (10)$$

III. RESULTS

In order to test the viability of this product, a simulation was run using COMSOL Multiphysics [12]. Using the included physics and material properties for Zinc Oxide, which were specified for such sub-micron range applications, a single cylindrical wire was modelled and tested on. The dimensions of the nanowires can be modified while they are being grown, with many diameters being smaller than 100nm, having possible lengths over 10 μ m and aspect ratios greater than 100 [13].

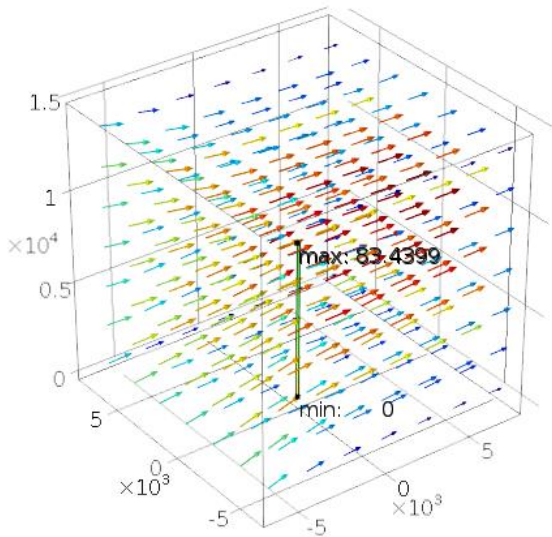


Figure 3: A nanowire simulated in a wind flow. The scale is in micrometers [μ m].

The first half of the simulation, calculation of the flow and the deflection of the wire was performed for various radii and lengths of the wire, with full results available in Appendix 1. It was seen that as the radius decreased, and the length increased, the deflection was greater.

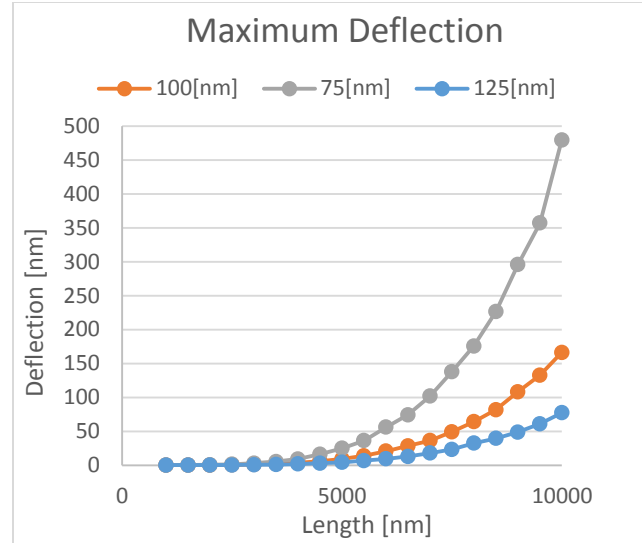


Figure 4: Maximum Deflection at the tip of the nanowire for changing lengths and radii.

The results showed that reducing the radius of the nanowire greatly increased the deflection. Furthermore, each increase in length also increased the deflection, with the longest nanowires bending the most. Generally a larger deflection at the tip of the nanowire, the more stress is imparted on the material and the higher the generated electric potential will be.

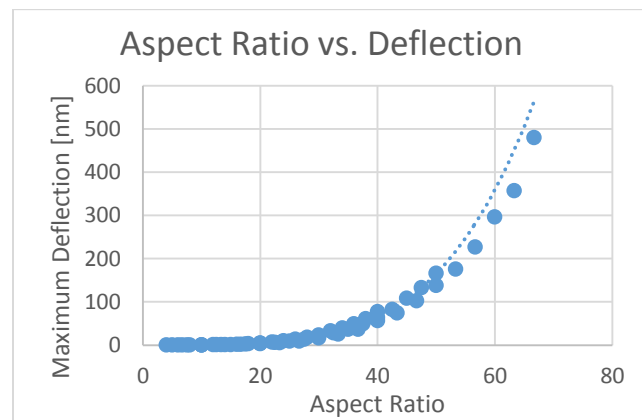


Figure 5: Aspect Ratio vs. the Maximum Deflection at the tip of the nanowire.

The aspect ratio, the length to the diameter, of the nanowires against their maximum deflection can be seen in Fig. 5. As expected the larger the aspect ratio the larger the deflection. The results followed a trend, shown by Eq. (11). This allowed for calculation of the possible deflection for a very high

aspect ratio of 100 to be $3.05\mu\text{m}$. Given that the deflection seems to be a function of the aspect ratio instead of simply just the length of the nanowire allows for larger nanowires that will not break even at the maximum recorded wind speeds.

$$y = (9 \times 10^{-6})x^{4.2649} \quad (11)$$

IV. CONCLUSIONS AND FUTURE WORK

This product will be able to bring energy production to places such as urban environments where previously there was no options. It is extremely flat and can be integrated onto the side of a building with ease. It is a very environmentally friendly material with a relatively straight forward manufacturing process given the proper equipment.

There is still a room for the simulation to be expanded on, by actually calculating the potential generated by the nanowire. Zinc Oxide also grows in a wurtzite structures, meaning that its crystals will be hexagonal in shape. Another step that can be taken to possibly increase the amount of deformation is to hollow out the nanowire via a chemical process, which could allow it to bend more. The simulation for the purpose of this paper was simplified due to the large amount of time each simulation took to run.

REFERENCES

- [1] "Global Analysis - December 2015." *National Centers for Environmental Information (NCEI) Formerly Known as National Climatic Data Center (NCDC)*. Web. 30 Mar. 2016. <<http://www.ncdc.noaa.gov/sotc/global/201512>>.
- [2] "National Climate Assessment." *National Climate Assessment*. Web. 30 Mar. 2016. <<http://nca2014.globalchange.gov/report#section-1947>>.
- [3] "Global Greenhouse Gas Emissions Data." *Global Emissions*. United States Environmental Protection Agency. Web. 30 Mar. 2016. <<https://www3.epa.gov/climatechange/ghgemissions/global.html>>.
- [4] "195 Countries Adopt the First Universal Climate Agreement." *COP21*. Web. 30 Mar. 2016. <<http://www.cop21.gouv.fr/en/195-countries-adopt-the-first-universal-climate-agreement/>>.
- [5] "Monthly Energy Review April 2016." U.S. Energy Information Administration, 26 Apr. 2016. Web. 2 May 2016. <<http://www.eia.gov/totalenergy/data/monthly/pdf/mer.pdf>>.
- [6] "Wind Energy Pros and Cons - Energy Informative." *Energy Informative*. 23 Mar. 2015. Web. 30 Mar. 2016. <<http://energyinformative.org/wind-energy-pros-and-cons/>>.
- [7] "Solar Energy Pros and Cons - Energy Informative." *Energy Informative*. 12 May 2014. Web. 30 Mar. 2016. <<http://energyinformative.org/solar-energy-pros-and-cons/>>.
- [8] "Sun Protection." *Radiation-Emitting Products*. U.S. Food and Drug Administration. Web. 30 Mar. 2016. <<http://www.fda.gov/Radiation-EmittingProducts/RadiationEmittingProductsandProcedures/Tanning/ucm116445.htm>>.
- [9] Xu, Sheng, Yaguang Wei, Melanie Kirkham, Jin Liu, Wenjie Mai, Dragomir Davidovic, Robert L. Snyder, and Zhong Lin Wang. "Patterned Growth of Vertically Aligned ZnO Nanowire Arrays on Inorganic Substrates at Low Temperature without Catalyst." *J. Am. Chem. Soc. Journal of the American Chemical Society* 130.45 (2008): 14958-4959. Web.
- [10] Chu, Dewei, Yoshitake Masuda, Tatsuki Ohji, and Kazumi Kato. "Facile Synthesis, Characterization of ZnO Nanotubes and Nanoflowers in an Aqueous Solution." *Journal of the American Ceramic Society* 93.3 (2010): 887-93. Web.
- [11] "Wind Speed at New York, New York." Web. 30 Mar. 2016. <<https://wind-speed.weatherdb.com/1/168/New-York-New-York>>.
- [12] "Design and Develop Better Products, Faster." *COMSOL Multiphysics® Modeling Software*. Web. 30 Mar. 2016.
- [13] Xu, Sheng, and Zhong Lin Wang. "One-dimensional ZnO Nanostructures: Solution Growth and Functional Properties." *Nano Res. Nano Research* 4.11 (2011): 1013-098. Web.

APPENDIX I: Flow and deflection of the wire performed for various radii and lengths of wire.

| Radius | Length | Max Deflection |
|--------|--------|----------------|
| 125 | 1000 | 0.003 |
| 125 | 1500 | 0.02 |
| 125 | 2000 | 0.069 |
| 125 | 2500 | 0.204 |
| 125 | 3000 | 0.477 |
| 125 | 3500 | 0.916 |
| 125 | 4000 | 1.672 |
| 125 | 4500 | 2.861 |
| 125 | 5000 | 4.229 |
| 125 | 5500 | 6.846 |
| 125 | 6000 | 9.274 |
| 125 | 6500 | 12.979 |
| 125 | 7000 | 17.88 |
| 125 | 7500 | 23.149 |
| 125 | 8000 | 32.499 |
| 125 | 8500 | 39.603 |
| 125 | 9000 | 48.786 |
| 125 | 9500 | 60.975 |
| 125 | 10000 | 77.198 |
| 100 | 1000 | 0.008 |
| 100 | 1500 | 0.043 |
| 100 | 2000 | 0.16 |
| 100 | 2500 | 0.453 |
| 100 | 3000 | 0.976 |
| 100 | 3500 | 1.963 |
| 100 | 4000 | 3.547 |
| 100 | 4500 | 6.076 |
| 100 | 5000 | 9.045 |
| 100 | 5500 | 13.696 |
| 100 | 6000 | 20.637 |
| 100 | 6500 | 28.414 |
| 100 | 7000 | 36.188 |
| 100 | 7500 | 49.255 |
| 100 | 8000 | 64.036 |
| 100 | 8500 | 81.862 |
| 100 | 9000 | 108.127 |
| 100 | 9500 | 132.705 |
| 100 | 10000 | 166.185 |

| Radius | Length | Max Deflection |
|--------|--------|----------------|
| 75 | 1000 | 0.019 |
| 75 | 1500 | 0.13 |
| 75 | 2000 | 0.477 |
| 75 | 2500 | 1.225 |
| 75 | 3000 | 2.993 |
| 75 | 3500 | 5.341 |
| 75 | 4000 | 9.187 |
| 75 | 4500 | 16.147 |
| 75 | 5000 | 24.908 |
| 75 | 5500 | 36.279 |
| 75 | 6000 | 55.96 |
| 75 | 6500 | 74.348 |
| 75 | 7000 | 101.907 |
| 75 | 7500 | 138.06 |
| 75 | 8000 | 175.842 |
| 75 | 8500 | 226.512 |
| 75 | 9000 | 295.875 |
| 75 | 9500 | 357.167 |
| 75 | 10000 | 479.761 |

A Deferred Action Battery for Home Backup Power

Patrick Calhoun
Rensselaer Polytechnic Institute
Department of Mechanical, Aerospace and Nuclear Engineering
Calhop2@rpi.edu

As dependency on electronic devices increases so does the age and unreliability of the electrical distribution network in the United States. The common solution to this problem is a small generator capable of supplying power to a home. This paper explores an alternative means of backup power. By harnessing chemical power only when there is a need for it, the lifetime of a battery can be extended. Specifically, by utilizing a deferred action galvanic battery, instantaneous and automatic backup power can be provided.

I. Introduction

In the United States, the average home is powered by the Electric Grid. The “Grid” is an intertwined web of transmission wires that supply various voltages to a multitude of buildings. While this network is generally reliable, there are instances where it fails.

Power failures or outages are usually limited to small regions and have short durations, ranging from a minutes to hours and sometimes days. On rare occasions, outages can be spread across large geographic areas or can last multiple weeks.

As dependency on electronic devices increases, so does the age of the Grid. External effects—other than age—also affect the reliability of power distribution. There are numerous threats to the power distribution network, including weather patterns, attacks from nefarious organizations, and solar activity to name a few.

Currently homeowners and corporations alike rely on backup generators to supply backup electrical power. There are three

methodologies for providing this power: stationary generators, portable generators, and backup batteries. The latter of the three is not widely used.

Stationary generators are widely used for industrial and large building applications where the cost of installation and fuel are outweighed by the revenue or necessity of maintaining power. These generators usually have a much larger capacity than portable generators. Stationary generators carry the additional cost of installation and are often hardwired to a manual or automatic bus transfer switch, which eliminates the need for additional wiring.

While large and small scale stationary generators are gasoline or diesel powered, current models can be powered by natural gas. Modern stationary backup generators are able to be supplied by domestic natural gas supplies that are used for cooking and heating.

Portable generators are small in size and are generally designed to be used on worksites where electrical power isn’t readily available. These generators tend to be quite robust, lightweight, and easy to move. They are usually gasoline powered, but some diesel options are available.

Portable generators are limited in capacity and can supply vital circuits in a home for as long as a fuel supply is present. These generators are not designed to be permanently installed in a circuit breaker and require a power cord to connect directly to components.

Both portable and stationary generators must be near a home or building’s ventilation supply for fresh air intake [2]. All options for these units require the combustion of some fuel type, and therefore all produce exhaust gasses that are hazardous to health when inhaled.

Both types of generator are limited by the volume of fuel in storage. Portable and stationary generators require a fuel tank which has limited capacity—the exception being stationary generators powered by a gas pipeline. In all cases, the cost of fuel and the need to refill that supply has economic drawbacks.

There is a new form of backup power being created. It requires no fossil fuel inputs and yields no hazardous byproducts. It can be kept indoors and provides instantaneous power upon loss of Grid power. Recently, there has been a new market emerging for backup power in home batteries. The batteries on the market and in development have commonalities in construction, location and function.

The batteries are rechargeable and are designed to be placed within living areas and can accept a charge from both AC and DC current. They are usually lithium ion batteries and are designed to operate on a daily basis. They are hardwired into the home and have an automatic control system. These systems are designed to activate during times of peak energy cost, minimizing the owner's electric bill. The systems automatically energize upon the loss of grid power, providing power to vital circuits.

A Deferred Action Saltwater Battery cannot provide the same capability for charge and discharge behavior that these lithium ion batteries can; however, they can provide near instantaneous backup power. The battery can be hardwired into a home and provide power to all vital circuits and some non-vital circuits based on power configurations in a structure.

By placing two dissimilar metals in an electrolytic solution, a reduction/oxidation can be initiated. When in proximity in such a solution the metals undergo galvanic corrosion. In this type of corrosion, electrons are transferred from the metal with a more negative potential to a metal with a more positive potential [3].

By connecting these dissimilar metals in an electrical circuit the difference in voltage will generate a current. Free electrons will be

transferred through the electrolytic solution from one metal to the other and then through the connecting wire, continuing cyclically. Eventually the system will drive toward equilibrium with one metal oxidizing and the other being plated.

I.A. Deferred Action Battery for Backup Power

In order for a battery to operate, three key components must be present: a positively charged electrode (anode), a negatively charged electrode (cathode), and an electrolytic solution.

If these three components are kept separate, the reduction/oxidation reaction will not take place, and galvanic corrosion will not occur in an appreciable way. Similarly, electric current will not be produced. Keeping these components separated until such time that there is a demand for power is known as deferred action.

When seeking an alternative to backup generators, a deferred action galvanic battery is preferable as it initiates current when needed and maintains charge when not in use.

A.1. Product Description

The deferred action battery for home backup power consists of four primary assemblies: the tank, battery core, terminal and controls, and the circulation unit. The tank—as shown in Figure 1—is the bottom portion of the unit. It houses the battery core and contains the electrolytic solution. The circulation unit (not shown) is attached with flanges to the ends of the tank. The terminal and controls portion is covered and sits atop the tank, as shown in Figure 1.

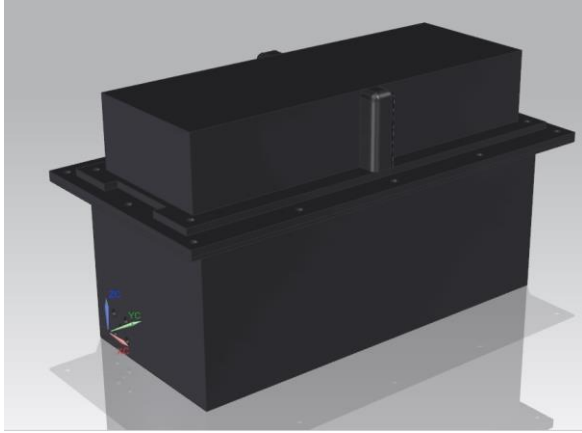


Figure 1: A Deferred Action Saltwater Battery Tank.

The control system maintains the battery core suspended above the electrolytic solution while AC power is supplied to the unit. Upon loss of power, the control unit drops the core into the electrolyte, and the power-producing chemical reaction begins.

The design intent is to have the battery be capable of providing electrical power sufficient to power an entire home for an extended period of time. Recent tests show that this type of battery can sustain two days of continuous operation at consistent voltage and current. The desired length of continuous operation is one month or greater. It is unlikely that a grid interruption will have a duration exceeding that time.

The terminal and controls system works in conjunction with an Automatic Bus Transfer switch (ABT). The ABT automatically shifts the power supply to the breaker box, by connecting the operating power supply. This allows power to be supplied nearly continuously with no operator action required. The ABT ensures that the higher voltage supply signal is online and the other is isolated which prevents backflow of electricity into the grid.

The electrolytic solution is comprised of Sodium Chloride and water. The solution used for testing was 3.5% sodium chloride with the remainder being water. During operation iron oxide entered solution as the circulation piping and inner rods experienced corrosion.

A.1. The Tank

The tank encloses the functional elements of the battery, as well as providing structural support for other components. Ideally the tank is made from an extrusion of ABS plastic and has rectangular dimensions of roughly 2'x1'x1'.

Using a plastic extrusion allows the tank to be inert with regard to the battery core. This extends the life of the core and prevents degradation of the tank.

The base of the tank holds in place two rectangular rods which are constructed of aluminum. These rods extend from the base up through the tank cover and make contact with the control system. The rods are the terminal contacts for the battery.

The rectangular shape allows for a relatively large contacting area while maintaining a slim profile. If the face of the rod were to extend significantly into the tank, the number of galvanic cells that could be housed in the battery would be affected.

The rods act as a guide for the battery cell upon ascent and descent and conduct current from the battery to the control system. The battery core is connected to the rods via a graphite brush, which provides axial support and lubrication as well as electrical connection.

A.3. Battery Core

The battery core consists of individual galvanic cells which are wired into a sub battery in the lateral direction and are then wired in parallel vertically.

The material selection for the galvanic cell is heavily influenced by the emf series of metals in flowing seawater [1]. The series gives the electrical potential difference between various metals that will react when in a saltwater solution. The electrolytic solution is not seawater, but is similar in composition.

Material consideration for the cells is a process that requires scrutiny. While the metals

with the highest electrical potential are the best option at first glance, some of these metals can be hazardous or have hazardous byproducts that are not immediately recognizable. For instance, magnesium and graphite are the best options based on electrical potential, but magnesium is explosive in moist environments, as is the next best option of zinc.

Graphite also has drawbacks. It is susceptible to degradation and scoring in a saltwater environment, however Graphene may be a usable material. Gold and platinum are the next best options, but they are limited by cost.

The materials chosen for testing in a battery to be used in a domestic application were copper and steel, and copper and aluminum. These metals are common and easily attainable for a reasonable cost.

The prototype cell that has undergone the most testing at this time consists of a copper tube with a steel rod held concentrically with the tube. The copper tube has an outside diameter of 1/4 inch and a wall thickness of 0.030 inches. The steel rod has a diameter of 1/8 inch. It is important that the rod and tube do not make contact and have enough of a clearance to allow electrolyte to flow in the channel between the metals. This is accomplished by holding the cells in an endcap. The cap is fitted with holes to align the rods and tubes of each cell and also contains the internal electrical connections. The endcaps are channeled to allow circulation of the electrolyte through the cell channels. The endcaps also provide the structure to wire appropriate rods and tubes in series to create battery groups. These batteries will produce a useful voltage and groups the batteries into a core. Wiring the cells in series will create a useful voltage, while placing those batteries in parallel will combine the electrical current.

The endcaps support a ferrous plate that is attached to the top (not shown). This plate allows for the core to lift out of solution by the terminal and controls portion of the battery. The entire assembly is shown in Figure 2.

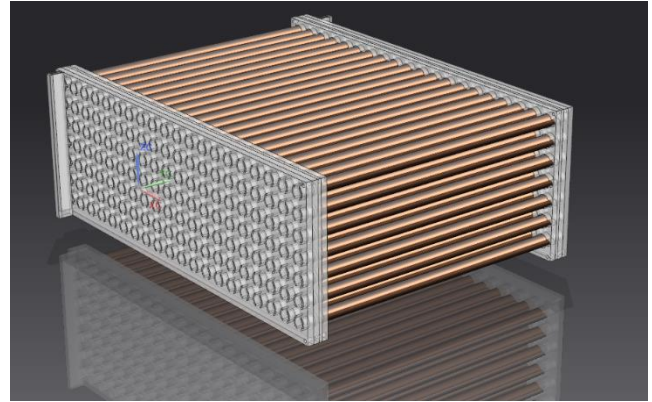


Figure 2: Entire assembly of the battery core.

A.4. Terminal and Control

The control components are contained inside the top cover, mounted on the tank lid. The outer protrusions of the lid are equipped with contacts that slide onto the terminal rods that protrude from the tank which supply an inverter. An electromagnet is mounted to the tank lid and is contained in the housing. The rectifier for the magnet is also located in the housing.

In order to energize the magnet from grid power, a rectifier is needed. The magnet is powered just upstream of the main breaker. The AC input is rectified to the DC power at an appropriate voltage for the magnet. This allows the magnet to stay energized when the main breaker of the house is open in order to allow for maintenance or other operation requiring the circuits to be dead.

When supply line power is interrupted, the magnet is de-energized, and the field instantaneously diminishes. This collapse of the magnetic field allows gravity to pull the battery core into the solution.

Once in solution, the battery begins operating, energizing the terminals. The output, however, is DC, and cannot power AC circuits. The terminals are connected to an inverter which converts the DC to AC. A portion of this current is directly fed to the recirculation pump. The rest is sent to house loads via an ABT switch.

A.5. Circulation

Upon insertion of the battery core into solution, the core enters a state of high activity. Tests with twelve cells, each acting as an individual battery (no voltage increase) produced an initial current exceeding 500 Amps. This was sustained momentarily, and the current decayed non-linearly. Within an hour, the cell was stagnant, producing no more current than baseline tests run with tap water.

When the water is circulated, however, the activity is sustained. Tests showed that the reaction can be sustained for 48 hours with a steady current output in excess of 300 Amps.

A small pump is capable of producing the circulation necessary to maintain the reaction. A 47 watt AC pump with a 3 gallon per minute capacity was used with quarter inch iron pipe. This provided adequate circulation, and has a low enough power rating to be run by the battery while still powering desired loads.

II. CONCLUSIONS

A deferred action galvanic battery can provide homeowners with a continuous power supply during grid failures. While other means are available, this methodology seems to be an environmentally friendly choice, and is safe to use within the home. The low voltage nature of the battery allows for high power densities to be achieved while maintaining relatively safe voltages for in home use.

While the battery core cannot be recharged in the home due to the creation of combustible and toxic gasses, the core can be swapped out. Much like a car battery exchange program, the cost to the user of purchasing a new cell is offset by a buy back of the old cell. These spent cells can be recharged at a facility capable to collect these gasses and use them for industrial purposes.

More research is required and is currently being conducted on material selection, electrolytic solution combinations and supplying power to large facilities.

ACKNOWLEDGMENTS

This research did not receive any specific grant from funding agencies in the public, commercial, or not-for-profit sectors

The author would like to acknowledge and thank Ashish Ghosh, Joonho Lee, Jacqueline Curtsinger, Kevin Lambert and Zachary Hileman for their contributions to research.

REFERENCES

- [1] 2016, "Galvanic Corrosion Series Chart of Metals Seawater", Corrosionist.com [Online]. Available: http://www.corrosionist.com/Galvanic_Series_of_Metal_in_Seawater.htm. [Accessed: 09- May-2016].
- [2] Occupational Safety and Health Organization, Using Portable Generators Safely.
- [3] Callister, W., 2005, Fundamentals of materials science and engineering, John Wiley & Sons, Hoboken, NJ.

Utilizing Regulations and Standards as Design Criteria in Innovative Design

Patrick Calhoun

Department of Mechanical, Aerospace and Nuclear Engineering

Calhop2@rpi.edu

The quality of potable water is highly regulated internationally. Each nation has its own standard that is based on the contaminants commonly found in the region. When designing an offshore desalination unit for the purpose of delivering drinking water to a multitude of nations, the difference in regulations became a large issue. This paper examines the process of using regulations and standards as a guideline for product design and development. A lack of understanding of regulations can lead to economical and physical losses, especially for large scale innovations. Understanding regulations and implementing them as design parameters can improve product design and lower overall cost.

I. Introduction

At the turn of the twentieth century there was a drive toward building things that were bigger and better. As the twentieth century has given way to the twenty-first, it seems that the drive is toward smaller and more efficient. There are still challenges that require large scale innovation, and as technology has decreased in size, regulation has grown in breadth and complexity.

This increase in regulation has created an opportunity for innovators. Once through the initial idea phase, the regulatory limits can become design parameters. Understanding the regulations and the basis for them, future changes can be predicted and components or features added or removed to ensure the final product remains viable.

The importance of regulation and adaptability of design became apparent in the early design of an offshore desalination plant. The function of the plant is to supply water to areas with a shortage, and to be able to respond quickly as water scarcity locations change.

The design for such a plant will be a long process and is still in early development stages. When evaluating how such a plant would maintain quality control of the water, it was clear that the

water would have to meet the applicable water standards of where it would be consumed.

It became rapidly apparent that there is no single water standard in place. Different countries have different standards, limits and required tests, as well as when those tests take place in the supply chain.

I.A. Designing for Water Standards

The United States and Canada are seemingly similar countries with strong water control programs. The standards between the two differs substantially. Canada has 39 chemical and organic substances that are monitored that the US neglects. Additionally, the United States tests for 42 substances that Canada does not [3, 4].

A.1. Understanding the regulation

In regards to monitoring disease causing bacterium, the United States only measures one bacterial contaminant that Canada does not: Legionella. The bacteria is the Cause of Legionnaires Disease, also known as Pontiac Fever. The bacteria grows in warm freshwater environments, and thus the risk of Legionella in drinking water is minimal. The country has less than 100 reported cases per year [1]. In 2009 the United States had 3,522 reported cases [2].

The divergence of standards for Canadian drinking water and US standards, are generally based on agricultural chemicals or water treatment chemicals that may have residual compounds in the water.

Understanding the reasons behind a regulation can help in the design process. If choosing a standard to use for designing an offshore desalination plant's quality assurance testing, the Canadian bacteria criteria may be the better option. Legionella is a freshwater bacteria, and therefore would not be found in seawater. A test would still have to be performed in order to sell that water in the United States, but filtering and killing that particular strain is not something that would have to be designed for.

Conversely Canada does not have a regulatory limit or required test for Mercury. The metal is most hazardous in the form of methylmercury, which is more prevalent in the ocean, especially in the aphotic regions. As the source of the water being purified is the oceans, it would be more prudent to follow the US standards and testing procedures, as well as to design the plant to eliminate the chemical.

The difference in Canadian and American water supplies illustrates how understanding a regulation can provide insight to design. Understanding and designing for a global scale is a much larger challenge, which can produce similar insights.

By comparing the standards of the United States and Canada, a baseline assumption can be made for evaluating quality controls for different countries. Regulation and testing of drinking water for microorganisms that may be hazardous to health is relatively consistent. Testing for organic and inorganic elements or chemicals is not standard and is based largely on the climate and practices of the country. In order to verify this assumption, The World Health Organization's reports "A Compendium of Drinking-Water Quality Standards in the Eastern Mediterranean Region." [5] All Nations evaluated in this report had some guideline in place for E.coli and thermotolerant bacteria in drinking water. The assumption that microorganism control is a consistent standard, especially coliform and thermotolerant bacteria.

A.2. Designing for the regulation

From the regulations above, it is clear that the treatment of water produced offshore needs to eliminate harmful bacteria, which will not be eliminated in boiling or reverse osmosis. There are many ways to filter or otherwise treat water after the desalination process to eliminate these types of bacteria. One such method that has been proven to work on seawater desalination units is chemical treatment.

The effluent water from a desalination unit is chemically treated with Bromine. The water passes through a unit that injects enough of the chemical to eliminate pathogens but in small enough concentrations that the water is potable and safe for consumption.

Bromine use has drawbacks; the chemical is a toxin. While this is beneficial because small amounts can kill microorganisms, small doses can be harmful

to humans and animals. Use of bromine requires sufficient testing to ensure that the chemical remains within safe drinking limits.

Another option is to treat the water using Ultraviolet Light (UV). At the proper wavelength, UV light will kill bacteria and viruses by altering their DNA structure. This methodology has proven useful in residential applications as well as laboratory conditions.

UV disinfection is challenging to use in a desalination plant. The water produced by desalination will have some mineral content present. The minerals in solution may produce fouling on the lighting surface or cause shadowing in solution, allowing bacteria to escape the treatment process. These effects can be mitigated by routine cleaning and 360 degree lighting of the treatment tube.

Another decontamination option for organic contaminants in an evaporative process could be the superheating of effluent steam. The steam exiting the evaporator, or boiler, is condensed into drinking water. If that steam is heated above the saturation temperature and above the temperature at which thermotolerant bacteria can survive, when the vapor is condensed it will be free of harmful pathogens.

This process is not energy efficient. A heat input to the steam is required and increased coolant flow in the condenser, or substantial expansion upstream of the condenser is required.

Of these choices, the UV light seems to be the most efficient and safe method for treatment. As it uses no chemicals, the standards for treatment chemicals are met for all regions to which water will be supplied.

In a desalination plant, whether it be reverse osmosis or evaporative, solid particulates will not be present in significant quantities. It is still prudent to monitor the final water produced for total dissolved solids and mercury, as methylmercury poses a significant threat to health if consumed orally. This test will also be able to provide feedback on plant operation.

The possibility exists with desalination that a lack of minerals will exist in the water. This should be tested for at a bottling or distribution station, as required vitamins, minerals and other electrolytes can be added to solution if concentrations are too low. The initial total dissolved solids test done at the plant can be a useful indicator for whether or not compounds must be added.

A.3. Regulation as a Process Step

When designing a new product, innovation or platform, it is easy to focus solely on performance criteria. This approach can lead to negative results. Asbestos for instance has excellent performance properties, but it is not a viable option for most applications.

The basic parameters for all designs are functionality. These parameters are usually established early in conceptualization and the proof of that concept. From a design perspective, once the functional limitations have been determined, it is easy to dive into optimization. Before optimization takes place, it is beneficial to add another parameterization process. This process is accounting for various regulations and standards that may apply.

Evaluating the appropriate government regulations and industry standards early in the design phase can minimize the time spent reevaluating a working design in order to ensure that it is up to code. In extreme cases, neglecting this step may render a working design unfeasible.

Table 1 shows the steps involved for evaluating regulations and standards as parameters for design. The inputs in the process are the regulations and codes set forth by governments, agencies and industries. These inputs are then used to establish parameters in the process step, shown in Table 2. The output of the process is drinking water that meets the standards and regulations of appropriate agencies.

| Suppliers | Inputs | Process | Outputs | Customers |
|---------------------|------------|-------------|---|---------------------------------------|
| Government Agencies | Laws/Codes | See Table 2 | Potable water that meets applicable standards | Bottled Water Consumers |
| NGOs | Guidelines | | | Regional entities with water scarcity |
| Industry Standards | Standards | | | |

| | |
|---|--|
| 1 | Determine appropriate field, industry and target consumer |
| 2 | Determine the appropriate governing agents for the market |
| 3 | Acquire and evaluate the appropriate regulations and standards |
| 4 | Set appropriate parameters based on step 5. |
| 5 | Reiterate the design for those parameters |

Understanding and incorporating regulatory parameters early in the design phase can be an advantage. This allows the design team to determine if components need to be added, removed or reconfigured to meet standards, or if a quality assurance process can ensure the final product is acceptable.

Testing for specific elemental products should be done in accordance with the locations to which the product is being sent. While particularly hazardous materials, such as mercury and lead, should be tested for always, other materials may require less stringent testing. It is unlikely that beryllium will be present in desalinated seawater, but water shipped to the US should be tested to ensure that it meets the drinking water standards of the EPA.

II. CONCLUSIONS

Regulations can pose a threat to a large scale innovation or projects. If not properly accounted for, an expensive process can become useless if it violates laws or standards.

Understanding the laws, standards and other regulations in place during the early phase in design can be useful in development. The limits set forth can be used as design parameters, as well as a resource in building a quality control program in the early stages, saving time and cost.

The use of UV lighting or heating methods eliminates the need for treatment chemical testing. EPA agents will periodically test the water produced by an offshore desalination plant. If no treatment chemicals were used, then those portions of the test will show negative.

Regulations can be a hindrance to innovation, or they can be a guide. When used properly they can be a valuable resource in developing a new product or process, especially when the scale of the design is large. Incorporating regulatory design early can result in significant cost reduction, both in design and operation.

ACKNOWLEDGMENTS

The author would like to acknowledge, and thank Ashish Ghosh for his contributions to this research.

REFERENCES

- [1] Public Health Agency of Canada, "Legionella-Infectious Diseases," 22 April 2016. [Online]. Available: <http://www.phac-aspc.gc.ca/id-mi/legionella-eng.php>.
- [2] World Health Organization, "A Compendium of Drinking-Water Quality Standards in the Eastern Mediterranean Region," 2006.
- [3] Center for Disease Control and Prevention, "Legionellosis," 19 August 2011. [Online]. Available: <http://www.cdc.gov/mmwr/preview/mmwrhtml/mm6032a3.htm>. [Accessed 24 April 2016].
- [4] Health Canada, "Guidelines for Canadian Drinking Water Quality - Summary Table," October 2014. [Online]. Available: http://www.hc-sc.gc.ca/ewh-semt/pubs/water-eau/sum_guide-res_recom/index-eng.php#t. [Accessed 24 April 2016].
- [5] U.S. EPA, "Table of Regulated Drinking Water Contaminants | Your Drinking Water," 3 May 2016. [Online]. Available: <https://www.epa.gov/your-drinking-water/table-regulated-drinking-water-contaminants>. [Accessed 24 April 2016].

Low-Cost Skeletal Tracking System for a Wearable Consumer Product

James Cazzoli

Rensselaer Polytechnic Institute

Department of Mechanical, Aerospace and Nuclear Engineering

jamescazzoli@gmail.com

Smartfit is a low-cost skeletal tracking system embedded in compression clothing which allows for fitness insights to be provided to the wearer during exercise. Smartfit system has inertial measurement units placed on various limbs of the body, which reveals the acceleration and orientation of the user's limbs. Through forward kinematic analysis, the resultant body position can be determined with acceptable certainty.

I. Introduction

The fitness space is full of different kinds of people, each with their unique motivation for going to the gym or participating in some form of exercise. A potential customer demographic is shown in Figure 1.

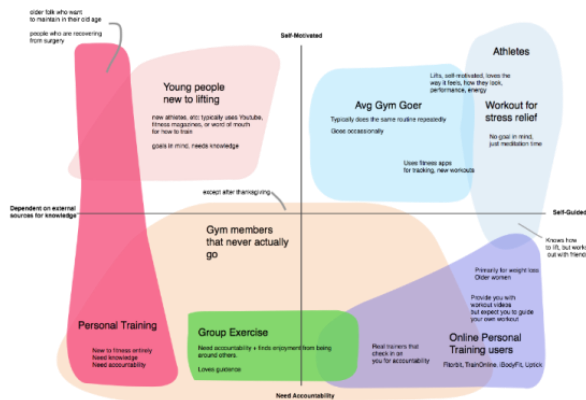


Figure 1: Potential customer demographic for the Skeletal Tracking System.

Narrowing the conversation to pertain only to individuals who go to the gym, you can sufficiently describe these people with a 2x2. The X-axis is a spectrum that describes people from those who are “dependent on external knowledge” to “self-guided”. The Y-axis describes people who are either motivated or require some form of accountability. The first quadrant describes athletes and the typical weightlifter. These people know

what they’re doing, and they get themselves in the gym each day. The second quadrant describes people who are entering into fitness for the first time. These people need to learn, but they are motivated and eager for results. The third quadrant describes a unique type of individual – the online personal trainer user. These people are self-guided but need someone to talk to, to push them to go to the gym. The fourth quadrant describes the personal training industry’s customer. They need knowledge and accountability.

SmartFit’s target audience serves a customer that is underserved today. The people who need help learning to exercise, yet are motivated to get themselves in the gym in order to lift weights. Currently, people who are new to fitness are either taught by peers, watch other people in the gym or watch youtube videos. A knowledgeable peer who can teach you is always a great source of information. However, you can never be quite sure what the quality of this information is. In fitness, there is a huge problem of misinformation, which can lead to injuries or time wasted.

Watching people in the gym, and copying them is a very dangerous way to learn how to exercise with free weights. You can easily injure yourself without having a trained pair of eyes on your posture. Additionally, you don’t know exactly what you’re working out when copying another person’s workout.

Youtube videos are great for inspiration but poor for teaching. People are able to learn how to exercise from them because of our mirror neurons, which fire the same neural pathways needed to move the skeletal muscle in a way that mirrors the kinematics of the person the observer is watching. Still, advanced lifts like deadlifts, pull ups, and squats can easily be done incorrectly. Injuries and misinformation are too common in the

fitness space. Smartfit solves these problems by leveraging exponential technology: sensors, cloud computing, and artificial intelligence.

I.A. Product Description

SmartFit is compression clothing with embedded IMUs that do skeletal tracking. Our product has a better look at the way your body is moving than a personal trainer does. It is able to tell if your body is in proper alignment during an exercise, how much endurance you may have left, and then make appropriate suggestions to improve your exercise.

This data from the IMUs are streamed from a Bluetooth low energy module to the wearer's smartphone, where the data is parsed in the cloud. The data is constantly being monitored for repetitive motions of known exercises. The quality of the exercises are then classified as good or bad form. If bad, a 3D model of the wearer's body is illustrated in app, showing them where they are going wrong, and how to correct the exercise. The user can learn how to do a workout, but attempting the motion, and letting SmartFit show them where they are going wrong. A host of tips and advice can be shared with the wearer to help them improve their exercise.

The benefits to an automated personal trainer are staggering. Now everyone can have personal trainer quality guidance for fitness. The fitness education learning curve is greatly reduced when everyone is able to have a teacher with them. This solution is massively scalable. As we acquire more users, we get more data, which allows us to further improve our algorithms. We can then do more complex training routines such as yoga, or even sports like boxing and baseball.

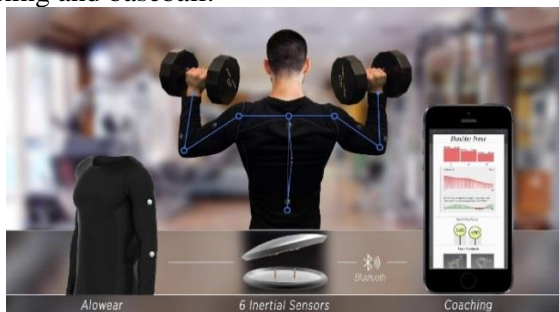


Figure 2: Product Rendering of the low-cost skeletal tracking system.

II. CONCLUSIONS

Injuries and misinformation are common in the fitness space. People who are new to exercise find it tremendously difficult to get over the learning curve required to be self-sufficient in the gym.

SmartFit is your wearable personal trainer. It is able to provide insight on your form and give intelligent feedback during your workout. SmartFit can be part of your fitness journey, from the moment you decide to start exercising, to when you become advanced. SmartFit is your coach, that can help prevent injuries and optimize your progress toward your fitness goals.

ACKNOWLEDGMENTS

The technology was developed in Google's 30 Weeks Incubator. The tools used in Inventor's Studio helped theoretically.

PERSONAL FACE WARMING DEVICE

Frank Charbonier
Rensselaer Polytechnic Institute
Department of Mechanical, Aerospace and Nuclear Engineering
charbf@rpi.edu

Severe cold weather can turn routine activities into uncomfortable, painful, and sometimes permanently scarring endeavors. Current methods for shielding the face from damaging exposure not only fail to provide complete protection, but interfere with communication and other necessary functions. The proposed solution is a personal device that provides a protective envelope of warm air to the face. This product will alleviate the major identified pain points by maintaining the user's face at a safe and comfortable temperature without leaving exposed skin, building up moisture, and inhibiting speech and consumption of food or drink.

I. INTRODUCTION

Severe cold weather is a natural phenomenon affecting millions of people across the globe. For many, this cold weather can interfere with daily activities. Specifically, exposure of the face to cold air can cause discomfort, pain, and even frostbite. Currently, one of the best methods for shielding faces from the cold is wrapping a scarf or similar garment around the neck and part of the head. This not only leaves the eyes and some patches of skin exposed (e.g. nose, ears, forehead), but it interferes with the wearer's ability to speak, breathe, and eat or drink. Scarves also tend to build up moisture from the user's breath and can fog up glasses or goggles. For certain user groups, this is a significant issue. News reporters, for example, are often found outdoors in inclement weather yet still need to be able to speak clearly into microphones and maintain a professional appearance. Construction workers on scaffolding hundreds of feet in the air need the ability to communicate without freeing up a hand to pull down their facemasks. Fans at outdoor sporting events and Arctic mountaineers alike would prefer to be able to eat and drink without removing scarves and exposing themselves to the elements. At this time,

there is no product on the market which meets these identified requirements. What is needed is a portable device that provides warmth to the entire face, without interfering with speech and eating or drinking. The proposed solution is a low-profile, neck-worn personal device which provides an envelope of warm air to surround the face.

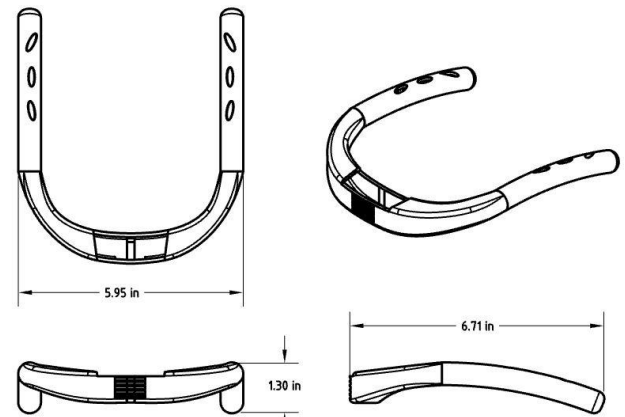


Figure 1: CAD Model with Dimensions.

II. PRODUCT DESCRIPTION

The main function of the product is to provide streams of warm air which flow over the face, thus protecting the user's skin from the harsh effects of severe cold weather without interfering with speech and eating or drinking. This is accomplished with a low profile, ergonomic design that sits around the user's neck for maximum comfort and ease of use. Within the device, air is passed over a heat source before being forced out and up onto the user's face. The temperature, speed, and direction of the air produced by the device can be adjusted to the user's preference, such that the entire face is maintained at a comfortable temperature.



Figure 2: Rendering of the Personal Face Warming Device.

III. RESULTS & DISCUSSION

This product alleviates the identified pain points by maintaining the entire face at a safe and comfortable temperature in a non-intrusive way. The product is superior to current solutions in that it does not require removal in order for the user to speak clearly, express emotions, and eat or drink. Additionally, the product alleviates the concerns associated with current solutions about protection of the eyes and any exposed skin not covered by a scarf or mask. Future generations of this product may include moisture control to alleviate issues associated with dry, cracked skin during winter months, as well as smart temperature monitoring and automatic adjustment to ensure optimal heat output given a desired comfort level and sensor readings of surrounding conditions. The product could also be adapted as a cooling device for use in warm climates.

ACKNOWLEDGEMENTS

This publication would not have been possible without the help of Dr. Asish Ghosh, who provided support and guidance throughout the entire process. Also, special thanks to Brad Matheus for his assistance with the initial prototype and to everyone who provided feedback and encouragement along the way.

APPLICATION OF BELL HOUSING FOR LED COOLING AND LIGHT DEFLECTION

Josh DeRosa
Rensselaer Polytechnic Institute
Department of Mechanical, Aerospace and Nuclear Engineering
derosatechnology@gmail.com

A unique LED mounting, cooling and reflecting configuration is described and the iterations it took to achieve the design. The future plans of the work and how it is set apart from currently issued patents is also discussed. The bell shape is aesthetically pleasing and efficient because it is used as the heat sink, reflector and structural component.

I. Introduction

Seasonal changes affect moods and productivity; especially in locations further from the equator. Those who work and play outdoors are the most affected. A typical user of the described device would be do-it-yourself, or traveling repairmen. Also, camping parties would benefit greatly from this technology.

The desire to continue the outdoor workday into the night has been a goal since the beginning of recorded history, and there are many current solutions. The solutions generally fall into one of two categories; the large and stationary, or the portable and gimmicky. The former are street lamps which provide ample light but have no portability. The latter are flashlights, often with features that seem “cool” in an infomercial, but prove unreliable in a demanding environment. Headlamps are one such device that provides portable light but they’re not typically bright and only illuminate a small area. The advantage of the described device is the unique construction which makes it rugged, powerful and portable. The light produced from this device can illuminate a large area and leave the user’s hands free. The details of the device are discussed in the next section.

II. Product Description

There are 2 aspects of this device that separate it from the rest of the solutions; the integrated heat sink & reflector, as well as the portability & configurability aspect. Figure 1 shows the device in

one configuration where the light emitting assembly is atop a pole. These poles are off the shelf and interlock with each other to achieve any desired height; even the same height as a street lamp. The interlocking nature ensures easy storage and assembly. The user could store the sections in a work truck or car easily and snap together and erect fast when needed. Another configuration is where the light emitting assembly is connected to a magnetic mount. Then this mount can be stuck to any ferrous surface, such as a car or steel pipe.

Figure 2 is a section view showing the internal structure of the device. The LED is mounted on an inside wall of the bell shaped housing. Then a diffuser is placed over the opening, for aesthetics and to protect the LED from damage. The housing functions as a heat sink and reflector; this sets it apart from other innovations. The “bell” or “trumpet” shaped housing has been used in previous devices as seen in patents US 8888319 B2 (Ref. 2) and CA 2820798 A1 (Ref. 1). The former uses the bell shape as a heat sink and not a reflector. The latter, CA 2820798 A1, uses the bell shape for aesthetics and chimney effect cooling of the LED. And US20140160737 A1 (Ref. 3) similarly uses the housing as a heat sink and not as a reflector. To date, no patents have been issued which utilizes the bell shape as a heat sink and reflector. Figure 3 shows the components with labels. The use of the integrated heat sink and reflector makes for a simpler design, and therefore more rugged and cost effective.



Figure 1: “Street Lamp” Configuration.

This innovation will enable campers and outdoor workers alike to obtain more usable hours in the day. Productivity will increase and the user will have an easier time working in their environment. The user will also be exposed to higher levels of light than before which will elevate mood and help regulate their circadian rhythm while in the winter months.

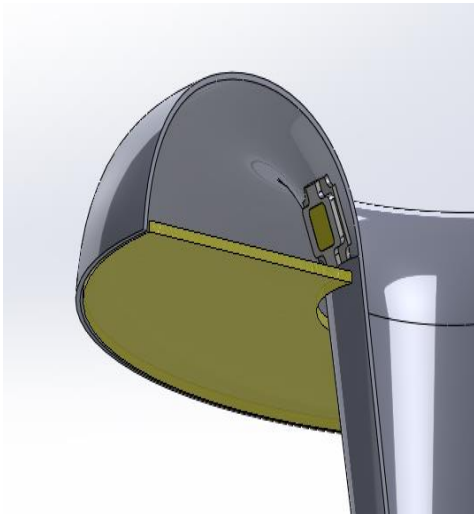


Figure 2: Cross section of the Street Lamp.

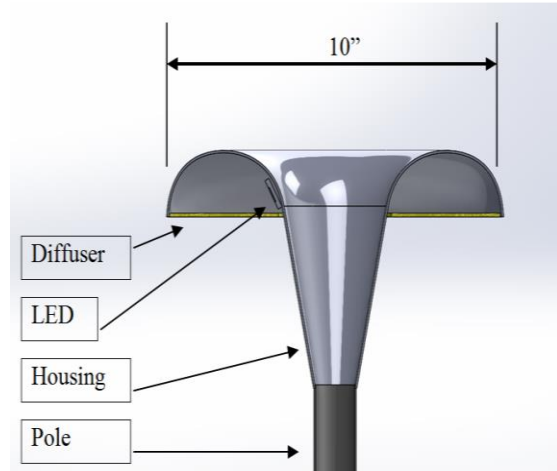


Figure 3: Labeled Components of the Street Lamp.

III. Results/discussion

A number of iterative prototypes have been made to reach the described configurations. The first prototypes were square and posed concerns for safety, aesthetics and cooling effectiveness. The device is to be user mounted high in the air and could pose a risk of falling if not mounted properly. The sharp square edges were believed to be too high of a risk of injury if it were to fall. The bell shape looks much more pleasing after talking to potential customers and the cooling can be more effective while taking advantage of the chimney effect caused in the center of the bell.

To reach the maximum number of people, the light emitting assembly containing the LED, housing and lens, can be mounted using various methods. The interlocking poles make for a portable “street lamp” type design and a magnetic mount makes it easily attached to anything magnetic. These mounting designs are excellent for rugged and changing work conditions outdoors, and in low light indoor environments. However, this design can also be applied to more refined environments. The light emitting assembly can be mounted to a typical desk lamp mount or track lighting as well, making it an aesthetic piece, and not just functional. The modular nature of the unit will even empower users to come up with their own mounting schemes. Those schemes can then be evaluated and brought into production if deemed viable.

The future plans for this innovation are to refine the interface between the LED and the heat sink. Currently the flat LED is mounting on a curved surface making poor thermal contact. It can be compensated for by using ample heat sink compound, but this is not ideal. Either a flat surface to mount on would be the next step or a custom LED with curved mounting.

IV. CONCLUSIONS

It's no secret that as a species we thrive on sunlight; it lifts our mood and enables us to be more productive. A close substitute for no actual sun is a bright enough and convenient enough light to allow the user to continue their work well into the night. The described device accomplished this goal in a beautiful and efficient form. The device is set apart from the other inventions and offers the unique combination of features for the benefit of the designer and user.

REFERENCES

- [1] Strelchuk, Joseph D. Led Heat Sink Apparatus. Anmeldung, assignee. Patent CA 2820798 A1. 6 June 2014.
- [2] Lee, Ke-Chin, and Hung-Chieh Chen. LED Projection Lamp Having a Cylindrical Heat Sink. Erteilung, assignee. Patent US 8888319 B2. 18 Nov. 2014. Print.
- [3] Strelchuk, Joseph D. Led Heat Sink Apparatus. ZUSAMMENFASSUNG, assignee. Patent US 20140160737 A1. 12 June 2014. Print.

Spoiler Alert Wasteless Refrigerator

Thomas Fajardo
Rensselaer Polytechnic Institute
Department of Mechanical, Aerospace and Nuclear Engineering
Fajart@rpi.edu

The Spoiler Alert is an app that works in conjunction with the waste less fridge and or compartments to help reduce food waste by alerting the consumer when a product is going to expire. After alerting the consumer, the app will display a variety of recipes to make using the food scanned inside the fridge along with a cost analysis based on the stored memory showing the consumer how much money has been lost due to spoiling. The purpose of this is to:

- 1) Minimize the amount of food thrown away.*
- 2) Determine if food left inside the fridge over a period of time is safe to eat.*
- 3) Make it easier to shop for necessary groceries.*
- 4) To save money.*

I. Introduction

Food waste is a problem that seems to be growing year after year. According to a report by UNEP around \$1 trillion in food production and consumption is wasted worldwide and a major portion of this waste is left in landfills negatively impacting the environment as a leading source of methane emissions [1]. Food dating also called food labeling is a major contributor to food waste and is a huge misconception [5]. Many believe that the labels are some sort of indication to determine the risk involved with eating food. “90% of Americans throw out food prematurely, and 40% of the U.S. food supply is tossed every year because of food dating” [2]. On average American family of four will throw away \$2,275 a year in food. Two-thirds of that waste is due to food spoilage which adds up to about \$1517 a year [3]. Food spoilage is not limited to the United States. All over the world people are subject to this misconception of food labeling. A research study in the U.K. led to the government revising how labels guide shoppers having “sell by” and “display until” removed from products [4]. The information is available and yet there is still little progress in coming up with a solution. Many are unaware but awareness alone will not resolve the issue. We are human with natural tendencies to avoid risk. The idea of putting oneself your loved ones in even the slightest amount on danger is not acceptable. There has to be a device that will allow for the detection of spoiled food so

that one can rest assured knowing no harm will follow.

I.A. Existing Technology


As of right now there are smart refrigerators that contain a screen embedded on the fridge door and allow for tracking on food inside using an app along with the ability to access a calendar and listen to music. There are also products such as the Nutrima food analyzer which can detect if the presence of certain toxins such as mercury and also be used as a scale or the Tell Spec which can provide a list or nutritional facts. Most chemical analysis equipment are in testing labs and require a small food sample to be tested.

Although smart refrigerators are already in the market, all of the current features satisfy wants but not any needs for the consumer. There is no current way to determine if a product inside is actually safe to eat. The price of these fridges are also expensive and although they provide useful applications the price outweighs its value. The gap in this technology is providing the user with something they need and can benefit from in the long run. The solution is a fridge or fridge compartments that can detect when food is about to spoil and alert the consumer using an app, that the food must be eaten to avoid health hazards. The app will also provide a cost analysis of how much food has been lost due to food spoilage and provide suggestions on how to reduce food spoilage by buying less and how much money would be saved in the long run.

I.B. Flysheet

Spoiler Alert Wasteless Fridge

Tired of being afraid to eat spoiled inside your fridge due to health hazards but hate letting it go to waste??



Fear No More with the Wasteless Fridge...



Who will benefit: College students, families, and anyone with a busy schedule. There are also possibilities for commercial use.

How: A fridge with compartments made to determine whether specific products inside are spoiled and will cause harm if eaten. It will also alert the owner when food is approaching a risk hazard and can give recipes and a monthly cost analysis.

I.C. Product Description

The Spoiler Alert is an app that is associated with the waste less fridge and or its separately sold refrigerator compartments. The waste less fridge is a fridge with removable compartments designed to detect when a product inside will spoil. Each compartment is specific to a food group (poultry, vegetables, dairy, etc.) and subject to a chemical and ultra violet light bacterial analysis. The app itself monitors the food inside the fridge and will alert the user when a product is about to spoil along with possible dishes one could make with that product using the food already inside the refrigerator. Every time a product is placed inside the fridge it can be

scanned in using the barcode the product came with. This will allow the Spoiler Alert app will keep track of purchasing patterns and data regarding how many times a specific product has gone bad. Each time the consumer goes to the grocery store they will be informed what is inside the fridge along with a recommended grocery list and reminder on how much money has been lost due to over purchasing and spoiling food.

This product will be the stepping stone to reducing premature food waste around the globe. Not only will it help assure the safety of food consumption, but it will cause an awareness eliminating the fear that food labels had instilled since the 1970s. Even those who have no concern for the environment and stick to their own selfish needs will think twice after the cost analysis shows the overall gain.

I.D. Design Sketches

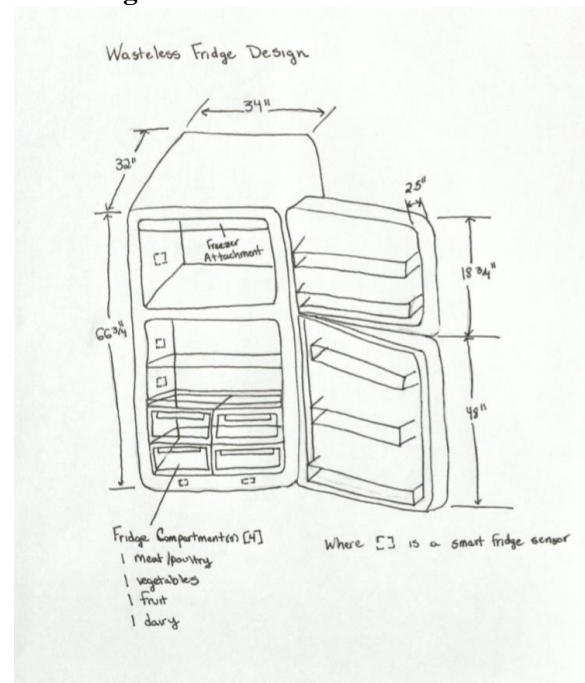


Figure 1: Wasteless Fridge Sketch with dimensions.

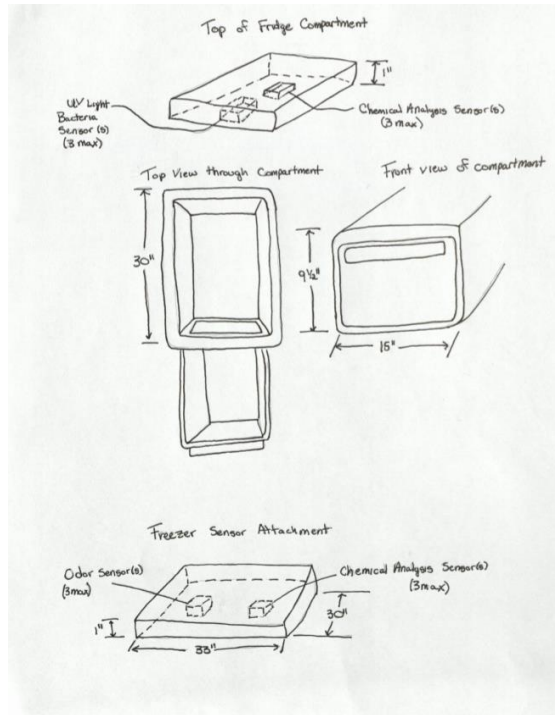


Figure 2: Individual compartment sketch with dimensions.

II. CONCLUSIONS

Based on customer interviews, the product must be reliable, efficient, easy to use, integrate able, convenient, and not too expensive. Due to the ability to purchase separate refrigerator components, the reduction of cost in the product will allow for a maximum number of people to benefit.

This product alleviates the issue of misinterpretation due to food labeling by providing the consumer with knowledge on whether or not a food product inside the fridge is safe to eat. It will allow for people to get rid of the myth that food is expired from a food label and help reduce food waste while helping save money after a cost benefit analysis.

In the future, technology should allow for a more efficient way to determine the freshness of food products which will continue to raise the quality of the product and help in lowering the overall cost of the product.

REFERENCES

[1] J. Goorley et al., "Initial MCNP6 Release Overview - MCNP6 verion 1.0 LA-UR-13-22934," 2013.

- [2] U.S. EPA, "Table of Regulated Drinking Water Contaminants | Your Drinking Water," 3 May 2016. [Online]. Available: <https://www.epa.gov/your-drinking-water/table-regulated-drinking-water-contaminants>. [Accessed 24 April 2016].
- [3] World Health Organization, "A Compendium of Drinking-Water Quality Standards in the Eastern Mediterranean Region," 2006.
- [4] U. N. E. Programme, "world food day usa," 15 October 2015. [Online]. Available: http://www.worldfooddayusa.org/food_waste_the_facts. [Accessed 15 March 2016].
- [5] E. Schwartz, "Econlife," 25 January 2016. [Online]. Available: <http://www.econlife.com/food-waste-from-dating-labels/>. [Accessed 9 March 2016].
- [6] B. Plumer, "The Washington Post," 22 August 2012. [Online]. Available: <https://www.washingtonpost.com/news/wonk/wp/2012/08/22/how-food-actually-gets-wasted-in-the-united-states/>. [Accessed 9 March 2016].
- [7] K. Benner, "Cartoon illustration of a refrigerator with an idea," [Online]. Available: http://www.123rf.com/photo_20015846_cartoon-illustration-of-a-refrigerator-with-an-idea.html. [Accessed 24 April 2016].
- [8] "Reduce your food waste," [Online]. Available: environment.utk.edu. [Accessed 24 April 2016].

APPENDIX:

Using the current existing technology today, modifications to a fridge or fridge components can be made to allow for a successful integration with food analyzing sensors.

The original concept for this product was changed twice before realizing what the main issue the product needed to solve. Customer interviews and the innovation tools learned in class such as backward imaging, 100 questions, 5/7/n Why, QFD, and FMEA were most helpful in creating an end product.

Pressure Washing in the 21st Century

David Haggerty
Rensselaer Polytechnic Institute
hagged@rpi.edu

Since the advent of the pressure washer in 1927 the design of pressure washing wands has been largely unchanged: a handle, a barrel, and an attachment point for water input. With rigid structuring and poor weight distribution, career pressure washers repeatedly encounter issues of wrist fatigue and pain, reducing their efficacy as employees. Design principles such as user centricity and design methods such as FMEA, SOTA, and Stakeholder Analysis were employed to innovate current technologies along this thread. The problem definition, design method, and value proposition generate and support the aim to redesign the pressure washer wand to be the first low-torque apparatus to date with simple additions such as a wrist guard and recoil spring.

I. Introduction

Commercial pressure washing is a prevalent industry in America. With nearly 63,000 car wash companies nationwide and innumerable business parks needing periodic maintenance, the pressure washer wand market is vast in all respects. The largest pitfall of the industry as a whole is their continuation down the path of tradition in their wand designs. For most, their center of mass falls from 3-5 inches in front of the user's hand, and their rigid structure transmits heavy torque to the user's hand upon activation. Couple that fact with the positioning of the water input directly below the hand, there is much stress applied directly to the user's wrist. In addition, the location of the water input line generates further problems of usability, being that maneuvering the hose is a constant task of the user's free hand, rendering some models free hand grip useless and ineffective.

While investigating this problem, a number of career pressure washers were interviewed at a local car wash. The results were strikingly similar. The general disposition: their handles are uncomfortable, too much forward weight, too much torque on the wrist leading to heavy fatigue, and poor location of the hose attachment site. Immediately new approaches to redesigning this

product to ameliorate the pain points expressed became apparent, and an alpha concept was generated.

I.A. Application of Design Strategies

Pressure washer wands have been designed following a static path for the 89 years they have been in existence. This primary design approach has led to distaste amongst the users of these artifacts, and there is space in this market to significantly alter both design understanding as well as quality of life for those individuals who make a living as a career pressure washer.

Explicitly, then, the problem as defined for purposes of this venture are as follows. Current pressure washer designs have been designed according to traditional principles which have not altered to best serve the needs of their customers. The result is that full time pressure washing professionals regularly experience wrist and arm fatigue that could potentially lead to chronic issues. Further, this fatigue coupled with the need to consistently adjust the location of the inflow hose with the user's free hand reduces the efficiency of the employee and affects the overall success of the business that employ them.

Thus, the mission is to generate a more effective pressure washer wand that reduces fatigue and improves quality of life of the users, as well as positively impacts the other stakeholders involved achieved by creating a low torque apparatus, that incorporates and leverages user-centered design principles.

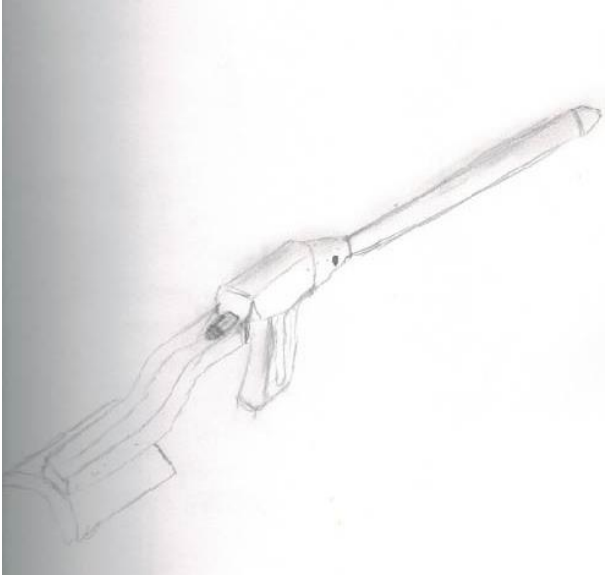


Figure 1: Rough ideation sketch of the pressure washer.

1.A.1. Design Principles

The design process in this space began with problem identification. Once the problem was identified and stated in broad terms, ethnographic data were collected from a number of sources. Primarily those sources were career pressure washers employed by Hoffman Car Wash on Hoosick Street in Troy, New York. Frequently, the Hoffman Car Wash has lines of 10-20 cars, two pressure washers working constantly, navigating around cars and other obstacles, moving their hoses everywhere with them with their free hand, and attacking every exposed inch of the vehicles they serve with their trade tool. Both interviewees complained of the weight of the device, as well as the location of the hose bib. These frustrations can be exponentiated under the immense stress this fast paced work environment can produce, as well as the fatigue generated by controlling their pressure washers. One individual interviewed commented that he can wash anywhere from 600-800 cars in a day, and by the end of his shift his right arm (washing arm) can be essentially useless due to the fatigue and pain onset by such strenuous work. Thus, the information ascertained from these individuals corroborated the initial problem identification, and lent to its validity.

At this point, market exploration began as well as a State of the Art analysis (SOTA). The results of the SOTA analysis made it readily apparent that the

design of pressure washers has remained largely unchanged in the past 60 years they have been commercially available. Both Big Box retailer Home Depot and various online retailers were surveyed and the results of this exploration were unsurprising, constancy. Of specific interest was the efforts made to reduce the torque applied to the wrist by adding a handle near the tip of the barrel for a second hand to assist. While this design idea has potential, interviews with professionals leads one to believe that appointment remains largely idle in the industry. Further, this addition absent of consult with end users seems to be more detrimental to the experience these users face by adding more weight at distance from the wrist.

As the last stage of problem exploration, a brief stakeholder analysis was conducted by conceiving the impacts of creating the product in mind. Obviously enough and at the most basic of levels exist the end users, who would benefit from this creation by having their fatigue and pain reduced, and potentially feeling more proud of their positions by being more apt to maintain a consistent service. From this would follow the employers of pressure washers. Employers would quite clearly benefit from this advent by having increased production generated by marginal investment, yielding a high ROI. Further, customers of pressure washing services would benefit in a number of ways, namely more consistent product as well as more accurate application of that service, achieved by increased control of the pressure washing unit. Peeling one degree further back, water districts may potentially benefit from the reduction of water waste influenced by sub-optimal accuracy as a product of the current apparatus on the market.

Design iterations commenced from this point, beginning with hand sketching and developing into rough CAD illustrations to assist the primary ideation phase of this product development. A number of iterations later, a preferred design emerged that balanced customer desire and material minimization. This design was the result of a concurrent use of hand sketching, CAD renders, and a decision matrix to comply with discovered criteria such as weight, bib location, length, and wrist support. The next step was to begin an initial failure modes and effects analysis, with modes such as pressure regulation and material strength being glaring aspects. With this information present, the initial prototyping phase began and should.

I.A.2. Value Generation

The pressure washing industry is a large and mostly stagnant market, and it is dominated by a few companies imposing outdated wand designs. Unfortunately, these designs have led to numerous end user problems, as previously mentioned. It is these facts that leads me to believe there is market potential for the introduction of a complete redesign of current concepts. At present, pressure washer wands can exert great torque on the wrist of users, varied almost entirely by the area of the barrel nozzle. This method is not highly viable, for that matter, as nozzles are job specific and must be maintained to a certain degree. Thus the needs of the end user are not met, and as a result, face wrist injury, work induced fatigue, and cascading issues that proceed from these into the user's personal life.

The proposed solution to these problems is simple and can be achieved with minimal additional effort than what already exists. With the inclusion of a wrist support piece, relocation of the hose inlet to the wrist support, and a recoil spring in the barrel assembly, many of the problems and pain points facing the end user may be assuaged, and an inherently dangerous profession may be made measurably safer. While weight may be slightly increased in the new design, weight distribution will be refined so as to have a negligible effect. Hose inlet rearrangement will allow for a single arm use of the apparatus, yielding to improved worker efficiency, and thus quality, by sparing more attention to be paid to such. The barrel recoil spring will further support torque, and therefore fatigue, reduction thereby increasing the value of each employee as their effective working hours will increase, with more energy present during the later hours of their shift.

Thus, for all the reasons previously portended this is a viable product. With further market research and refinement of design focused on end user needs, the value of such a product to both employees and employers will only increase. With the aforementioned additions and a competitive price point, this innovation shows great promise both in user experience and profit potential.

II. CONCLUSIONS

Currently the pressure washer wand market is saturated with antiquated design strategies. With

performance being the only measure of success, the user experience has been almost entirely overlooked, with the exception of ergonomic improvements of the trigger handle. Unsurprisingly, many end users are dissatisfied with such relegation, and for this reason the forward facing intention is to empower pressure washer professionals by returning them their freedom of choice, and an inclusion into the design process. The devised system will reduce fatigue, water wastage, and employee downtime, thereby increasing productivity of each and the employers bottom line.

ACKNOWLEDGMENTS

The author would like to acknowledge Hoffman Car Wash, Inc., Rensselaer Polytechnic Institute, and The Lemelson Foundation for their support of this work.

REFERENCES

- [1] "Carwashes in the United States." *Manta*, Apr. 2016. <http://www.manta.com/mb_34_B121E_000/carwashes>.
- [2] "Pressure Washing Ethnography." Interview by David Haggerty.
- [3] "Pressure Washer Safety." Centers for Disease Control, Apr. 2016. <http://emergency.cdc.gov/disasters/pressurewasher_safety.asp>.

LifeSource; Daily Vital Sign Monitoring System

Maxen Haveles
Rensselaer Polytechnic Institute
Department of Mechanical, Aerospace, and Nuclear Engineering
havelj@rpi.edu

Even though American medical teams are extremely skilled and effective at making an accurate diagnosis, there is still a lack of medical support when a patient is released from the hospital. This creates gaps in the medical coverage that is given to patients because they are only able to be monitored while they are in the hospital. This gap creates many problems when dealing with patients who are prone to reoccurring diseases, such as heart attacks, but are not in the intensive care unit of a hospital. LifeSource is a way for a doctor and their team to monitor their patients while they live their lives. By using vital sign sensors and giving the information that is collected daily to doctors, the risk for a patient after they are released from a hospital will greatly decrease.

I. Introduction

There is currently a problem of the lack of accurate long term information available for the human body. When a patient leaves a hospital, the doctor and medical staff that they were seeing loses contact with them and their health until the next scheduled appointment. This creates large gaps in data for the doctors that could result in another serious injury.

This problem creates the biggest risk for patients. Cardiovascular diseases currently cause the most deaths in the United States and they are some of the most common reoccurring illnesses. Although it is not possible to determine exactly how much higher the chances of having a second heart attack are, it is proven that there is a much higher risk. The elderly are also affected by a lack of healthcare information. Because they are at a greater risk for nearly all diseases, the lack of information is even more deadly. Creating a system that could fill in the gaps between medical checkups will help to lengthen all people's lives.

The technology that is currently available is not enough to solve this problem. There has been a great rise in the last five years of wearable technology, but none of the products on the market have the main focus of tracking all of a person's

vital signs. The closest system that currently exists is the Fitbit because it keeps track of heart rate and promotes daily health. This system however has an entirely different goal than LifeSource. Fitbit is a daily fitness tracker while LifeSource is going to be a link between the doctor's office and the patient's home. The medical devices that are currently available are bulky and do not record data over a long period of time. They are also very expensive to purchase.

LifeSource will be a solution to this problem by being a device that is used daily for about fifteen minutes. It will track several vital signs including heart rate, blood oxygen level, and blood pressure and store the information in an online portal. The portal will be able to be accessed by both the patient and their doctors so that daily health can be monitored. This will allow doctors to keep a better eye on their patients, especially those prone to disease, without the patients having to be in the office.

II. Product Description

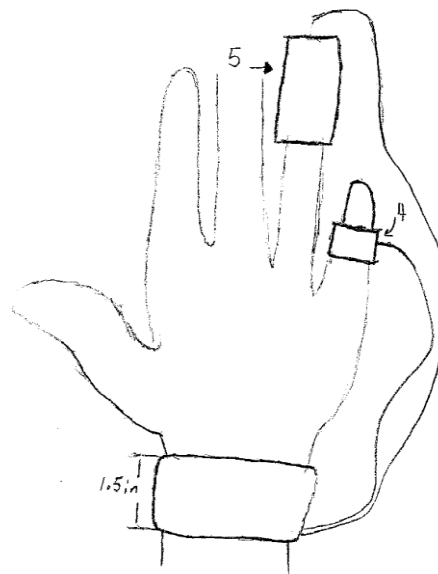


Figure 1: Early design of LifeSource.

The main goal of the LifeSource is to connect patients and their personal data to doctors. The first task of the system is to collect accurate data and store it securely. Once the data is available through an online portal, the doctor and patient will both be able to access all of the information whenever they need to. The system will also be able to examine the data and alert a medical team when there are abnormalities in any of the figures that were entered.

Because the system will be monitoring the patient's health on a daily basis rather than a weekly or monthly timeframe, there will be a higher chance of a disease, especially heart attack or stroke, to be identified before they strike. If a person is using the system and has to go to the hospital, the medical team will have more information at their disposal and will be able to make a faster, more accurate diagnosis. By collecting the vital signs of a person over a long period of time, a bank of data is built that will help doctors see where symptoms started to occur.

III. Development

Creation of LifeSource started by identifying sensors that would be capable of being mounted in a device on the wrist and give accurate readings. The choice was made to make this a device that will be worn every day for a short period of time instead of a constantly worn device so that the device can have a larger size. With a larger size, the emphasis of LifeSource is accuracy of readings rather than a full day's worth of data. While size was not a main concern in the design process, a goal was set to keep the device limited to the user's wrist and hand.

Interviews were conducted with multiple different medical professionals and after hearing their inputs and pain points, the focus of LifeSource was changed to cardiovascular diseases. Although the original goal of LifeSource was to be able to help medical teams prevent all kinds of diseases, illnesses that attack the nervous system are harder to notice without being in the presence of a doctor so they can see how a patient interacts with their environment. After these conversations, the three measurements that were chosen to be taken were blood pressure, heart rate, and blood oxygen level.



Figure 2: Vasotrac Blood Pressure Monitor.

The hardest of these numbers to record accurately on a wrist system is blood pressure. There are currently two types of technology that exist to take a blood pressure reading from the wrist. The first is called a Vasotrac that works in a similar way to a cuff on the arm, but has a large system that needs to accompany the wrist cuff. The second option is a device that is being developed at MIT that would use points of reference on the wrist and finger to give an accurate reading. Because Vasotrac was created in 1995, there are ways to minimize the equipment that it uses. This makes both systems viable options for LifeSource.

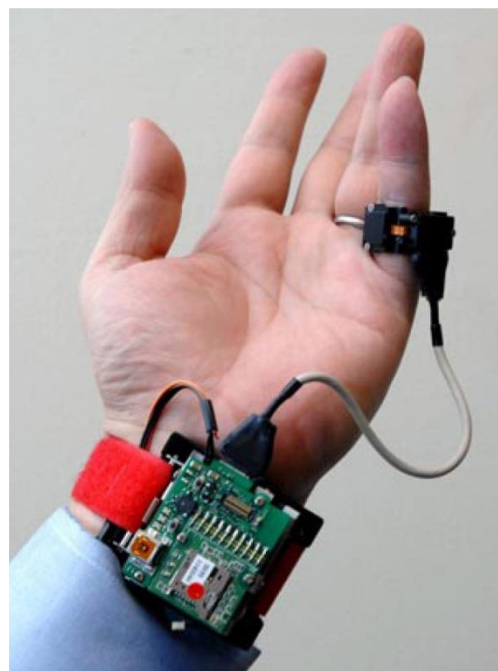


Figure 3: MIT Blood Pressure Monitor.

The most accurate readings for both heart rate and blood oxygen level are taken from arteries in the

fingers, therefore an additional system that sits on any finger will be wired to the blood pressure cuff. Taking the readings at the finger will allow the user to move around while the system is working without worry that they are altering their data.

A prototype of LifeSource is being built to model the data collection and storage system. The goal of the prototype is to demonstrate a system that is capable of reading data off of a sensor and storing it in an easy to read format. A finger heart rate monitor was chosen as the prototype sensor because of its ease of accusation and proven accuracy. Once a viable data system is developed, integrating other sensors onto the system will become the main goal of development.

IV. CONCLUSIONS

Based on interviews with multiple different people who work in different parts of the medical industry, this is a viable product. LifeSource relieves the pain points described in the first section by creating a way for doctors and their staffs to easily and accurately monitor patients when they are released from the hospital. By presenting a clear data set, the medical staff will also have more information at their disposal when working with a patient to diagnose their ailment.

Currently, the main focus is building the prototype and ensuring that the data that is collected is organized in an easy to understand format for both the medical teams and the patients. Once a prototype is created, more sensors will be integrated to ensure that they are compatible.

ACKNOWLEDGMENTS

Special thanks to Professors Asish Ghosh and Paul Schoch for all of the guidance and support that was given.

REFERENCES

- [1] Health & Medicine Report. (2007, April 16). Clinical Chemistry; Data on PreMD's New PREVU(x) Tape POC Format to be Presented at American Association for Clinical Chemistry Meeting. *Helth & Medicine Week*, p. 383.
- [2] Profis, S. (2014, May 24). *Do wristband heart trackers actually work? A checkup*. Retrieved

- from CNET: <http://www.cnet.com/news/how-accurate-are-wristband-heart-rate-monitors/>
- [3] Yilmaz, T. R. (2010). Detecting Vital Signs with Wearable Sensors. *Sensors*.

SolarSystem: A New Solar Powered Battery System

Adam Hennick
Rensselaer Polytechnic Institute
Department of Mechanical, Aerospace and Nuclear Engineering
hennia2@rpi.edu

The ‘SolarSystem’, a portable, modular and personal solar power battery system is a project developed in the Inventor’s Studio Class at Rensselaer Polytechnic Institute. Although still in the design and prototyping stage, the innovation seeks to provide a solution to the problem to power accessibility in remote areas. The modular system allows for the user to utilize as many panels as needed at any one time, while easily detachable for transportation and storage. The battery ensures that there is always power when a user needs it most. Design and prototyping of the innovation is nearing completion and full scale model testing will proceed through May of 2016.

I. THE PROBLEM

How many times has a nice day outside at the park or at the beach resulted in a dead phone battery, dead camera battery, or dead music player before you were ready to go home or done using it? You could have a backup supply if you prepared, but perhaps you didn’t anticipate having all your electronics die around the same time. The introduced solution is in the form of a renewable energy source that never runs out. Before now, hooking up a usable solar panel power system was expensive and was not conducive to transportation or portability. Real or perceived, a disconnect from electronics, cell phones and other devices is a fear many users experience on a daily basis. Running for a charger when a phone is almost dead, fearing that they will miss out on some form of communication if their phone dies is very real and ever increasing. The introduction of power banks is novel but useless once drained of their power before being able to get back to a plug. Traditional solar chargers don’t incorporate a battery which causes an unbearably slow charge as power is converting directly as it is being harnessed from the sun. The poor efficiency of traditional solar panel charger makes them unattractive to potential consumers. The proposed solution described in the next section looks to solve that issue and make solar power desirable for all.

II. PROPOSED SOLUTION

The solution provides virtually unlimited and cost efficient power to your electronic devices through a modular, user friendly portable solar panel powered system. The ‘SolarSystem’ which consists of solar panels mounted to an adjustable arm incorporated with a battery to store power for use when it’s needed most. A modular setup of the solar powered battery system is shown in Figure 1.

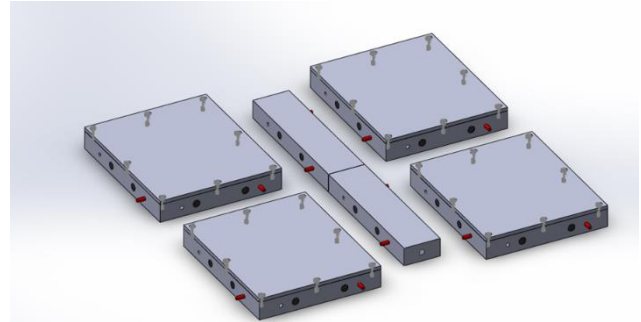


Figure 1: Modular setup of the solar powered battery system.

Currently, alternative solutions for backup batteries for personal devices range from traditional AA or AAA batteries which are both heavy and obsolete once the stored power is used, not to mention poor for the environment. Other rechargeable solutions include battery packs which also are obsolete once the power stored is used in a remote area. Lastly, small personal solar chargers are present in the marketplace although without a battery, in conjunction with size of the panels; they are not conducive to providing enough power to adequately and conveniently charge a device.

II.A. Main Functions

The proposed solution, as seen below in Figure 1 is a modular unit where the user can choose how many panels they would like to use at any given moment. The main functions of this innovation are

the easily attachable and detachable modular solar units, along with the convenient battery and bendable arm for maximum exposure to the sunlight.

II.B. Modularity

The panels, incased in a plastic frame, attach and detach rather easily with magnets and dowel pins holding the frames together. The bendable arm provides placement flexibility for the user. Ideally, the user sets up the “SolarSystem” by clamping it to the back of a chair on the beach, or a table in the park when they arrive. At this point, devices should still have battery. While the day goes on, the panels will collect energy and store it in the attached battery. Therefore, when the user needs the power, it is there waiting for them.

II.C. Proposed Electronics

Each panel outputs 6v, 583ma and 3.5W of power. Connected in parallel, the system, with a maximum of 6 panels can output 3.5A. Using a diode enables a step-down of 0.7v to use with the micro-usb wire that will carry the power from panels to battery. The panels are attached to a “modular hub” which enables the user to connect and disconnect the panels, using “Tamiya Style” connectors as they are attached and detached from the system. A model of this setup can be seen in Figure 2 below.

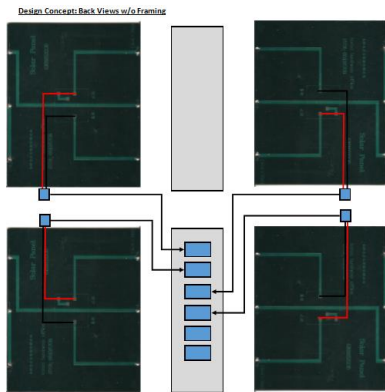


Figure 2: Design of solar battery’s electronic connections

III. PROGRESS REPORT

The project is in the prototyping stage with a first model expected to be completed by the

beginning of May. Once the prototype is complete, electrical and mechanical testing will begin and tweaks to the first prototype made. The iterative process will ensure a product ready for the marketplace is the result. The initial prototype is a 3D printed body integrated with project components that are readily available in the marketplace. This initial sourcing of materials from suppliers is adequate for the purposes of initial phases of testing although a development of supply chains for manufacturing is crucial to the success of the product to ensure a competitively priced product.

IV. FUTURE PLANS

The plan, once a working product has been completed, is to expand the offering to the other applications to ensure that the most amount of people is benefitting from renewable energy sources. By creating a portable power system for everyday users to enjoy, the hope is to increase the use of renewable energy sources, while simultaneously improving the convenience of charging electronic devices where power is not readily available.

ACKNOWLEDGMENTS

Thanks to the Inventors Studio II and III classmates, along with Professor Asish Ghosh for continued support and guidance. Special thanks to the help of Nick Madonna and Bradley Matheus for hands-on work on the project.

REFERENCES

- [1] "How Are Your Panels Going to Be Wired?" *Photovoltaic Solar Panels*. Web. 12 Apr. 2016.
- [2] "What Is 3D Printing? How Does 3D Printing Work?" *3D Printing*. Web. 3 Mar. 2016.
- [3] Solidworks Education, 2015 Edition

RELOAD: AN AUTOMATIC ORDERING SYSTEM

Jacqueline Peret
Rensselaer Polytechnic Institute
Department of Mechanical, Aerospace and Nuclear Engineering
peretj2@rpi.edu

Reload is a device that is targeted to busy college students to help them receive the items they need on a daily basis. The purpose of this is to save them both the time of having to either drive or take public transportation to a store and the money it would cost to pay for the car's gas. It would also indirectly prevent many accidents and slow the increase in global warming by taking vehicles off the road.

Reload consists of a device that can measure mass. It is a small scale that is connected to the internet. Once the product being placed on the scale is inputted from an online marketplace, the scale has access to how much the full product weighs and how much of that weight includes the carrying container. The Reload scale will reorder the product at a desired increment, for example when 10% of the product is left. It will also be connected to a secure website with the customer's credit card information to automatically pay for the item. The product will be delivered to the customer's door within twenty-four hours.

I. INTRODUCTION

The product was originally targeted to busy college students without cars on their college campuses. With shops being too far away to walk, many must either wait until friends are available to drive them or take the bus. The former is inconvenient if an item is needed right away and no one is willing or able to drive. The latter is also often not possible because of the time it takes for the bus to make the journey to and from the shopping area.

Receiving necessary items proves difficult for the elderly and people living in cities as well. Many elderly people are unable to drive anymore and, similarly to college students, rely on friends and relatives to bring them items when it is convenient.

People living in large cities may have a difficult time transporting products from the store to their homes. They often do not have cars and can only bring home what they can carry, which is only food for four days at a maximum. Reload would

automatically deliver everything to their doors, so they will have more of a selection of food to eat.

Though the aforementioned groups would benefit the most from a product such as Reload, any individual could use it. The user would never have to worry about restocking on essentials again.

Lastly, in a commercial setting, Reload could eliminate the need for inventory to be taken on both raw materials and manufactured goods available for sale.

I.A. Existing Competition

Amazon Dash is currently on the market. It delivers a product to the user after he or she pushes the product-specific button. However, the user must first recognize that the product needs to be restocked or refilled. Amazon Dash will not automatically order anything [1].

II. PROPOSED SOLUTION

The final concept is called Reload. It is a series of small scales that can be ordered for a minimal fee each. Reload connects to Wi-Fi and, once the product to be weighed is input, has access to the weight of the full container. As the product is used, the scale recognizes that and reorders the product at a user-specified time. If the product is not placed back on the scale, it will recognize that because the weight of the container is not felt. The user may choose what type of product and how much he or she wants ordered directly from Reload's website or phone application.

The scale is connected to an online marketplace that it orders from. The user's credit card is automatically charged for the amount of the item, and a drone will deliver it to the user's home the next day. A drawing of the product and a flowchart of the process can be seen below.

III.

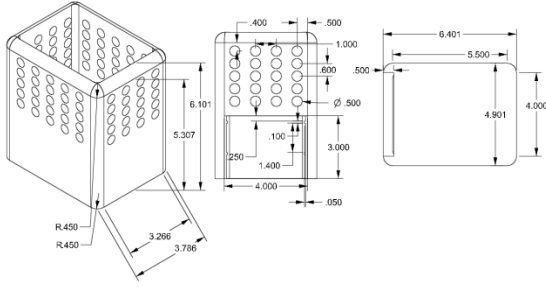


Figure 1: Drawing of Reload caddy.

If the warehouse that stores the product is too far away for the delivery to be efficiently made by a drone, the product will also have partnerships with local convenience stores. A delivery person would take products by car to the customer's home.

II.A. User Input

The user would select one time what product he or she wants to put on the scale to be monitored. He or she would also only input once when the product should be reordered, either in length of time or amount left of the item. The user can adjust both things later if he or she so chooses. Lastly, once the credit card information is inputted, the customer does not need to do anything to ensure the products are in stock, except when he or she picks them up at the front door.

II.B. Manufacturing

The first manufacturing model is a shower caddy with multiple slots for shampoo, conditioner, etc., to be weighed. The prototype is 3D printed using ABS plastic, but the final product is to be made by plastic injection molding.

The overall system will achieve fast and automatic delivery by incorporating each subsystem efficiently. The aim is to manufacture the Reload shower caddy system to respond to customer needs within one minute, send the information within five minutes, and achieve delivery to the home within one day.

III. RESULTS AND DISCUSSION

One of the most important things to have is an easy-to-navigate website. This will allow for an easy

set-up of the product, as well as facilitation of the ordering process. If this product is to be marketed to the elderly, it cannot be complicated for them to use. If this occurs, a large consumer base will be lost.

Another thing that needed by the user is less time driving. A reduction in the gas bill of the user is also necessary, but that goes hand-in-hand will less driving time. This will free up money and time for the user.

III.A. A Larger Impact

Not only would Reload give certain demographics more independence, it would also be beneficial to the environment. Fewer cars would be on the road. Greenhouse gases would be reduced, and numbers of accidents could decrease from reducing unnecessary driving.

III.B. Future Plans

Reload could be expanded from a scale system to full integration into current domestic objects and appliances in use, such as a refrigerator. This would eliminate the need to have many bulky scales. It could also be manufactured for a commercial market.

ACKNOWLEDGMENTS

The author would like to thank Yuhan Shi for her help with the electronics and Zachary Shute for his help with programming. Additional appreciation is extended to Dr. Asish Ghosh for his guidance and support for the duration of the project.

REFERENCES

- The lower side of the shower ca
- [1] Amazon, "Introducing Amazon Dash," 2016. [Online]. Available: <https://fresh.amazon.com/dash/>. [Accessed 11 May 2016].

INTER-CONNECTING CLAMP (ICC)

Daryian Rhysing

¹Rensselaer Polytechnic Institute

Department of Mechanical, Aerospace and Nuclear Engineering

rhysid@rpi.edu

The Inter-Connecting Clamp (ICC) is a rapid prototyping clamp designed to secure bundles of wires or longitudinal tubes to each other without the use of metallic hardware. The purpose of this clamp is to solve one of the many problems that affect the aviation industry when it comes to weight and performance. By changing the material of the clamp and eliminating the hardware used today for the installation, aircraft weight can be reduced significantly. The ICC consists of two halves that connect to each other through a quick snapping mechanism. This allows for easy assembly without stressing the wires upon removal or replacement.

I. PROBLEM STATEMENT

A great amount of fuel is used worldwide by airplanes and military aircraft in the course of a flight. This quantity is approximately proportional to the drag of an aircraft. Weight and drag are very much related; by adding weight to an aircraft, a greater lifting force is required as it moves through the air increasing the drag. Scientists dedicate most of their attention to shaping the aircraft's architecture to decrease this drag. Airlines are not able to control the price of fuel, but they are constantly working on ways to reduce how much fuel they use. In order to accomplish this, they must cut the weight wherever possible. There is a need in the aviation industry to reduce the weight of an aircraft in order to improve its performance.

I.A. Evolution of the problem

In contrast to ground vehicles, which do not need to be improved for effectiveness to the same magnitude as an aircraft due to the fact

that they can refuel regularly, long-distance traveling aircraft must bring all their fuel with them. On top of fuel taking up a great deal of storage room, old metal clamps that secure wire bundles and tubes are heavy and their weight is distributed along the entire aircraft. There are many different sizes of clamps that are installed from the cockpit, to the cabin, wings, tail, engines, and rotor assemblies. This weight, when added together, will most likely limit efficiency and affect the payload able to be carried.

I.A.1. Scope of the problem

Modifying an aircraft with new technology also implies, in most of the cases, increasing the size of the clamps or adding more clamps to the new wire bundles and consequently, increasing the weight. Aircraft are very complex and entail intricate arrangements of systems with networks of electrical wires, pneumatic cables, and heating technology. With every new aircraft model, the demands on these systems become a necessity and are required to be quickly implemented. According to the Air Transport Action Group, "The recent addition of personal seat-back televisions has added hundreds of meters of wiring to the aircraft" [1]. They have analyzed the scope of the problem previously by noticing that "There is a growing and contradictory requirement to reduce the weight of these systems while increasing their performance and reliability levels" [1]. For these reasons reinventing the clamp is crucial.

II. VISION STATEMENT

A major area of aerodynamic development in recent phases of aircraft architecture is

completing a good design while keeping a positive balance between conflicting elements. For example, “In older aircraft, the control surfaces such as the flaps and slats on the wings and the rudder and ailerons used to be controlled mechanically from the cockpit through cables or heavy, hydraulically-powered systems. These have been replaced with lighter and more powerful electrical systems which are electronically-controlled ‘fly-by-wire’ management systems” [1]. It seems that as technology makes its advances, there has been a steady rise in the amount of ‘composite’ materials used in aircraft manufacturing. Many aviation companies are now experiencing the weight savings generated by these materials over traditional aluminum alloys. The purpose of the ICC is to provide a relatively strong but flexible design to secure the wires and tubes through vibration without the use of heavy hardware for installation. With additive manufacturing, the ICC can be formed into a more complex shape than its metallic and non-metallic equivalents since the new market technology still requires the use of metallic hardware. The ICC can reduce the number of parts and the need for fasteners and joints during preventive maintenance.

II. CONCEPT SPECIFICATIONS

The new ICC innovation focuses on potential reduction of aircraft weight by optimizing the operational design. The new inter-connecting, light-weight clamp is a challenge that pushes efficiency in the aviation sector while ensuring it remains the safest form of transport. With a dual locking mechanism, two equally designed halves are connected together in order to reduce the labor and Foreign Object Damage (FOD) hazards. A single slide-through channel allows interconnection within each other. Two alternatives are featured:

- A fixed sliding high friction strip and channel, Figure 1.
- A sliding clip-in that allows for rotation, Figures 2 and 3.

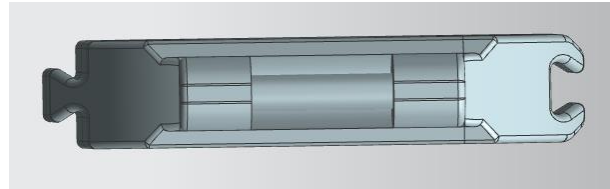


Figure 1: Strip and channel for easy assembly.

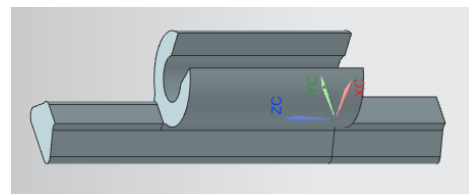


Figure 2: Clip attachment.

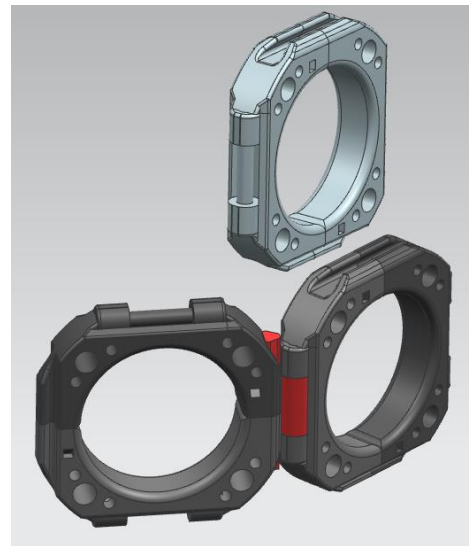


Figure 3: Clamp assembly.

The key material preferred for this rapid prototyping is a resin that could offer the highest heat resistance, chemical resistance, and tensile strength. There are many methods to accomplish this and Fused Deposition Modeling (FDM) thermoplastics could be an ideal selection for

this innovation. The initial prototype is manufactured at the Rensselaer Polytechnic Institute (RPI) using their 3D printing machine.

II.A. Feasibility of Concept

Concept feasibility of the ICC is shown in Table I.

Table I: Concept feasibility of the ICC.

| Feature | Manufacturing | Flexibility | Composite | Technology |
|------------|----------------------------------|------------------------------------|----------------------------------|------------------------------|
| Half Clamp | Two equally designed halves | Highly temperature resistant | Non-conducting, lighter material | Attaches to another clamp |
| Attachment | Fixed sliding strip with channel | Easy to install in compacted areas | Non-corrosive | Dual connecting device |
| Assembly | Easy locking mechanism | Multiple sizes | Withstands vibrations and shock | Can turn at different angles |

III. CONCLUSION

Throughout the conceptual evaluation and development of the ICC, the new modern design is shown to cover more than the configuration of the standardized clamps. This advantage allows for the assessment of technological and operational scenarios having the potential to ‘right first time design’. For that purpose, the ICC was developed on the basis of the former metal clamp by evolutionarily introducing modern inter-connecting sophistication under the premise of maximum reusability of existing parts. New modeling and geometry are integrated into the new design for flexibility in dealing with typical optimization problems.

REFERENCES

[1] “Beginner’s Guide to Aviation Efficiency,” Air Transport Action Group, 2010.

Limb Ease: A New Concept for Transfemoral Prosthetic Sockets

James Sherman

Rensselaer Polytechnic Institute

Department of Mechanical, Aerospace, and Nuclear Engineering

shermj5@rpi.edu

Prosthetic attachments or artificial limbs are artificial extensions used to replace a missing body part as a result of injury or congenital defect. For this report, the focus will be on the technologies surrounding transfemoral prostheses, which are prosthetic limbs utilized when the limb is missing above the knee joint—more specifically, the sockets which are used to attach the artificial limb to the stump. Using current literature, interviews with an industry representative, an amputee, and benchmarking with current market technologies, several issues with the current state of prosthetic sockets have been identified. These issues include—but are not limited to—the expensive and often extensive fitting sessions, which require a prosthetist or orthotist. Additionally, the inconvenience of current market sockets can cause pain and other injuries to the user. We propose the development of Limb-Ease, a novel method of approaching a custom socket which will revolutionize the way that current prosthetic sockets are designed and fitted. Limb-Ease will be based upon the newest research in the use of bi-stable electroactive polymers, whose shape and stiffness can be modified by applying heat and voltage. These ‘memory’ polymers have the potential to shift the fitting process to the user while maintaining the safety and accuracy in design of sockets fitted by a prosthetist, and may ultimately reduce price and increase the comfort of artificial limbs.

I. INTRODUCTION

When a person is born without a limb or becomes an amputee, they are faced with several lifelong problems, including the physical, emotional, and financial burden of buying prostheses and services [1]. Among these

services, the fitting of artificial limbs and sockets requires the expertise of a prosthetist or orthotist. While this may not seem to be a hindrance, the number of times an amputee may visit a prosthetist per year can exceed 9 ± 11 times [2]. The high frequency for fittings and physical therapy is required by children who have congenital birth defects or who have suffered injury, as they are growing and must have fittings in order to prevent injury from ill-fitting sockets. Additionally, the cost of prosthetic limbs can reach exorbitant levels, with transfemoral prostheses running costs into the tens of thousands of dollars. The reason for the high cost is that prostheses must be custom-made for each user, which prevents mass production of artificial limbs and sockets [1]. Finally, the socket fitting for most prostheses, especially those of transfemoral amputees can cause pain and lingering skin problems despite the high cost required for even baseline models.

As a result, there is a dire need in the market to be able to create a design for prosthetics and sockets which may be mass produced, reducing the cost, time, and stress associated with fitting and purchasing a prosthetic limb.

I.A. Scope of the Problem

Currently, records show that approximately 500 Americans lose limbs daily as a result of injury, disease, congenital defects, and trauma, with a total of over 185,000 per year. There is an estimated total of 2 million amputees currently in the United States [4].

I.A.1. Average Cost of Transfemoral Prosthetics

The cost of new prosthetic limbs ranges from about \$6,000 to about \$46,000, with sockets for transfemoral limbs ranging from \$200 to \$3,200

[5]. While health insurance may cover a portion of the fees for the fabrication of a prosthetic limb, approximately 10% of the US population was without health insurance for the entirety of 2014, with about 12% of the population experiencing a lack of health insurance for at least a portion of that year [6]. This means that there are a vast number of Americans who do not receive assistance in the purchase of prostheses, and of those that do have health insurance, many do not receive adequate coverage of prosthetics. The result is that many patients who are suffering cannot afford the care they need when it comes to prosthetic fitting, and many more families are strained by the financial burden of the cost of prosthetics.

I.A.2. Design Issues with Prosthetic Sockets

Finally, there are a number of problems with current designs which result in injury to amputees both in the short and long terms. Since the majority of prosthetic sockets utilize a molded cup where the stump is first covered in a silicone or fabric sleeve before being placed inside (see Figure 1), the skin on the stump is not allowed to breathe, resulting in numerous issues.

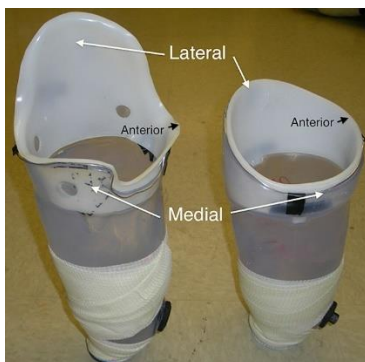


Figure 1: Transfemoral Prosthetic Socket [7].

Since skin is not suited for this type of contact, a multitude of skin issues can arise including the ones tabulated in Table 1 of Appendix A.

I.B. Current Designs to Address Socket Issues

Several companies currently produce alternatives to traditional sockets, and are characterized by their strength and weaknesses below.

I.B.1. Lim Innovations: Infinite Socket

The Infinite Socket is an adjustable socket designed for users who have active lifestyles. This socket is characterized by rigid, molded arms which are held together and whose fit may be adjusted by Velcro straps (Figure 2).



Figure 2: Infinite Socket [8].

This socket provides a level of comfort not seen in traditional transfemoral sockets, and allows the user to adjust the fit as needed. However, the arms and baseplate must still be custom fitted and designed for each user, resulting in increased end-cost to the consumer.

I.B.2. Martin Bionics: Socketless Socket

The Socketless Socket provides a similar level of comfort as the Infinite Socket. The design is also similar, and as a result has the same shortcomings of the Infinite Socket (Figure 3).



Figure 3: Socketless Socket [9].

I.B.2. Osseointegration

Osseointegration is the fusing of a metal rod to the bone in the amputated limb (Figure 4). This metal rod can then be attached directly to the prosthetic limb. In terms of providing the best fit and comfort, this method is clearly the best. However, the process also requires invasive surgery with a high risk for infection. This would initially result in pain for the user, as well as the risk of further amputation due to infection.

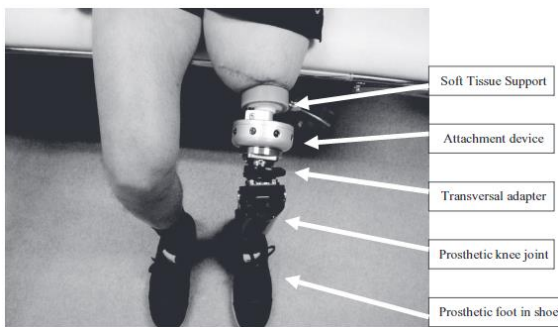


Figure 4: Osseointegration [10].

II. DESIGN PROCESS

II.A. Initial Design Parameters

The user of Limb-Ease will be any patient who requires the use of a prosthetic. This means that the new socket attachment should be able to be applied towards any type of amputee, including transtibial, transfemoral, transhumeral,

or transradial. In addition to this, the Limb-Ease system should be able to withstand any use, especially those shown in Figure 4, from minimal use to high impact activities. Finally, the Limb-Ease should be easily affordable, allowing anyone, even those without adequate insurance to be able to afford it.

II.B. Post-Benchmarking Parameters

After benchmarking and discussing design parameters with an industry representative, thereby reframing the initial issue, I concluded that in order to revolutionize the prosthetic socket, several new needs had to be met:

- i) Provide custom fit without custom manufacturing
- ii) Provide same or greater quality fit as that provided by prosthetist
- iii) Provide this level of comfort and fit without user input (automatic)

Given these criteria, it was necessary that the materials and control system for this socket would be the defining factor of the innovation. A literature search yielded a paper published recently regarding bi-stable electroactive polymers. Bi-stable electroactive polymers (BSEPs) have the ability to ‘remember’ the shape to which they are forced by heating and applied voltage, followed by cooling below the glass transition temperature [11]. An example of the mechanics of a BSEP is shown in Figure 5.

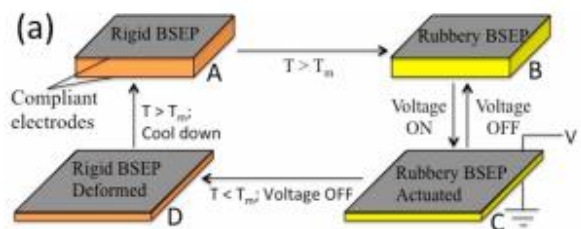


Figure 5: BSEP mechanism demonstration [11].

This technology is still in its infancy, but the potential uses have been shown in robotics, such as the ability to pick up sensitive objects, as well

as for the medical industry. However, the potential benefits for the prosthetics industry could revolutionize how prosthetic sockets are fitted. As a result, I propose the evaluation of the technology as a self-regulating prosthetic socket. This type of socket would utilize pressure transducers along the length of the polymer in order to insure that pressure applied to a limb matches the average pressures exerted by a prosthetic socket. An example of this is shown in Figure 6 along with an idea of how an actuated BSEP arm could be integrated into a prosthetic socket system.

II.C. Initial Concept Design

Based on the design parameters and the use of BSEPs, the following concept for a transfemoral socket was created (Figure 6).

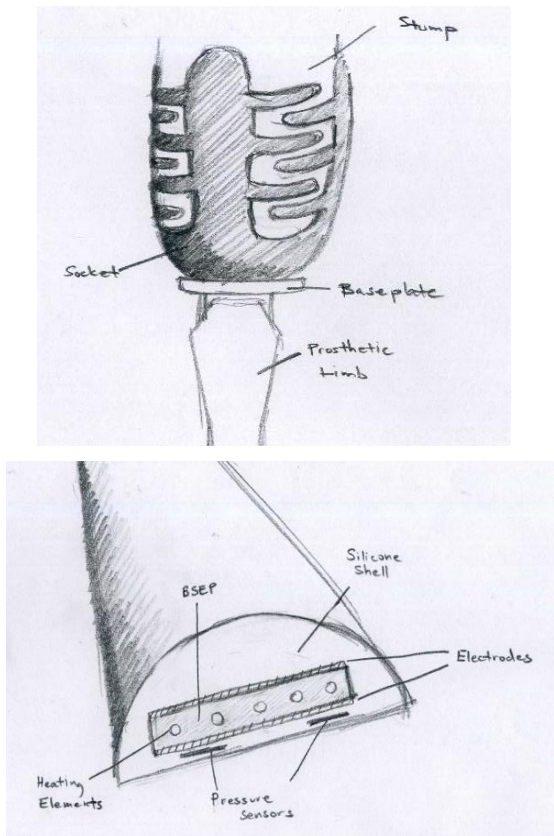


Figure 6: Lime-Ease Concept Design.

This design concept features several key aspects, including embedding the BSEP within a

silicone shell, as well as integrated heating, electrode, and pressure transducer circuits.

II.C.1. Design Parameters

To develop this concept further, it is necessary to characterize baseline parameters for strength, applied load, and the geometry of the stumps of transfemoral amputees. However, there is a significant lack of data with respect to these characteristics.

To calculate the amount of pressure needed to insure that the socket and limb will not separate from the stump, the average mass of an artificial limb, the friction coefficient between the skin and socket, and the applied upwards and downwards force along the upper leg are needed.

Average transfemoral prosthetic weight is 8 lbf (pounds-force), which equates to a 35.6 N load [12]. The average acceleration of the upper leg during gait has not been characterized (no publicly available data has been found to date). As a result, for the initial acceleration in the vertical direction will be assumed to be a maximum of 2g, where g is the gravitational acceleration (9.81 m/s²). This will equate to a maximum applied force of 71.2 N, given the initial load applied by the weight of the prosthetic. Silicone will be used as the material between the skin and the BSEP. The frictional coefficient (μ_f) between skin and silicone is 0.7 [13]. Finally, the average area of the upper leg is $3.077 \times 10^{-3} \text{ m}^2$ [14]. The equation for pressure is:

$$P = \frac{F}{A} = \frac{ma}{A} \quad (1)$$

where P is pressure, F is force, A is area, m is mass, and a is the acceleration. However, since the total area will be the area of the arms of the prosthetic socket, the dimensions of the arms must be designed such that the socket does not cut off circulation (create pressure points).

II.C.2. Polymer Selection and Concept Design

The arms of the prosthetic socket must be rigid enough to resist bending and deformation during use. As a result, a high elastic modulus (E) is required.

A polymer known as PtBAS4 [15] has a modulus of 994 MPa at 50 °C. PtBA is a known BSEP, while PtBAS4 consists of PtBA mixed with styrene. PtBAS4 must be tested in order to determine whether it exhibits the properties of a BSEP, but at the moment, will be used for its modulus in the design process.

50 °C is close to the glass transition temperature of the material, meaning that as it is cooled, its elastic modulus increases. The lower E will be used in order to ensure that the design meets the necessary requirements (i.e. the components will not buckle or bend under the given static load).

For the purposes of the concept drawings shown in Figure 6, a simple beam bending and buckling analysis will be carried out for the horizontal and vertical arms. A simple beam bending analysis is shown in Figure 7, and the maximum deflection characterized by the following equation

$$\delta = \frac{qL^4}{8EI} \quad (2)$$

where δ is the maximum deflection of the beam, q is the distributed load, L is the length of the beam, E is the elastic modulus and I is the moment of inertia.

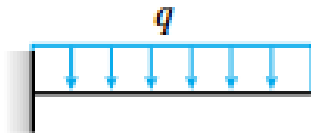


Figure 7: Cantilever beam with distributed load [16].

The moment of inertia, I , for a rectangular cross section is given by the following equation

$$I = \frac{bh^3}{12} \quad (3)$$

where b is the length of the base, and h is the height.

Finally, for a fixed, vertical beam, buckling is characterized by the following equation:

$$P_{cr} = \frac{\pi^2 EI}{4L^2} \quad (4)$$

where P_{cr} is the critical load at which buckling occurs, and the other variables are as described previously.

The deflection (Equation 2) must be kept to a minimum, and preferably at 0.0 m. For the purposes of this design, the deflection will be set at 0.0001 m. Additionally, the cross sectional geometry must be set in order to produce this minimal deflection. The base will be 0.0127 m, and the height will be 0.0508 m. Given these parameters, the length of a single arm of the socket may not exceed 0.1157 m. The height of the vertical portion of the socket arm must not exceed 2.1862 m, which is far greater than needed for a transfemoral socket.

III. CONCLUSIONS

The need for current patients requiring prostheses is a method of reducing the cost and amount of professional help needed to fit a socket, the overall comfort of the socket, and an adjustable socket which can be utilized far longer than existing sockets.

The Limb-Ease system has the potential to meet all these needs. However, there is much work to be done in order to provide a proof of concept by the end of the semester. The following lists what must be accomplished before a proof of concept can be attempted:

- Materials used in BSEP must be analyzed to determine parameters of Limb-Ease components using dynamic analysis
- Controller and voltage source for Limb-Ease must be determined based on BSEPs
- Potential methods of creating proof of concept must be explored (i.e. additive manufacturing, injection molding, etc.)

Once these details have been worked out, the development of a proof of concept or working prototype may begin.

ACKNOWLEDGMENTS

Special thanks to Nathaniel Winters, TaiLor Made Prosthetics, Professor Asish Ghosh, and Rensselaer Polytechnic Institute for helping in the development of this concept.

REFERENCES

- [1] G. McGimpsey, "Limb Prosthetics Services and Devices," 3 March 2016. [Online]. Available: 2016.
- [2] L. Pezzin, "Use and satisfaction with prosthetic limb devices and related services," *Archives of physical medicine and rehabilitation*, pp. 723-729, 2004.
- [3] J. H. J. K. M. Jason Highsmith, "Identifying and Managing Skin Issues with Lower Prosthetic Use," *In Motion*, 2011.
- [4] K. Ziegler-Graham, "Estimating the Prevalence of Limb Loss in the United States: 2005 to 2050," *Archives of Physical Medicine and Rehabilitation*, pp. 422-429, 2008.
- [5] D. K. Blough, "Prosthetic Cost Projections for Servicemembers with Major Limb Loss from Vietnam and OIF/OEF," *The Journal of Rehabilitation Research and Development*, p. 387, 2010.
- [6] "US Census Bureau," 8 March 2016. [Online]. Available: census.gov.
- [7] M. J. H. Jason T. Kahle, "Transfemoral Sockets with Vacuum-Assisted Suspension Comparison of Hip Kinematics, Socket Position, Contact Pressure, and Preference: Ischial Containment Versus Brimless," *Journal of Rehabilitation Research and Development*, pp. 1241-1252, 2013.
- [8] LIM Innovations, "Infinite Socket - LIM Innovations," 8 March 2016. [Online]. Available: liminnovations.com.
- [9] Martin Bionics, "Socket-less Socket," Martin Bionics, [Online]. Available: martinbionics.com. [Accessed 8 March 2016].
- [10] E. H. K. H. E. E. Haggstrom, "Comparison of Prosthetic Costs and Service Between Osseointegrated and Conventional Suspended Transfemoral Prostheses," *Prosthetics and Orthotics International*, pp. 152-160, 2012.
- [11] Z. Ren, "Phase-Changing Bistable Electroactive POLYMER Exhibiting Sharp Rigid-To-Rubbery Transition," *Macromolecules*, pp. 134-140, 2016.
- [12] CPO Inc., "Prosthetics Questions and Answers," 29 April 2016. [Online]. Available: cpo.biz.
- [13] M. Z. a. A. Mak, "In Vivo Friction Properties of Human Skin," *Prosthetics and Orthotics International*, pp. 135-141, 1999.
- [14] M. C. A. N. Alan Cross, "Body Segment Differences in Surface Area, Skin Temperature, and 3D Displacement and the Estimation of Heat Balance During Locomotion in Homonins," *PLoS ONE*, 2008.
- [15] M. Cerrada, "Preparation of Poly(Tert-Butyl Acrylate-G-Syrene) as Precursors of Amphiphilic Graft Copolymers: Relaxation Processes and Mechanical Behavior," *Polymer*, pp. 2803-2810, 2002.
- [16] R. Hibbeler, *Mechanics of Materials*, Jurong: Pearson/Prentice Hall, 2005.

APPENDIX A: Skin disorders as a result of prosthetic use [3].

| Diagnosis (Name) | History (Signs/Symptoms) | Physical Exam Findings | Acute Management | Long-Term Management |
|-----------------------------------|---|---|---|--|
| Pressure sores (Decubitus ulcers) | Pain and/or redness over bony prominences | Erythema (redness) or ulceration over bony prominences | <ul style="list-style-type: none"> Stop using prosthesis Antibiotic ointment (e.g., Polysporin*) | <ul style="list-style-type: none"> Prosthetic adjustment New socket |
| Allergic Contact Dermatitis | <ul style="list-style-type: none"> First exposure causes no reaction (type IV delayed hypersensitivity reaction) Itching and redness appears 1-5 days after second exposure and affects everywhere the allergen contacts the skin May extend beyond allergen contact areas if severe | <ul style="list-style-type: none"> Acutely, may have well-demarcated erythema, weeping or blisters Subacutely, erythema, less well-demarcated, maybe scaly skin Chronically, erythema and dry, thick, scaly skin | <ul style="list-style-type: none"> Moisturizer Topical steroids (e.g., hydrocortisone) | Allergen avoidance (substitute allergen for materials that do not aggravate symptoms) |
| Irritant Contact Dermatitis | <ul style="list-style-type: none"> Itching and redness typically appear immediately after contact (even with first exposure) Severity related to duration & amount of exposure Never extends beyond contact area | Same as allergic contact dermatitis | <ul style="list-style-type: none"> Barrier cream [zinc oxide] Moisturizer Topical steroids | Avoid or minimize irritant exposure (e.g., perspiration from heat or friction) |
| Negative Pressure Hyperemia | <ul style="list-style-type: none"> Negative pressure socket, pain and erythema under prosthesis in a well-circumscribed pattern Usually a history of limb volume change (i.e., weight gain/loss, edema) | Well-demarcated erythema that is exquisitely tender to palpation | <ul style="list-style-type: none"> Stop using prosthesis Moisturizer | <ul style="list-style-type: none"> Correct underlying problems: Curb weight gain (diet/exercise) Treat edema New socket? |
| Folliculitis | Itching, possibly pain, "pimple" (properly termed pustule) | <ul style="list-style-type: none"> Direct visualization of folliculocentric pustule Typically with erythema | <ul style="list-style-type: none"> Decrease heat and friction (remove prosthesis if possible) Topical or systemic antibiotics | Avoid shaving area (increases incidence) |
| Abscess | Inflammation with erythema and severe pain | Visualization of erythematous nodule that is exquisitely painful | Incision and drainage absolutely necessary by physician, may also need systemic antibiotics | <ul style="list-style-type: none"> Keep area clean Avoid shaving affected area |
| Xerosis | Dry skin, may have erythema and/or itching | Dry scaly or flaky skin, may have excoriations or erythema | Moisturizers (over-the-counter) | <ul style="list-style-type: none"> Keep area clean Maintain hydration (systemically and locally) |

AUTONOMOUS UAS TARGET IDENTIFICATION

Sage Trudeau¹, James Hanford¹, Diego Cepeda¹, Jacob Keats¹,
Jesse Greaves¹, Vincent Cerati¹, Stanley Cheung¹, Alexander Link¹, Grant Barron¹
¹Rensselaer Polytechnic Institute
Department of Mechanical, Aerospace and Nuclear Engineering
²MIT Lincoln Laboratories
Trudes@rpi.edu

Despite their intense training and incredibly rapid response times, search and rescue teams are often unable to identify locations of surviving victims during disaster scenarios. They rely heavily on local tips and tend to resort to overlaying a grid on the disaster area and searching square by square. Search time could be reduced, and lives saved increased, if there was a better way to determine the location and density of survivors in disaster areas. The team proposes to use Commercial Off The Shelf COTS quadcopter and sensor technology in addition to open-source software to enable Unmanned Aerial Systems UAS to find and relay information about survivors. Commercial quadcopters already have excellent Global Positioning System GPS capabilities, while guidance and collision avoidance systems are beginning to appear on the market. Coupling these with additional image recognition software and thermal vision will allow UAS to identify targets while mapping the area around them. This will allow human users to optimize their search, spending more time saving lives and less time searching empty buildings.

I. INTRODUCTION

To achieve the most effective disaster relief two major steps should be taken that can be broken into subtasks. First and foremost the aid must be swift and accurate, minimizing the amount of time people are left in danger. To do this, the solution must be able to scope out the affected area, identify points of interest, and provide suggested routes for responders. Second, the first responders should maintain a maximum level of safety for themselves. This can be achieved by returning information about hazards, scouting difficult terrain, and relaying information between responders.

In recent years, mobile platforms such as small UAS have undergone rapid development showing high potential for disaster relief. However, current

technology lacks the “smarts” to perform these tasks, especially in a manner that requires a minimal amount of assistance from the user. To this end, the team aims to create a system that allows a user to task a UAS to perform autonomous target identification through the use of cheap, lightweight onboard sensors.

The direct beneficiaries of this research are first responders who include but are not limited to: fire fighters, police officers, paramedics, and the National Guard. First responders are often injured while on-duty, which can hinder search efforts and shorten their careers. To that end, this project has been designed to reduce the risk associated with search and rescue from collapsed or damaged buildings. Implementation of the UAS as a preliminary disaster surveillance device should inform first responders of feasible entrances, create floor plans, and help avoid obstacles. By providing this information to rescuers first responders will be better equipped to handle the situation and triage appropriately. Minimizing risk and injury in disaster relief situations has the potential to increase the likelihood of victim discovery and protect the heroes in the field.

As seen in recent floods, drones have been piloted to help search rooftop to rooftop for survivors with great success[1]. The team set out to improve on this effort and automate the search. The purpose of the system is to create an autonomous platform capable of performing disaster relief tasks with minimal human interaction. With increasing standards and restrictions, it is proposed that through open-source algorithms and COTS, the capabilities UAS can have for saving lives will be demonstrated.

A necessary step for this demonstration is an effective collision avoidance system on UAS. Researchers at institutions such as Massachusetts Institute of Technology (MIT) are developing algorithms for fixed-wing UAS collision avoidance systems using stereoscopic imaging and a myriad of

startup companies are packaging ultrasonic sensors to retrofit commercial UAS[2][4].Unfortunately, most of this information falls under proprietary property, making integration with the Humanitarian Aid and Disaster Relief (HADR) community difficult. Additionally, thermal imaging is rapidly dropping in price and the benefits it can provide to situational awareness for Disaster Relief and Emergency Response missions are well accepted within the community [8]. Due to these factors it is proposed to develop a combination of sensors such as visual, infrared, ultrasonic, and radar that would allow advanced autonomous tasking in dangerous and communication disadvantaged environments such as collapsed buildings. This system is shown in Figures 1 and 2.

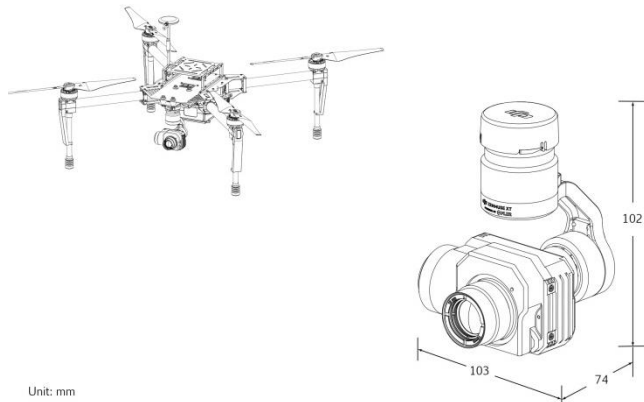


Figure 1: Matrice 100 Development Platform with Zenmuse XT Thermal Imaging Camera. Component drawings courtesy of DJI[3].

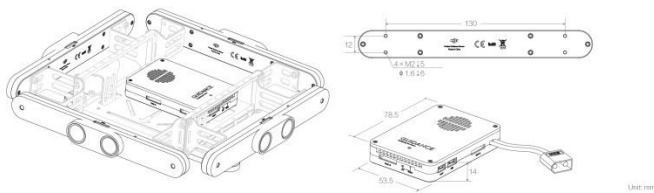


Figure 2: Guidance collision avoidance system with decision support. Component drawings courtesy of DJI[3].

II. PRODUCT DESCRIPTION

The UAS will feature autonomous flight navigation to traverse between specified areas input by the user. At each waypoint, the drone will scan the surrounding area and perform on-board image

processing to locate possible entrances in a collapsed building for the UAS to explore. Within a building, the UAS will maintain indoor positioning using Light Detection And Ranging (LIDAR) and stereoscopic imaging. The drone will also utilize thermal imaging to detect nearby survivors and notify ground station of such. The UAS will use collision avoidance algorithms to navigate around obstacles as it performs its mission.

Operators can rapidly build up situational awareness in a given disaster relief situation by delegating the task of searching for survivors to the proposed system. The UAS is significantly faster than humans at reaching target locations, especially when road infrastructure is damaged or obstructed with debris. This reduces the time needed to search for survivors, and speeds up the time sensitive task of rescuing survivors. The system is easily scalable for larger regions by having more drones simultaneously searching. Users can operate many UAS, reducing the manpower needed to perform an extensive search. Overall, the proposed system reduces manpower needed, speeds up search and rescue operations, and scales easily.

III. APPROACH/ DISCUSSION

A major challenge in the development of an autonomous UAS is fine tuning navigation and collision avoidance algorithms without risking the hardware. In order to reduce collisions during testing, a testing cycle has been created where all algorithms are first tried numerous times in a simulation on a dedicated machine. These are then imported as hardware in the loop simulations using the aircraft's onboard computer and finally tested in live exercises. The Robot Operating System (ROS) provides open-source tools for simulations as well as allowing for existing tools to be easily extended with custom code. ROS was chosen because it facilitates the management of complex systems by providing a unifying layer for synchronous and asynchronous communication between complex models and subsystems. An ROS computation graph, showing the flow of network processes, can be seen in Figure 3 [7].

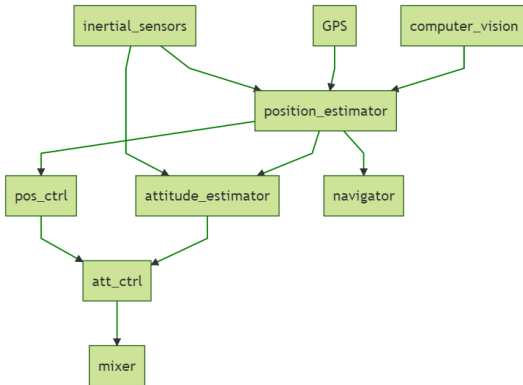


Figure 3: ROS Computation Graph.

To test the operation of the ROS components, the official simulator integrated with ROS was used. Through its built-in physics engine the simulator is able to faithfully reproduce the dynamics of a system taking into account gravity, contact, and friction forces. This can also be further extended with plugins. For UAS simulation the package “Hector quadrotor” by Technische Universitat Darmstadt was modified to simulate both a quadrotor craft’s low level controls as well as high level behavior[6]. All sensor data is merged using Extended Kalman Filters to obtain a single representation of the vehicle. This information is then used to drive the navigation and collision avoidance algorithms. Pictured in Figure 4 is a simulation of the quadcopter where LIDAR readings gathered on the Gazebo generated environment are used to generate a map and intelligently navigate through the use of SLAM algorithms.

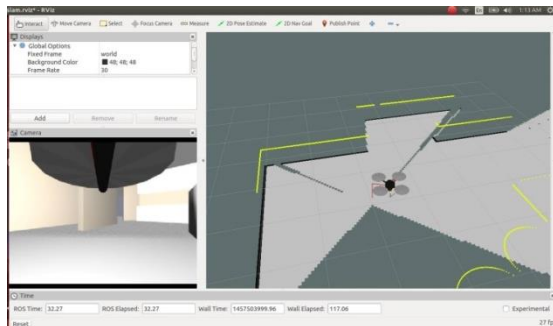


Figure 4: LIDAR Mapping Simulation.

Red Green Blue (RGB) camera data is also used in the simulation. The second incarnation of the SLAM algorithm implemented Octomap to process LIDAR data and generated an accurate 3d representation of the environment around the aircraft, as shown in Figure 5 [5].

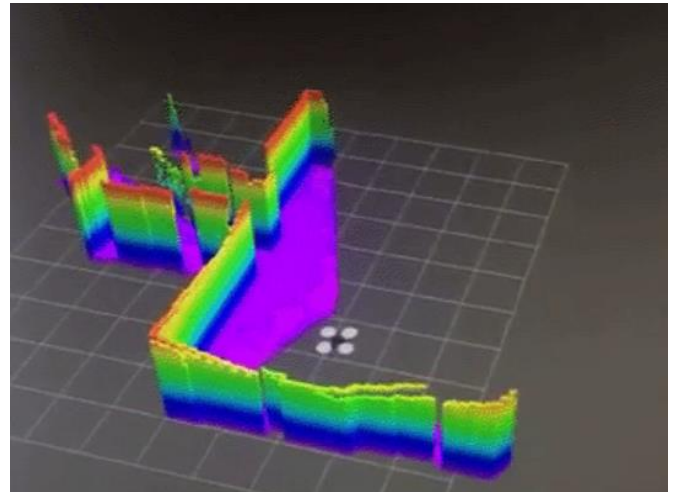


Figure 5: 3D Simultaneous Localization And Mapping (SLAM) Simulation.

IV. FUTURE DEVELOPMENT

Moving forward, the team would like to expand the capabilities of the drone using the current onboard sensors. Using the onboard LIDAR combined with the stereoscopic imaging, the team envisions being able to create detailed three dimensional floor plans of spaces to be sent back to first responders. This will enable first responders to better assess threats and reduce risk. The current system focuses on visual threats, however unseen threats such as carbon monoxide or explosives are yet to be tackled. The goal is to push the capabilities of commercial off the shelf hardware and so as that hardware improves new research explorations reveal themselves. Even the administration of basic first aid could soon be seen as a possibility.

V. APPENDIX

Table 1: List of Abbreviations.

| | |
|-------|---------------------------------------|
| COTS | Commercial Off The Shelf |
| GPS | Global Positioning System |
| UAS | Unmanned Aerial Systems |
| MIT | Massachusetts Institute of Technology |
| HADR | Humanitarian Aid and Disaster Relief |
| LIDAR | Light Detection And Ranging |
| ROS | Robot Operating System |
| RGB | Red Green Blue |

ACKNOWLEDGEMENTS

Special thanks to Amna Greaves of MIT Lincoln Laboratory and Professor Ali Tajer of Rensselaer Polytechnic Institute for invaluable help and guidance.

This project was conducted with support from the Department of Homeland Security Science and Technology Directorate.

REFERENCES

- [1] AP Exchange (2015, September 26). Drones used in search for missing in Central Texas flooding. Retrieved April 09, 2016, from <http://kxan.com/2015/09/26/drones-used-in-search-for-missing-in-central-texas-flooding/>
- [2] Conner-Simons, A. (2015, October 26). Self-flying drone dips, darts and dives through trees at 30 mph. Retrieved April 14, 2016, from http://www.csail.mit.edu/drone_flies_through_forest_at_30_mph
- [3] DEVELOPER | DJI. Retrieved April 14, 2016, from <http://www.dji.com/products/developer>
- [4] Gageik, N., Benz, P., & Montenegro, S. (2015). Obstacle Detection and Collision Avoidance for a UAV With Complementary Low-Cost Sensors. *IEEE Access*, 3, 599-609. doi:10.1109/access.2015.2432455
- [5] Hornung, K.M. Wurm, M. Bennewitz, C. Stachniss, and W. Burgard, "OctoMap: An Efficient Probabilistic 3D Mapping Framework Based on Octrees" *Autonomous Robots*, 2013; DOI: 10.1007/s10514-012-9321-0.

- Software available at <http://octomap.github.com>.
- [6] Kohlbrecher, S., Meyer, J., Petersen, K., & Graber, T. (2012). Hector SLAM for robust mapping in USAR environments. *Technische Universität Darmstadt*. Retrieved from http://tedusar.eu/cms/sites/tedusar.eu.cms/files/Hector_SLAM_USAR_Kohlbrecher_RRSS_Graz_2012.pdf
 - [7] ROS.org | Powering the world's robots. (n.d.). Retrieved April 14, 2016, from <http://www.ros.org/>
 - [8] Fairfax County Urban Search and Rescue Team (2015, October 21). Interview with Lorton Search and Rescue [Personal interview].